Volume 86, Number 1,
January 2025

ISSN 0005-1179
CODEN: AURCAT

AUTOMATION AND REMOTE CONTROL

Automation and Remote Control

Vol. 86, No. 1, January 2025

http://ait.mtas.ru

Automation and Remote Control

ISSN 0005-1179

SCOPE

Automation and Remote Control is one of the first journals on control theory. The scope of the journal is control theory problems and applications. The journal publishes reviews, original articles, and short communications (deterministic, stochastic, adaptive, and robust formulations) and its applications (computer control, components and instruments, process control, social and economy control, etc.).

Automation and Remote Control is abstracted and/or indexed in *ACM Digital Library, BFI List, CLOCKSS, CNKI, CNPIEC Current Contents/Engineering, Computing and Technology, DBLP, Dimensions, EBSCO Academic Search, EBSCO Advanced Placement Source, EBSCO Applied Science & Technology Source, EBSCO Computer Science Index, EBSCO Computers & Applied Sciences Complete, EBSCO Discovery Service, EBSCO Engineering Source, EBSCO STM Source, EI Compendex, Google Scholar, INSPEC, Japanese Science and Technology Agency (JST), Journal Citation Reports/Science Edition, Mathematical Reviews, Naver, OCLC WorldCat Discovery Service, Portico, ProQuest Advanced Technologies & Aerospace Database, ProQuest-ExLibris Primo, ProQuest-ExLibris Summon, SCImago, SCOPUS, Science Citation Index, Science Citation Index Expanded (Sci-Search), TD Net Discovery Service, UGC-CARE List (India), WTI Frankfurt eG, zbMATH.*

Journal website: http://ait.mtas.ru

0005-1179/25. *Automation and Remote Control* (ISSN: 0005-1179 print version, ISSN: 1608-3032 electronic version) is published monthly by Trapeznikov Institute of Control Sciences, Russian Academy of Sciences, 65 Profsoyuznaya street, Moscow 117997, Russia.

Volume 86 (12 issues) is published in 2025.

Publisher: Trapeznikov Institute of Control Sciences, Russian Academy of Sciences.

65 Profsoyuznaya street, Moscow 117997, Russia; e-mail: redacsia@ipu.rssi.ru; http://ait.mtas.ru, http://ait-arc.ru

Contents

Automation and Remote Control

Vol. 86, No. 1, 2025

Linear Systems

Nonlinear Systems

Control in Technical Systems

Intellectual Control Systems, Data Analysis

Optimization, System Analysis, and Operations Research

ISSN 0005-1179 (print), ISSN 1608-3032 (online), Automation and Remote Control, 2025, Vol. 86, No. 1, pp. 1–19.

LINEAR SYSTEMS

Incomplete Measurements-Based Finite Stabilization of Neutral Systems by Controllers with Lumped Commensurate Delays

V. E. Khartovskii[*,a] **and O. I. Urban**[*,b]

[*] *Yanka Kupala State University of Grodno, Grodno, Belarus*
e-mail: [a] *hartovskij@grsu.by,* [b] *urban_ola@mail.ru*

Received July 16, 2024
Revised September 22, 2024
Accepted September 23, 2024

Abstract—This paper considers a linear autonomous differential–difference system of neutral type with lumped delays. For such systems, an output-feedback controller is proposed that simultaneously solves the finite stabilization (complete damping) problem and ensures a finite (albeit, nonarbitrary) spectrum of the closed loop system. For this controller, an existence criterion is derived and a constructive design method is presented. The distinctive feature of the controller is the absence of any distributed delay in the structure, which is important for its practical implementation. The results are illustrated by a numerical example.

Keywords: differential–difference system, neutral type, delay, finite stabilization, controller

DOI: 10.31857/S0005117925010011

1. INTRODUCTION

Systems of differential equations with delay are used to model many processes in ecology, medicine, electrodynamics, deformed solid mechanics, engineering, economics, and other fields [1–3]. On the one hand, considering delay in a model improves reliability in describing real phenomena and predicting the behavior of the corresponding systems. On the other hand, incorporating process characteristics at previous time instants into the evolution law of the system increases its complexity. In this connection, quite a lot of research works have been devoted to the general theory of delayed systems and their applications (for example, see the Introduction in [3]). This paper addresses the issue of the finite stabilization of linear neutral systems with lumped delays in the state and control variables.

Stabilization problems for delayed systems are rather difficult [4–11] and have not been fully investigated to date. One possible approach is based on calculating the unstable eigenvalues of the spectrum and then replacing them with suitable numbers. However, finding such values is a nontrivial task. Therefore, a more universal method is to assign a finite spectrum to a closed loop system [12–15], usually consisting of numbers with negative real parts.

Generally speaking, the set of eigenvalues of a linear system with aftereffect is infinite, so it seems natural to control all eigenvalues of such a system by tuning the coefficients of its characteristic quasipolynomial (the problem of modal control [16–19]). Another line of stabilization-related research consists [14, 20–22] in designing a feedback controller that ensures, after a finite time, zero values for all components of the state vector of the the original open-loop system (the finite stabilization problem [23, 24], in other words, providing the complete 0-controllability by a feedback controller). An original idea for solving the finite stabilization problem is to introduce a feedback loop so that the closed loop system becomes a system with a finite spectrum pointwise degenerate

in the directions corresponding to the solution components of the original system. Such ideas were further developed to systems of neutral type [15, 17, 21, 22]; a systematic presentation of these results can be found in the monograph [25].

In this paper, a finite stabilization output-feedback controller is designed for linear autonomous systems of neutral type with lumped commensurate delays. This is an output-feedback controller based on measurements of an observed signal that ensures both finite stabilization and a finite spectrum. In the case of a delayed system with scalar input and output, such a problem with the choice of any finite spectrum was studied in [24] and, for multi-input neutral systems, in [26]. A disadvantage of the approach described in [26] is the presence of distributed delay terms in the controller, although the original plant has only a lumped delay. During practical implementation, the integrals containing a distributed delay are replaced by finite sums, which may lead to undesirable consequences even when using high-precision quadrature formulas (e.g., the loss of stability) [27, 28]. The fundamental difference between this paper and [26] is the new structure of the controller, which contains purely lumped commensurate delays. The idea is to construct a discontinuous feedback defined by two controller loops (inner and outer). The inner loop "smoothens" the solution over time by using a feedback law that transforms the original system into a delayed one. After the solution reaches the necessary smoothness, the second loop is activated to ensure the pointwise degeneracy of the closed loop system in the directions corresponding to all solution components of the original (open-loop) system.

2. PROBLEM STATEMENT

Let the plant under consideration be described by a linear autonomous differential–difference system of neutral type with lumped commensurate delays:

$$\dot{x}(t) - \sum_{i=1}^{m} D_i \dot{x}(t-ih) = \sum_{i=0}^{m} \Big(A_i x(t-ih) + B_i u(t-ih) \Big), \quad t > 0,$$
$$y(t) = \sum_{i=0}^{m} C_i x(t-ih), \quad t \geqslant 0,$$

where x is the state vector of this system, u is the control input, y is the observed output, and $h = \text{const} > 0$; $D_i \in \mathbb{R}^{n\times n}$, $A_i \in \mathbb{R}^{n\times n}$, $B_i \in \mathbb{R}^{n\times r}$, and $C_i \in \mathbb{R}^{l\times n}$.

We introduce the following notations: $I_i \in \mathbb{R}^{i\times i}$ is an identity matrix, and λ_h is the shift operator defined by the rule $(\lambda_h)^k f(t) = f(t-kh)$, $k \in \mathbb{N}$, for a given value $h > 0$ and an arbitrary function f. With the polynomial matrices

$$D(\lambda) = \sum_{i=1}^{m} D_i \lambda^i, \quad A(\lambda) = \sum_{i=0}^{m} A_i \lambda^i, \quad C(\lambda) = \sum_{i=0}^{m} C_i \lambda^i, \quad B(\lambda) = \sum_{i=0}^{m} B_i \lambda^i,$$

the original plant can be written in the operator form

$$\big(I_n - D(\lambda_h)\big)\dot{x}(t) = A(\lambda_h)x(t) + B(\lambda_h)u(t), \quad t > 0, \tag{1}$$
$$y(t) = C(\lambda_h)x(t), \quad t \geqslant 0. \tag{2}$$

The solution of equation (1) is uniquely determined by the initial condition

$$x(t) = \varphi(t), \quad u(t) \equiv 0, \quad t \in [-mh, 0]. \tag{3}$$

Suppose that $\varphi \in \widetilde{\mathcal{C}}^1([-mh, 0], \mathbb{R}^n)$ is an unknown function, where $\widetilde{\mathcal{C}}^k(\cdot)$ indicates the class of $k-1$ times continuously differentiable functions with a piecewise continuous derivative of order k. The control input u is a piecewise continuous function.

Let $\mathbb{R}^{n\times m}[p,\lambda]$ ($\mathbb{R}^{n\times m}[\lambda]$) be the set of all matrices of dimensions $n\times m$ whose elements represent polynomials of the variables p, $\lambda\,(\lambda)$ (if $m=n=1$, the superscript will be omitted), where $p_{_D}=d/dt$ is the differentiation operator.

We define an output-feedback controller of the form

$$\begin{aligned} u(t) &= U_{11}(p_{_D},\lambda_h)y(t)+U_{12}(p_{_D},\lambda_h)\tilde{x}(t),\\ \dot{\tilde{x}}(t) &= U_{21}(p_{_D},\lambda_h)y(t)+U_{22}(p_{_D},\lambda_h)\tilde{x}(t),\quad t>t_0. \end{aligned} \tag{4}$$

Here, $\tilde{x}\in\mathbb{R}^{\tilde{n}}$ is an auxiliary variable, $t_0>0$ is some number chosen below ($u(t)\equiv 0$, $t\leqslant t_0$), $U_{11}(p,\lambda)\in\mathbb{R}^{r\times l}[p,\lambda]$, $U_{12}(p,\lambda)\in\mathbb{R}^{r\times\tilde{n}}[p,\lambda]$, $U_{21}(p,\lambda)\in\mathbb{R}^{\tilde{n}\times l}[p,\lambda]$, and $U_{22}(p,\lambda)\in\mathbb{R}^{\tilde{n}\times\tilde{n}}[p,\lambda]$. For implementing the controller (4), we specify the initial condition

$$\tilde{x}(t)=\tilde{\varphi}(t),\quad t\in[t_0-\tilde{h},t_0]\quad \Big(\tilde{h}=\tilde{\alpha}h,\quad \tilde{\alpha}=\max\{\deg_\lambda U_{k2}(p,\lambda),\,k=1,2\}\Big), \tag{5}$$

where $\tilde{\varphi}\in\widetilde{\mathcal{C}}^{\tilde{p}}([t_0-\tilde{h},t_0],\mathbb{R}^{\tilde{n}})$ is any function, $\tilde{p}=\max\{\deg_p U_{k2}(p,\lambda),k=1,2\}$, and the notation $\deg_\lambda f(\lambda)$ means the degree of a polynomial (including a matrix one).

The goal of this paper is to design the controller (4) ensuring the following conditions:

(a) Regardless of the initial functions φ in (3) and $\tilde{\varphi}$ in (5), there exists a number $t_1>0$ such that the vector component x of the solution vector $\mathrm{col}[x,\tilde{x}]$ of the closed loop system (1), (4) is zero starting from a time instant t_1, i.e.,

$$x(t)\equiv 0,\quad t\geqslant t_1. \tag{6}$$

(b) The closed loop system (1), (4) is a linear autonomous system of neutral type with a finite spectrum.

Remark 1. (a) By a linear autonomous homogeneous neutral system with commensurate delays we mean a linear autonomous system $\Upsilon(p_{_D},\lambda_h)x(t)=0$, $\Upsilon(p,\lambda)\in\mathbb{R}^{n\times n}[p,\lambda]$ with a characteristic quasipolynomial of the form $|\Upsilon(p,\lambda)|=\sum_{i=0}^{\nu}p^i\tilde{d}_i(\lambda)$, where $\nu=n\deg_p\Upsilon(p,\lambda)$, $\tilde{d}_i(\lambda)$ are polynomials, $\tilde{d}_\nu(0)=1$, and the symbol $|\cdot|$ stands for the determinant of a matrix. By introducing auxiliary variables, such a system can be rewritten as (1). Linear autonomous differential–difference systems with delay ($\tilde{d}_\nu(\lambda)\equiv 1$) and ordinary systems are treated as a special case of neutral systems.

(b) Since $U_{ij}(p,\lambda)$ are polynomial matrices, system (1), (4) has only lumped commensurate delays.

Definition 1. A controller (4) implementing conditions (a) and (b) will be called a finite stabilization output-feedback controller.

Let us denote $W(p,\lambda)=p\big(I_n-D(\lambda)\big)-A(\lambda)$.

Lemma 1. *Assume that for system* (1), (2), *there exists a finite stabilization output-feedback controller* (4). *Then*

$$\operatorname{rank}\big[W(p,e^{-ph}),B(e^{-ph})\big]=n\quad\forall p\in\mathbb{C}, \tag{7}$$

$$\operatorname{rank}\big[I_n-D(\lambda),B(\lambda)\big]=n\quad\forall\lambda\in\mathbb{C}, \tag{8}$$

$$\operatorname{rank}\begin{bmatrix}W(p,e^{-ph})\\ C(e^{-ph})\end{bmatrix}=n\quad\forall p\in\mathbb{C}, \tag{9}$$

$$\operatorname{rank}\begin{bmatrix}I_n-D(\lambda)\\ C(\lambda)\end{bmatrix}=n\quad\forall\lambda\in\mathbb{C}. \tag{10}$$

The proof is postponed to the Appendix.

3. THE MAIN RESULT

Now we formulate the main result of this paper.

Theorem 1. *For system* (1), (2) *there exists a finite stabilization output-feedback controller* (4) *iff conditions* (7)–(10) *are valid.*

Proof. Necessity follows from Lemma 1. **Sufficiency.** The sufficient nature of the conditions of Theorem 1 will be established in two parts. In the first part, we design a controller implementable under the condition that the output $y(t)$ is a $(\rho_0 - 1)$ times continuously differentiable function with a piecewise continuous derivative of order ρ_0, where the number ρ_0 is determined when constructing the controller (see Remark 2). To satisfy the above condition for the function $y(t)$, we suppose that $\varphi \in \widetilde{\mathcal{C}}^{\rho_0}$. The second part of the proof considers the general case $\varphi \in \widetilde{\mathcal{C}}^1$ and $\rho_0 > 1$, i.e., the smoothness of the initial function does not ensure the same property for the output $y(t)$, which is described above.

3.1. The Case $\varphi \in \widetilde{\mathcal{C}}^{\rho_0}$

To prove the sufficiency of the theorem's conditions, we design the controller (4). The design process will consist of the following steps: 1) constructing a finite stabilization state-feedback controller; 2) constructing a finite observer; 3) designing a finite stabilization output-feedback controller based on the parameters of the controller and observer constructed at the previous steps.

1. Constructing a finite stabilization state-feedback controller

Due to (7) and (8), for system (1), there exists [22; 25, p. 358] a controller (further called a finite stabilization state-feedback controller) of the form

$$\begin{aligned} u(t) &= L_{00}(p_{_D}, \lambda_h)x(t) + L_{01}(p_{_D}, \lambda_h)\bar{x}(t), \\ \dot{\bar{x}}(t) &= L_{10}(p_{_D}, \lambda_h)x(t) + L_{11}(p_{_D}, \lambda_h)\bar{x}(t), \quad t > 0, \end{aligned} \tag{11}$$

where $\bar{x} \in \mathbb{R}^{\bar{n}}$ is an auxiliary variable, $L_{00}(p, \lambda) \in \mathbb{R}^{r\times n}[p, \lambda]$, $L_{01}(p, \lambda) \in \mathbb{R}^{r\times \bar{n}}[p, \lambda]$, $L_{10}(p, \lambda) \in \mathbb{R}^{\bar{n}\times n}[p, \lambda]$, $L_{11}(p, \lambda) \in \mathbb{R}^{\bar{n}\times \bar{n}}[p, \lambda]$, and $\deg_p L_{ij}(p, \lambda) = 1$, with the following conditions:

(1) It is possible to find a number $\bar{t}_1 > 0$ such that, regardless of the initial condition of system (1), (11), we have

$$x(t) \equiv 0, \quad t \geqslant \bar{t}_1. \tag{12}$$

(2) System (1), (11) is a linear autonomous neutral system with lumped commensurate delays and a finite (albeit, not a priori given) spectrum. Since the spectrum of the closed loop system is finite, the determinant of the characteristic matrix of this system will be a polynomial, i.e.,

$$\left|W_0(p, \lambda)\right| = d_0(p). \tag{13}$$

Here, $d_0(p)$ is some polynomial and $W_0(p, e^{-ph})$ is the characteristic matrix of system (1), (11) given by

$$W_0(p, \lambda) = \begin{bmatrix} W(p, \lambda) - B(\lambda)L_{00}(p, \lambda) & -B(\lambda)L_{01}(p, \lambda) \\ -L_{10}(p, \lambda) & pI_{\bar{n}} - L_{11}(p, \lambda) \end{bmatrix}. \tag{14}$$

We present the idea of constructing the controller (11) [22; 25, p. 358]. Conditions (7) and (8) are necessary and sufficient for the existence of matrices $L_{ij}(p, \lambda)$ in (11) such that the system corresponding to the matrix (14) is pointwise degenerate in the directions $\bar{e}_i$, $i = \overline{1, n + \bar{n} - 1}$,

where $\bar{e}_i$ is the ith column of the matrix $I_{n+\bar{n}}$. This implies [29] the existence of a time instant $\bar{t}_1$ such that $\bar{e}_i'\mathrm{col}[x(t), \bar{x}(t)] \equiv 0$, $t \geqslant \bar{t}_1$, $i = \overline{1, n+\bar{n}-1}$. (The prime $'$ indicates transpose.) The latter identity ensures (12). The construction procedure for the matrices $L_{ij}(p, \lambda)$ from (11) was described in [22; 25, p. 358].

2. Constructing a finite observer

By a finite observer we mean [30, 31] a linear autonomous delayed differential system dependent on the output (3) with lumped commensurate delays, a finite spectrum, and the output v that has the following property: there exists a time instant $t_* > 0$ starting from which, regardless of the initial conditions of the observer and equation (1), the observer's output v is equal to the solution x of equation (1) generating the output y, i.e., $x(t) = v(t)$, $t \geqslant t_*$.

As was shown in [30, 31], conditions (9) and (10) are necessary and sufficient for the existence of a finite observer. In this case, the observer can be constructed both as a system with distributed delays and any given finite spectrum [30] and as a system without distributed delays with a finite (albeit, not a priori given) spectrum [31]. For the goal of this paper, we will modify one observer from [31].

By condition (10), there are matrices $L_1(\lambda) \in \mathbb{R}^{n\times l}[\lambda]$ and $L_2(\lambda) \in \mathbb{R}^{l\times l}[\lambda]$ such that [17, 22]

$$|I_{n+l} - D_L(\lambda)| \equiv 1, \quad D_L(\lambda) = \begin{bmatrix} D(\lambda) & \lambda L_1(\lambda) \\ C(\lambda) & \lambda L_2(\lambda) \end{bmatrix}. \tag{15}$$

Let $\Pi(\lambda) = [\Pi_{ij}(\lambda)]_{i,j=1}^2$ be the adjoint matrix for the matrix $(I_{n+l} - D_L(\lambda))$, where $\Pi_{11}(\lambda) \in \mathbb{R}^{n\times n}[\lambda]$, $\Pi_{12}(\lambda) \in \mathbb{R}^{n\times l}[\lambda]$, $\Pi_{21}(\lambda) \in \mathbb{R}^{l\times n}[\lambda]$, and $\Pi_{22}(\lambda) \in \mathbb{R}^{l\times l}[\lambda]$. From (15) it follows that $\Pi(\lambda) = \big(I_{n+l} - D_L(\lambda)\big)^{-1}$. We introduce the new function

$$\chi(t) = \big(I_n - D(\lambda_h)\big)x(t), \quad t \geqslant 0. \tag{16}$$

Let $\tilde{\chi}(t)$ $(\tilde{\chi} \in \mathbb{R}^l,\ t \in \mathbb{R})$ be an arbitrary function. Applying the operator $\Pi(\lambda_h)$ to the equality

$$\begin{bmatrix} I_n - D(\lambda_h) & -\lambda_h L_1(\lambda_h) \\ -C(\lambda_h) & I_l - \lambda_h L_2(\lambda_h) \end{bmatrix} \begin{bmatrix} x(t) \\ \tilde{\chi}(t) \end{bmatrix} = \begin{bmatrix} \chi(t) \\ -y(t) \end{bmatrix} + \begin{bmatrix} -\lambda_h L_1(\lambda_h)\tilde{\chi}(t) \\ (I_l - \lambda_h L_2(\lambda_h))\tilde{\chi}(t) \end{bmatrix}, \quad t \geqslant 0,$$

on the left allows establishing the relation

$$x(t) = \Pi_{11}(\lambda_h)\chi(t) - \Pi_{12}(\lambda_h)y(t), \quad t \geqslant \gamma_2 h, \tag{17}$$

where $\gamma_2 = \max\{\nu_{1j},\ j = 1, 2\}$ and $\nu_{ij} = \deg_\lambda \Pi_{ij}(\lambda)$. Next, let us denote

$$\widetilde{A}(\lambda) = A(\lambda)\Pi_{11}(\lambda), \quad \widetilde{C}(\lambda) = \begin{bmatrix} C(\lambda)\Pi_{11}(\lambda) \\ (I_n - D(\lambda))\Pi_{11}(\lambda) - I_n \end{bmatrix},$$

$$\tilde{y}(t) = C_y(\lambda_h)y(t), \ \ t \geqslant \gamma_3 h, \ \ C_y(\lambda) = \begin{bmatrix} I_l + C(\lambda)\Pi_{12}(\lambda) \\ (I_n - D(\lambda))\Pi_{12}(\lambda) \end{bmatrix}, \ \ \gamma_3 = m + \gamma_2.$$

Based on (16) and (17), system (1), (2) can be written as an inhomogeneous linear autonomous differential–difference system with commensurate delays and the known output $\tilde{y}$:

$$\dot{\chi}(t) = \widetilde{A}(\lambda_h)\chi(t) + B(\lambda_h)u(t) - A(\lambda_h)\Pi_{12}(\lambda_h)y(t), \quad t > \gamma_3 h, \tag{18}$$

$$\tilde{y}(t) = \widetilde{C}(\lambda_h)\chi(t), \quad t \geqslant \gamma_3 h. \tag{19}$$

In view of (9), system (18), (19) satisfies the condition [30, 31]

$$\operatorname{rank}\begin{bmatrix} pI_n - \widetilde{A}(e^{-ph}) \\ \widetilde{C}(e^{-ph}) \end{bmatrix} = n \quad \forall p \in \mathbb{C}. \tag{20}$$

From (20) it follows that, for any $i_0 \in \{1, \dots, n+l\}$, there exists a matrix $V_{i_0}(\lambda) \in \mathbb{R}^{n\times(n+l)}[\lambda]$ such that

$$\operatorname{rank}\begin{bmatrix} pI_n - \widetilde{A}(e^{-ph}) - V_{i_0}(e^{-ph})\widetilde{C}(e^{-ph}) \\ \tilde{c}_{i_0}(e^{-ph}) \end{bmatrix} = n \quad \forall p \in \mathbb{C}, \tag{21}$$

where $\tilde{c}_{i_0}(\lambda)$ is the i_0th row of the matrix $\widetilde{C}(\lambda)$ [12]. Letting

$$\widetilde{A}_V(\lambda) = \widetilde{A}(\lambda) + V_{i_0}(\lambda)\widetilde{C}(\lambda), \quad K_0(\lambda) = -A(\lambda)\Pi_{12}(\lambda_h) - V_{i_0}(\lambda)C_y(\lambda) \tag{22}$$

and using equations (18), (19) and formulas (22), we replace system (1), (2) with

$$\begin{gathered} \dot{\chi}(t) = \widetilde{A}_V(\lambda_h)\chi(t) + B(\lambda_h)u(t) + K_0(\lambda_h)y(t), \quad t > \tilde{t}_1, \\ \tilde{y}_{i_0}(t) = \tilde{c}_{i_0}(\lambda_h)\chi(t), \quad t \geqslant \tilde{t}_1, \end{gathered} \tag{23}$$

where $\tilde{y}_{i_0}(t)$ is the i_0th component of the vector $\tilde{y}$, $\tilde{t}_1 = (\nu_0 + \gamma_3)h$, and $\nu_0 = \deg_\lambda V_{i_0}(\lambda)$.

Due to condition (21), for system (23), there exists [31] a finite observer in the form of a finite-spectrum system with purely lumped commensurate delays:

$$\dot{z}(t) = Q(p_{_D}, \lambda_h)z(t) + K(\lambda_h)y(t) + \overline{B}(\lambda_h)u(t), \quad t > \tilde{t}_1; \tag{24}$$

in addition, the output v_z determining the estimate of the solution χ of system (23) is given by

$$v_z(t) = [I_n, 0_{n\times 3}]z(t), \quad t \geqslant \tilde{t}_1. \tag{25}$$

Here, $z = \operatorname{col}[z_1, z_2]$, $z_1 \in \mathbb{R}^n$, $z_2 \in \mathbb{R}^3$, $z_1 = \operatorname{col}[z_{11}, \dots, z_{1n}]$, $z_2 = \operatorname{col}[z_{21}, z_{22}, z_{23}]$, $Q(p, \lambda) \in \mathbb{R}^{(n+3)\times(n+3)}[p, z]$, $0_{n\times m}$ denotes a zero matrix of dimensions $n \times m$,

$$\overline{B}(\lambda) = \begin{bmatrix} B(\lambda) \\ 0_{3\times r} \end{bmatrix}, \tag{26}$$

and the matrix $K(\lambda)$ is found from the equality

$$K(\lambda_h)y(t) = \begin{bmatrix} K_0(\lambda_h) \\ 0_{3\times l} \end{bmatrix} y(t) - e_{n+1}\tilde{y}_{i_0}(t) = \left(\begin{bmatrix} K_0(\lambda_h) \\ 0_{3\times l} \end{bmatrix} - e_{n+1}\,\tilde{e}'_{i_0} C_y(\lambda_h) \right) y(t), \tag{27}$$

where e_i and $\tilde{e}_i$ are the ith columns of the matrices I_{n+3} and I_{n+l}, respectively. The matrix $Q(p, \lambda)$ is obtained by the scheme for constructing the finite observer matrix for a homogeneous delayed system with scalar output [31]. The elements of the matrix $Q(p, \lambda)$ are such that, after introducing auxiliary variables, the homogeneous system (24) can be written in the standard form of a linear autonomous delayed system (i.e., as $\dot{X}(t) = \Sigma(\lambda_h)X(t)$, where $\Sigma(\lambda)$ is a polynomial matrix), and

$$|pI_{n+3} - Q(p, \lambda)| = d_1(p), \tag{28}$$

where $d_1(\lambda)$ is a polynomial. The matrix $Q(p,\lambda)$ has the form

$$Q(p,\lambda)=\left[\begin{array}{ccc|ccc} \tilde a^V_{11}(\lambda) & \dots & \tilde a^V_{1n}(\lambda) & g_{11}(\lambda) & \tilde g_{12} & 0 \\ \dots & \dots & \dots & \dots & \dots & \dots \\ \tilde a^V_{n1}(\lambda) & \dots & \tilde a^V_{nn}(\lambda) & g_{n1}(\lambda) & \tilde g_{n2} & 0 \\ \hline \tilde c^1_{i_0}(\lambda) & \dots & \tilde c^n_{i_0}(\lambda) & g_{n+1\,1}(p,\lambda) & 1 & 0 \\ 0 & \dots & 0 & \lambda g_{n+2\,1}(p,\lambda) & g_{n+2\,2}(p,\lambda) & g_{n+2\,3}(\lambda) \\ 0 & \dots & 0 & \lambda g_{n+3\,1}(\lambda) & g_{n+3\,2}(\lambda) & g_{n+3\,3}(\lambda) \end{array}\right], \tag{29}$$

where $\tilde a^V_{ij}(\lambda)$ are the elements of the matrix $\widetilde A_V(\lambda)$, $\widetilde A_V(\lambda)=\left[\tilde a^V_{ij}(\lambda)\right]_{n\times n}$, $\tilde c^j_{i_0}(\lambda)$ are the elements of the vector $\tilde c_{i_0}(\lambda)$, $\tilde c_{i_0}(\lambda)=[\tilde c^1_{i_0}(\lambda),\dots,\tilde c^n_{i_0}(\lambda)]$, $g_{ij}(p,\lambda)$ and $g_{ij}(\lambda)$ are polynomials of the variables p, λ and λ, respectively, and $\tilde g_{i2}\in\mathbb{R}$.

Remark 2. Let $\rho_0=\max\{\deg_p g_{n+2\,1}(p,\lambda)-\deg_p(g_{n+1\,1}(p,\lambda)-p),1\}$. The component z_{21} depends on the output y; therefore, $z_{21}\in\widetilde{\mathcal{C}}^{\rho_0}([\tilde t_1,+\infty),\mathbb{R})$ is a necessary condition for the term $\lambda_h g_{n+2\,1}(p_{_D},\lambda_h)z_{21}$ to exist in system (24). Hence, we require $\tilde y_{i_0}\in\widetilde{\mathcal{C}}^{\rho_0}([\tilde t_1,+\infty),\mathbb{R})$, which is achieved by $\varphi\in\widetilde{\mathcal{C}}^{\rho_0}([-mh,0],\mathbb{R}^n)$.

The components of the initial function $z(t)$, $t\in[\tilde t_1-h_0,\tilde t_1]$ (h_0 specifies the delay of system (24)), are taken smooth enough with a piecewise continuous senior derivative. (For each component, the order of this derivative is determined by the maximum degree of the variable p of the corresponding polynomials in the matrix (29).) In particular, it is possible to set $z(t)\equiv 0$, $t\in[t_0-h_0,t_0]$.

Now we explain the idea of choosing the elements of the matrix $Q(p,\lambda)$. Let $\zeta=v_z-\chi=z_1-\chi$ denote the estimation error and $\tilde\zeta=\operatorname{col}[\zeta,z_2]$. In view of (29) and (25), the vector function $\tilde\zeta(t)$ is given by the linear autonomous delayed system

$$\dot{\tilde\zeta}(t)=Q(p_{_D},\lambda_h)\tilde\zeta(t),\quad t>\tilde t_1. \tag{30}$$

The elements of the matrix $Q(p,\lambda)$ are chosen so that system (30) is pointwise degenerate in the directions corresponding to the first $(n+2)$ columns of the matrix I_{n+3}, i.e., in the directions e_i, $i=\overline{1,n+2}$. Hence, there exists a time instant $\tilde t_2$ such that $e_i'\tilde\zeta(t)\equiv 0$, $t\geqslant\tilde t_2$, $i=\overline{1,n+2}$, regardless of the initial function defining the solution of system (30). Consequently, the equality

$$\chi(t)=v_z(t),\quad t\geqslant\tilde t_2, \tag{31}$$

holds for any initial functions of systems (1) and (24).

Finally, we estimate the solution of system (1), (2) using formula (17). With

$$v(t)=\Pi_{11}(\lambda_h)[I_n,0_{n\times 3}]z(t)-\Pi_{12}(\lambda_h)y(t),\quad t\geqslant\tilde t_1, \tag{32}$$

from equality (31) and formula (17) it follows that

$$x(t)=v(t),\quad t\geqslant\tilde t_3, \tag{33}$$

where $\tilde t_3=\tilde t_2+\nu_{11}h$. Thus, the finite observer (24), (32) has been constructed.

3. Designing a finite stabilization output-feedback controller

Let us derive expressions for the controller (4). To this end, the control inputs $u(t)$ in equations (24) are replaced using the first formula of (11); the variable x in the resulting equation and

the relations (11) is expressed through z, y using (33) and (32). Next, denoting the variables $\bar{x}$, z by x_1, x_2, respectively, we write the controller

$$u(t) = R_{01}(p_{_D}, \lambda_h)x_1(t) + R_{02}(p_{_D}, \lambda_h)x_2(t) + R_{00}(p_{_D}, \lambda_h)y(t), \tag{34}$$

$$\dot{x}_1(t) = R_{11}(p_{_D}, \lambda_h)x_1(t) + R_{12}(p_{_D}, \lambda_h)x_2(t) + R_{10}(p_{_D}, \lambda_h)y(t), \tag{35}$$

$$\begin{aligned}\dot{x}_2(t) = R_{22}(p_{_D}, \lambda_h)x_2(t) + \overline{B}(\lambda_h)\Big(R_{01}(p_{_D}, \lambda_h)x_1(t)\\ + R_{02}(p_{_D}, \lambda_h)x_2(t) + R_{00}(p_{_D}, \lambda_h)y(t)\Big) + K(\lambda_h)y(t), \quad t > t_0,\end{aligned} \tag{36}$$

where $x_i \in \mathbb{R}^{n_i}$, $i = 1, 2$ $(n_1 = \bar{n}, \quad n_2 = n + 3)$, are auxiliary variables, $t_0 = \alpha_0 h$, $\alpha_0 = \max\{\deg_\lambda R_{00}(p, \lambda) + m, \deg_\lambda R_{10}(p, \lambda), \deg_\lambda K(\lambda)\}$, and

$$\begin{gathered}R_{i0}(p, \lambda) = -L_{i0}(p, \lambda)\Pi_{12}(\lambda), \quad R_{i1}(p, \lambda) = L_{i1}(p, \lambda),\\ R_{i2}(p, \lambda) = L_{i0}(p, \lambda)\Pi_{11}(\lambda)[I_n, 0_{n\times 3}], \quad i = 0, 1, \quad R_{22}(p, \lambda) = Q(p, \lambda).\end{gathered} \tag{37}$$

Letting $\tilde{x} = \mathrm{col}[x_1, x_2]$, $U_{11}(p, \lambda) = R_{00}(p, \lambda)$, $U_{12}(p, \lambda) = \mathrm{col}[R_{01}(p, \lambda), R_{02}(p, \lambda)]$, and

$$U_{21}(p, \lambda) = \begin{bmatrix} R_{10}(p, \lambda) \\ \overline{B}(\lambda)R_{00}(p, \lambda) + K(\lambda)\end{bmatrix},$$

$$U_{22}(p, \lambda) = \begin{bmatrix} R_{11}(p, \lambda) & R_{12}(p, \lambda) \\ \overline{B}(\lambda)R_{01}(p, \lambda) & R_{22}(p, \lambda) + \overline{B}(\lambda)R_{02}(p, \lambda)\end{bmatrix}$$

allows representing the controller (34)–(36) in the form (4).

Let $\hat{e}_i$ be the columns of the identity matrix $I_{n+n_1+n_2}$.

Proposition 1. *System* (1), (2), (34)–(36) *is pointwise degenerate in the directions* $\hat{e}_i$, $i = \overline{1, n + n_1 - 1}$, $i = \overline{n + n_1 + 1, n + n_1 + n_2 - 1}$, *and the set of its spectral values and their multiplicity are determined by the roots of the polynomial* $d_0(\lambda)d_1(\lambda)$.

The proof is provided in the Appendix.

By Proposition 1, the constructed controller (34)–(36) is a finite stabilization output-feedback controller. In the case $\varphi \in \widetilde{\mathcal{C}}^{\rho_0}$, Theorem 1 is proved.

3.2. The Case $\varphi \in \widetilde{\mathcal{C}}^1$

If $\rho_0 = 1$ (see Remark 2), then the controller (34)–(36) is the desired finite stabilization controller and the considerations of Section 3.2 become unnecessary. In what follows, we assume that $\rho_0 > 1$.

The finite stabilization output-feedback controller will be constructed as a variable structure (discontinuous feedback) controller [33] consisting of two serially connected loops: inner $\widehat{u}$ and outer v:

$$u(t) = \begin{cases} 0, & t \leqslant t_5 \\ \widehat{u}(t), & t \in (t_5, t_6] \\ \widehat{u}(t) + v(t), & t > t_6. \end{cases} \tag{38}$$

The inner loop $\widehat{u}$ ensures "smoothing" of the solution of the corresponding closed-loop system (1) over time. Once the solution of the system is $\rho_0 - 1$ times continuously differentiable and has a piecewise continuous derivative of order ρ_0, the outer loop v (34)–(36) is activated to ensure the pointwise degeneracy of the closed loop system.

Remark 3. In general, the loops $\widehat{u}$ and v may contain auxiliary variables as their arguments. Therefore, the full description of the finite stabilization output-feedback controller will be the relation (38) supplemented by differential equations with initial conditions describing the behavior of the auxiliary variables similar to the relations (4) and (5).

Let us impose a condition on the parameters of the homogeneous ($u \equiv 0$) system (1) under which the smoothness of its solution will increase over time. We denote by $\Pi_D(\lambda)$ the adjoint matrix for the matrix $(I_n - D(\lambda))$, $m_0 = \deg_\lambda A(\lambda)\Pi_D(\lambda)$.

Lemma 2. *Assume that the homogeneous* ($u \equiv 0$) *system* (1) *satisfies the condition*

$$\left|I_n - D(\lambda)\right| \equiv 1 \tag{39}$$

and $\varphi \in \widetilde{\mathcal{C}}^1$ *in the initial condition* (3). *Then, for any* $\rho_1 \in \mathbb{N}$ *and the solution* x *of system* (1), *we have* $x \in \widetilde{C}^{\rho_1}\big([t_4 + \rho_1 m_0 h, +\infty), \mathbb{R}^n\big)$, *where* $t_4 = h \deg_\lambda \Pi_D(\lambda)$.

The proof is given in the Appendix.

Remark 4. The identity (39) is equivalent to the fact that the characteristic quasipolynomial of system (1) has the form $\left|W(p,\lambda)\right| = p^n + \sum_{i=0}^{n-1} p^i \hat{d}_i(\lambda)$, where $\hat{d}_i(\lambda)$ are polynomials.

Remark 5. By the proof of Lemma 2 (see the Appendix), under (39), the homogeneous system of neutral type is reduced, through a nondegenerate change of the variables, to a delayed system whose solution will smoothen over time. Let us present other considerations showing that if (39) holds for the homogeneous system of neutral type, the smoothness of the solution will increase with t. For clarity, let $D_1 \neq 0$ and $D_i = 0$, $i = \overline{2,m}$, i.e., system (1) has the form

$$\dot{x}(t) - D_1 \dot{x}(t-h) = A(\lambda_h)x(t), \quad t > 0.$$

Then we obtain the following chain of equalities:

$$\begin{aligned} \dot{x}(t) &= A(\lambda_h)x(t) + D_1\dot{x}(t-h) \\ &= A(\lambda_h)x(t) + D_1\big(A(\lambda_h)x(t-h) + D_1\dot{x}(t-2h)\big) \\ &= \ldots = \sum_{i=0}^{\tilde{m}-1} D_1^i A(\lambda_h)x(t-ih) + D^{\tilde{m}}\dot{x}(t-\tilde{m}h), \quad t > \tilde{m}h, \quad \tilde{m} \in \mathbb{N}. \end{aligned} \tag{40}$$

In this case ($D_1 \neq 0$ and $D_i = 0$, $i = \overline{2,m}$), condition (39) becomes $\left|I_n - \lambda D_1\right| \equiv 1$. This means that the matrix D_1 is nilpotent. Let $\tilde{m}_0$ be the nilpotency index of the matrix D_1, $D_1^{\tilde{m}_0} = 0$. Then from (40) we obtain

$$\dot{x}(t) = \sum_{i=0}^{\tilde{m}_0-1} D_1^i A(\lambda_h)x(t-ih), \quad t > \tilde{m}_0 h. \tag{41}$$

System (41) is a delayed system with $m(\tilde{m}_0 - 1)$ commensurate delays. Therefore, for $t > k\tilde{m}_0 h$, $k = 1, 2, \ldots$, the smoothness of the solution increases by k units.

Similar reasoning is valid for an arbitrary polynomial matrix $\widetilde{D}(\lambda)$. (Condition (39) as necessary and sufficient for the nilpotency of some matrix at the derivatives of the solution containing delays was discussed in [25, p. 218]; see Lemma 4.10.)

Lemma 3. *Under conditions* (8) *and* (10), *there exist matrices* $\widetilde{U}_{11}(\lambda) \in \mathbb{R}^{r\times l}[\lambda]$, $\widetilde{U}_{12}(\lambda) \in \mathbb{R}^{r\times(r+n+l)}[\lambda]$, $\widetilde{U}_{21}(\lambda) \in \mathbb{R}^{(n+r+l)\times n}[\lambda]$, *and* $\widetilde{U}_{22}(\lambda) \in \mathbb{R}^{(r+n+l)\times(r+n+l)}[\lambda]$ *such that*

$$\begin{gathered} \left|I_{2n+r+l} - \widetilde{D}(\lambda)\right| \equiv 1, \\ \widetilde{D}(\lambda) = \begin{bmatrix} D(\lambda) + B(\lambda)\widetilde{U}_{11}(\lambda)C(\lambda) & B(\lambda)\widetilde{U}_{12}(\lambda) \\ \widetilde{U}_{21}(\lambda)C(\lambda) & \widetilde{U}_{22}(\lambda) \end{bmatrix}, \ \widetilde{D}(0) = 0_{(2n+r+l)\times(2n+r+l)}. \end{gathered} \tag{42}$$

The proof is postponed to the Appendix.

We define the inner loop controller by the relations

$$\begin{aligned} \widetilde{u}(t) &= p_{_D}\widetilde{U}_{11}(\lambda_h)y(t) + p_{_D}\widetilde{U}_{12}(\lambda_h)x_3(t) + v_1(t), \\ \dot{x}_3(t) &= p_{_D}\widetilde{U}_{21}(\lambda_h)y(t) + p_{_D}\widetilde{U}_{22}(\lambda_h)x_3(t) + v_2(t), \quad t > t_5, \end{aligned} \tag{43}$$

where $x_3 \in \mathbb{R}^{n+r+l}$ is an auxiliary variable, $v = \operatorname{col}[v_1, v_2]$, the matrices $\widetilde{U}_{ij}(\lambda)$ ensure (42), $t_5 = h\max\{m + \deg_\lambda \widetilde{U}_{11}(\lambda),\, \deg_\lambda \widetilde{U}_{21}(\lambda)\}$. We write system (1), (43):

$$\begin{aligned} (I_{2n+r+l} - \widetilde{D}(\lambda_h)) \begin{bmatrix} \dot{x}(t) \\ \dot{x}_3(t) \end{bmatrix} &= \begin{bmatrix} A(\lambda_h) & 0_{n\times(n+r+l)} \\ 0_{(n+r+l)\times n} & 0_{(n+r+l)\times(n+r+l)} \end{bmatrix} \begin{bmatrix} x(t) \\ x_3(t) \end{bmatrix} \\ &+ \begin{bmatrix} B(\lambda_h) & 0_{n\times(n+r+l)} \\ 0_{(n+r+l)\times r} & I_{n+r+l} \end{bmatrix} v(t), \quad t > t_5. \end{aligned} \tag{44}$$

Due to the condition $\widetilde{D}(0) = 0_{(2n+r+l)\times(2n+r+l)}$, system (44) has neutral type; in view of (42), it also satisfies the condition of Lemma 2.

Let us specify the initial condition $x_3(t) = \varphi_3(t)$, $t \in [t_5 - h_3, t_5]$, where $\varphi_3 \in \mathcal{C}^1([t_5 - h_3, t_5], \mathbb{R}^{n+r+l})$ is any function and $h_3 = h\max\left\{\deg_\lambda \widetilde{W}_{13}(\lambda), \deg_\lambda \widetilde{W}_{23}(\lambda)\right\}$.

For system (44) we add the output signal

$$y_1(t) = \begin{bmatrix} C(\lambda_h) & 0_{l\times(n+r+l)} \\ 0_{(n+r+l)\times n} & I_{n+r+l} \end{bmatrix} \begin{bmatrix} x(t) \\ x_3(t) \end{bmatrix}, \tag{45}$$

where $y_1(t) = \operatorname{col}[y(t), x_3(t)]$. Clearly, system (44), (45) satisfies the conditions of Theorem 1.

Let $v(t) = 0$, $t \leqslant t_6$, in system (44). For $t > t_6$, we construct the loop v according to the scheme of Section 3.1 but for system (44), (45). The number t_6 is appropriately chosen to fulfill the smoothness requirement described in Remark 2.

Remark 6. In several cases, there may exist a polynomial matrix $\widetilde{U}(\lambda)$ such that $\left|I_n - D(\lambda) - \lambda B(\lambda)\widetilde{U}(\lambda)C(\lambda)\right| \equiv 1$. Then, to reduce the size of the matrices of the finite stabilization output-feedback controller, we should take the inner loop controller in the form $\widetilde{u}(t) = p_{_D}\widetilde{U}(\lambda_h)y(t) + v(t)$ instead of (43). In this case, the output (45) is replaced by the output (3), whereas the variable x_3 and the corresponding blocks in (44) disappear (see the example below).

Example 1. We demonstrate the method of constructing a finite stabilization controller of the form (4) (see the proof of Theorem 1) on an example of system (1), (2) with $h = \ln 2$ and the matrices

$$D(\lambda) = \begin{bmatrix} \lambda + \lambda^2 & 0 \\ \lambda^2 & 0 \end{bmatrix},\ A(\lambda) = \begin{bmatrix} 1 - \lambda & 1 \\ 0 & 0 \end{bmatrix},\ B = \begin{bmatrix} 1 \\ 1 \end{bmatrix},\ C(\lambda) = \begin{bmatrix} 1 + \lambda, & 0 \end{bmatrix}. \tag{46}$$

In this case, the conditions of Theorem 1 are valid. In accordance with Remark 6, we find

$$\widetilde{u}(t) = p_{_D}[\lambda_h]y(t) + v(t), \quad t > t_5 = 2h. \tag{47}$$

(Here, $[\lambda_h]$ is a matrix of dimensions 1×1.)

For the case (46), (47), system (44), (45) takes the form

$$\left(I_2 - \begin{bmatrix} 0 & 0 \\ -\lambda_h & 0 \end{bmatrix}\right)\dot{x}(t) = \begin{bmatrix} 1 - \lambda_h & 1 \\ 0 & 0 \end{bmatrix} x(t) + \begin{bmatrix} 1 \\ 1 \end{bmatrix} v(t), \quad y(t) = [1 + \lambda_h, 0]x(t), \quad t > t_5. \tag{48}$$

Interpreting it as system (1), (2), we follow steps 1)–3) of Section 3.1.

1. The controller (11) is constructed as described in [22]:

$$\begin{aligned} v(t) &= \left[-\frac{2}{3}\lambda_h^3+\lambda_h^2+\frac{8}{3}\lambda_h-2,\ -\frac{2}{3}\lambda_h^2+\lambda_h-\frac{4}{3}\right]x(t) \\ &\quad+\left[\lambda_h^3-\frac{7}{2}\lambda_h^2+\frac{7}{2}\lambda_h-1\right]\bar{x}(t), \\ \dot{\bar{x}}(t) &= \left[-\frac{4}{9}\lambda_h^2+\frac{10}{9}\lambda_h+\frac{8}{3},\ \frac{4}{9}\lambda_h+\frac{10}{9}\right]x(t)+\left[\frac{2}{3}\lambda_h^2-3\lambda_h+\frac{7}{3}\right]\bar{x}(t). \end{aligned} \tag{49}$$

Consider system (48) closed with the controller (49). The characteristic matrix $W_0(p,\lambda)$ (see (14)) has the form

$$W_0(p,\lambda)=\begin{bmatrix} p+1+\frac{2}{3}\lambda^3-\lambda^2-\frac{5}{3}\lambda & \frac{2}{3}\lambda^2-\lambda+\frac{1}{3} & -\lambda^3+\frac{7}{2}\lambda^2-\frac{7}{2}\lambda+1 \\ p\lambda+\frac{2}{3}\lambda^3-\lambda^2-\frac{8}{3}\lambda+2 & p+\frac{2}{3}\lambda^2-\lambda+\frac{4}{3} & -\lambda^3+\frac{7}{2}\lambda^2-\frac{7}{2}\lambda+1 \\ \frac{4}{9}\lambda^2-\frac{10}{9}\lambda-\frac{8}{3} & \frac{4}{9}\lambda-\frac{10}{9} & p-\frac{2}{3}\lambda^2+3\lambda-\frac{7}{3} \end{bmatrix}. \tag{50}$$

Direct verification shows that $d_0(p)=p^3-p$. To investigate pointwise degeneracy we can apply, e.g., [29, Theorem 1.1]. Let us briefly illustrate this process. The elements of the first two rows of the matrix adjoint to the matrix $W_0(p,e^{-ph})$ in (50) vanish on the roots of the polynomial $d_0(p)$; therefore, the elements of the first two rows of the matrix $\left(W_0(p,e^{-ph})\right)^{-1}$ are integer functions. This property implies [29] pointwise degeneracy in the directions $[1,0,0]$ and $[0,1,0]$, i.e., condition (12) holds. The maximum degree of the variable λ in these rows does not exceed 5, so $\bar{t}_1=5h$.

2. We construct the finite observer (24), (32). In the case under consideration,

$$D_L(\lambda)=\begin{bmatrix} \lambda & 0 & -\frac{\lambda}{2} \\ 0 & 0 & 0 \\ 1+\lambda & 0 & -\frac{\lambda}{2} \end{bmatrix},\quad \Pi(\lambda)=\begin{bmatrix} \frac{\lambda}{2}+1 & 0 & -\frac{\lambda}{2} \\ 0 & 1 & 0 \\ 1+\lambda & 0 & 1-\lambda \end{bmatrix},$$

$$\widetilde{C}(\lambda)=\begin{bmatrix} \frac{\lambda^2}{2}+\frac{3}{2}\lambda+1 & 0 \\ -\frac{\lambda^2}{2}-\frac{\lambda}{2} & 0 \\ 0 & 0 \end{bmatrix},\quad C_y(\lambda)=\begin{bmatrix} -\frac{\lambda^2}{2}+\frac{\lambda}{2}+1 \\ \frac{\lambda^2}{2}-\frac{\lambda}{2} \\ 0 \end{bmatrix},$$

$$V_2(\lambda)=\begin{bmatrix} 0 & -1 & 0 \\ 0 & 0 & 0 \end{bmatrix},\ (i_0=2).$$

System (23) takes the form

$$\dot{\chi}(t)=\begin{bmatrix} 1 & 1 \\ 0 & 0 \end{bmatrix}\chi(t)+\begin{bmatrix} 1 \\ 1 \end{bmatrix}u(t),\quad \tilde{y}_2(t)=\left[-\frac{\lambda_h^2}{2}-\frac{\lambda_h}{2},\ 0\right]\chi(t). \tag{51}$$

Using (51), we finally arrive at the relations (24), (32):

$$\dot z(t) = Q(p_D, \lambda_h) z(t) + \begin{bmatrix} 0 \\ 0 \\ -\frac{\lambda_h^2}{2} + \frac{\lambda_h}{2} \\ 0 \\ 0 \end{bmatrix} y(t) + \begin{bmatrix} 1 \\ 1 \\ 0 \\ 0 \\ 0 \end{bmatrix} u(t),$$

$$x(t) = \begin{bmatrix} \frac{\lambda_h}{2} + 1 & 0 \\ 0 & 1 \end{bmatrix} z_1(t) + \begin{bmatrix} \frac{\lambda_h}{2} \\ 0 \end{bmatrix} y(t).$$

Here are the elements of the matrix $Q(p, \lambda)$ located in blocks nos. (1,2) and (2,2):

$$g_{11}(\lambda) = 0, \quad g_{21}(\lambda) = 0, \quad g_{31}(p, \lambda) = -1,$$

$$\begin{aligned} g_{41}(p,\lambda) = {} & \frac{428\,259\,827\,248}{370\,825\,875} + \frac{13\,308\,418}{37\,975}p + \frac{3\,263\,970\,139}{410\,130}p\lambda^2 - \frac{64\,061\,677\,864\,590\,419}{683\,506\,252\,800}\lambda^7 \\ & - \frac{4\,504\,350\,207\,517}{370\,825\,875}\lambda + \frac{10\,314\,197}{36\,325\,800}\lambda^{14} + \frac{109\,094\,554\,247\,916\,287}{683\,506\,252\,800}\lambda^6 \\ & - \frac{17\,328\,104\,121\,953\,0591}{854\,382\,816\,000}\lambda^5 - \frac{5\,199\,361\,041\,200\,909}{379\,725\,696\,000}\lambda^9 + \frac{47\,137\,018\,631\,639\,513}{1\,139\,177\,088\,000}\lambda^8 \\ & + \frac{1\,145\,930\,623\,773\,433}{341\,753\,126\,400}\lambda^{10} - \frac{3631}{605\,430}\lambda^{15} - \frac{21\,985\,862\,341}{3\,645\,600}p\lambda^5 + \frac{460\,650\,668\,593}{43\,747\,200}p\lambda^4 \\ & - \frac{154\,784\,798\,249}{13\,124\,160}p\lambda^3 + \frac{255\,035\,489\,398}{4\,944\,345}\lambda^2 + \frac{3\,925\,747\,081}{1\,749\,888}p\lambda^6 - \frac{90\,876\,950\,917}{15\,256\,836\,000}\lambda^{13} \\ & - \frac{1\,159\,012\,171}{2\,187\,360}p\lambda^7 - \frac{1\,743\,623\,839\,315\,721}{14\,239\,713\,600}\lambda^3 + \frac{30\,878}{315}p^2 + \frac{222\,361}{2520}p^2\lambda^4 \\ & - \frac{433\,453}{1008}p^2\lambda^3 + \frac{819\,967}{1008}p^2\lambda^2 - \frac{718\,133}{1260}p^2\lambda - \frac{3\,824\,219\,437}{1\,367\,100}p\lambda - \frac{3631}{630}p^2\lambda^5 \\ & + \frac{160\,864\,251\,357\,763\,979}{854\,382\,816\,000}\lambda^4 - \frac{101\,487\,682\,282\,697}{170\,876\,563\,200}\lambda^{11} - \frac{3\,412\,403}{585\,900}p\lambda^9 + \frac{3631}{19\,530}p\lambda^{10} \\ & + \frac{2\,474\,356\,747}{32\,810\,400}p\lambda^8 + \frac{4\,478\,040\,783\,667}{61\,027\,344\,000}\lambda^{12}, \end{aligned}$$

$$\begin{aligned} g_{51}(\lambda) = {} & - \frac{7\,991\,397\,801\,907\,001}{3\,218\,768\,595\,000}\lambda + \frac{430\,769\,061\,660\,938\,381}{51\,500\,297\,520\,000}\lambda^4 - \frac{90\,522\,930\,353\,255\,419}{794\,576\,018\,880\,000}\lambda^9 \\ & + \frac{7\,882\,042\,993\,003\,211}{397\,288\,009\,440\,000}\lambda^{10} + \frac{38\,819\,644\,979\,750\,780\,339}{11\,124\,064\,264\,320\,000}\lambda^6 \\ & + \frac{5\,294\,886\,380\,912\,311\,157}{11\,124\,064\,264\,320\,000}\lambda^8 - \frac{16\,491\,589\,988\,451\,048\,767}{11\,124\,064\,264\,320\,000}\lambda^7 \\ & - \frac{2\,550\,527\,148\,568\,185\,769}{309\,001\,785\,120\,000}\lambda^3 - \frac{68\,686\,980\,782\,797}{28\,377\,714\,960\,000}\lambda^{11} \\ & + \frac{440\,289\,519\,864\,500\,737}{77\,250\,446\,280\,000}\lambda^2 - \frac{7\,699\,195\,015\,471\,454\,567}{1\,236\,007\,140\,480\,000}\lambda^5 + \frac{3631}{18\,768\,330}\lambda^{14} \\ & - \frac{384\,159}{41\,707\,400}\lambda^{13} + \frac{30\,684\,351\,847}{157\,653\,972\,000}\lambda^{12} + \frac{23\,072\,498\,192\,986}{44\,705\,119\,375}, \end{aligned}$$

$$\tilde g_{12}=0,\quad \tilde g_{22}=2,$$

$$\begin{aligned}g_{42}(p,\lambda)=&-\frac{22\,963\,886}{1\,177\,225}-\frac{6049}{1085}p-p^2-\frac{237\,550\,583}{1\,367\,100}\lambda-\frac{113\,747}{1260}p\lambda+\frac{1\,277\,029\,067}{607\,600}\lambda^2\\&+\frac{1\,419\,991}{2520}p\lambda^2-\frac{1\,644\,438\,853}{234\,360}\lambda^3-\frac{817\,177}{1008}p\lambda^3+\frac{92\,476\,221\,137}{8\,202\,600}\lambda^4+\frac{2\,164\,661}{5040}p\lambda^4\\&-\frac{14\,100\,715\,427\,003}{1\,356\,163\,200}\lambda^5-\frac{6\,890\,671}{78\,120}p\lambda^5+\frac{131\,464\,618\,651}{21\,873\,600}\lambda^6+\frac{3631}{630}p\lambda^6\\&-\frac{3\,920\,013\,073}{1\,749\,888}\lambda^7+\frac{1\,930\,062\,779}{3\,645\,600}\lambda^8-\frac{2\,473\,263\,067}{32\,810\,400}\lambda^9+\frac{105\,765\,593}{18\,162\,900}\lambda^{10}-\frac{3631}{19\,530}\lambda^{11},\end{aligned}$$

$$\begin{aligned}g_{52}(\lambda)=&-\frac{36\,874\,722\,147}{5\,109\,156\,500}-\frac{2\,362\,315\,264\,557}{20\,436\,626\,000}\lambda+\frac{20\,884\,081\,349\,269}{61\,309\,878\,000}\lambda^2\\&-\frac{538\,059\,413\,076\,769}{1\,103\,577\,804\,000}\lambda^3+\frac{1\,793\,665\,758\,154\,211}{4\,414\,311\,216\,000}\lambda^4\\&-\frac{1\,445\,125\,981\,988\,557}{6\,621\,466\,824\,000}\lambda^5+\frac{1\,026\,288\,639\,816\,701}{13\,242\,933\,648\,000}\lambda^6\\&-\frac{8\,405\,817\,164\,119}{472\,961\,916\,000}\lambda^7+\frac{1\,174\,407\,170\,347}{472\,961\,916\,000}\lambda^8-\frac{106\,666\,081}{563\,049\,900}\lambda^9\\&+\frac{3631}{605\,430}\lambda^{10},\end{aligned}$$

$$g_{43}(\lambda)=-\frac{63}{4}\lambda^5+\frac{651}{8}\lambda^4-\frac{1395}{8}\lambda^3+\frac{651}{4}\lambda^2-63\lambda+\lambda^6+8,$$

$$g_{53}(\lambda)=-\frac{1}{31}\lambda^5+\frac{31}{60}\lambda^4-\frac{155}{56}\lambda^3+\frac{155}{24}\lambda^2-\frac{31}{4}\lambda+\frac{3879}{1085}.$$

(The form of the other elements is obvious.)

In this case, $d_1(p)=(p-2)(p-1)p(p+1)(p+2)(p+3)$ (see (28)). By [29, Theorem 1.1], the first 4 components of system (30) are degenerate.

3. Now we write the matrices of the finite stabilization controller (34)–(36) for system (48):

$$R_{00}(p,\lambda)=\Big[-\frac{1}{3}\lambda^4+\frac{1}{2}\lambda^3+\frac{4}{3}\lambda^2-\lambda\Big],\quad R_{01}(p,\lambda)=\Big[\lambda^3-\frac{7}{2}\lambda^2+\frac{7}{2}\lambda-1\Big],$$

$$R_{02}(p,\lambda)=\Big[-\frac{1}{3}\lambda^4-\frac{1}{6}\lambda^3+\frac{7}{3}\lambda^2+\frac{5}{3}\lambda-2,-\frac{2}{3}\lambda^2+\lambda-\frac{4}{3},0,0,0\Big],$$

$$R_{10}(p,\lambda)=\Big[-\frac{2}{9}\lambda^3+\frac{5}{9}\lambda^2+\frac{4}{3}\lambda\Big],\quad R_{11}(p,\lambda)=\Big[\frac{2}{3}\lambda^2-3\lambda+\frac{7}{3}\Big],$$

$$R_{12}(p,\lambda)=\Big[-\frac{2}{9}\lambda^3+\frac{1}{9}\lambda^2+\frac{22}{9}\lambda+\frac{8}{3},-\frac{4}{9}\lambda+\frac{10}{9},0,0,0\Big],$$

$$R_{22}(p,\lambda)=Q(p,\lambda),\quad K(\lambda)=\operatorname{col}\Big[0,0,\frac{1}{2}\lambda^2-\frac{1}{2}\lambda,0,0\Big].$$

We compose the characteristic matrix $W_1(p,\lambda)$ of the closed loop system (48), (34)–(36) (see the proof of Proposition 1). Direct verification shows that $\big|W_1(p,\lambda)\big|=d_1(p)d_0(p)$. By [29, Theorem 1.1], components nos. 1, 2, 4–7 of system (48), (34)–(36) become degenerate in time $16h$. (Here, 16 is the maximum degree of the variable λ of the polynomials representing the elements of the matrices of the controller (4).) Step 3) is completed. In this case, $\rho_0=2$; letting $\rho_1=2$ and $t_4=4h$ in Lemma 2, we observe that it is possible to take $t_6=t_5+t_4+4h=10h$ since $m_0=2$ (see Lemma 2). Finally, the finite stabilization output-feedback controller is given by formula (38), and $t_1=t_6+16h=26h$ can be set in the identity (6).

4. CONCLUSIONS

In this paper, we have derived an existence criterion for a finite stabilization output-feedback controller as well as have proposed its design method. Conditions (7) and (8) represent [25, p. 206; 32] a complete 0-controllability criterion for system (1), (2) (a complete damping/calming criterion for this system). Conditions (9) and (10) are [25, p. 204; 32] represent a final observability criterion for system (1), (2) (i.e., the existence of a single-valued continuous operator for reconstructing the state of system (1) by the past output (2)). Thus, a finite stabilization output-feedback controller exists iff system (1), (2) is both completely 0-controllable and finally observable. The design procedure of a finite stabilization output-feedback controller is based on the methods for constructing controllers and observers [22, 25, 31], which involve algebraic operations implemented in most modern computer mathematics systems. Therefore, it is possible to automate the computational procedures proposed above when developing automatic control systems.

FUNDING

This work was supported by the State Scientific Research Program "Convergence–2025."

APPENDIX

Proof of Lemma 1. If for any initial function φ in (3) there exists a control input u (a programmed or feedback law) ensuring (6), then system (1) is completely 0-controllable. Hence [32], conditions (7) and (8) are necessary. Let us establish the necessity of condition (9). Supposing the existence of a finite stabilization output-feedback controller of the form (4), we assume on the contrary that condition (9) is violated for some $p_0 \in \mathbb{C}$. Choosing a vector $g_0 \in \mathbb{C}^n$ as the solution of the algebraic system $W(p_0, e^{-p_0 h})g_0 = 0$, $C(e^{-p_0 h})g_0 = 0$, we define the function $x_{p_0}(t) = \mathbf{Re}\big(g_0 e^{p_0 t}\big)$, $t \geqslant -mh$, if it is nonzero and $x_{p_0}(t) = \mathbf{Im}\big(g_0 e^{p_0 t}\big)$, $t \geqslant -mh$, otherwise.

The controller (4) ensures the identity (6) regardless of the initial conditions (3) and (5). We set $\varphi(t) = x_{p_0}(t)$, $t \in [-mh, 0]$, and $\tilde{\varphi}(t) = 0$, $t \in [t_0 - \tilde{h}, t_0]$, in (3) and (5), respectively. The characteristic matrix of system (1), (4) is given by

$$W_1(p,\lambda) = \begin{bmatrix} W(p,\lambda) - B(\lambda)U_{11}(p,\lambda)C(\lambda) & -B(\lambda)U_{12}(p,\lambda) \\ -U_{21}(p,\lambda)C(\lambda) & pI_{\tilde{n}} - U_{22}(p,\lambda) \end{bmatrix}, \tag{A.1}$$

where $e^{-ph} = \lambda$. From (A.1) it follows that the function $\mathrm{col}[x_{p_0}(t),\, 0]$, $t > t_0$, is a nonzero solution of the closed loop system (1), (4). This obviously contradicts (6).

Now we show the necessity of condition (10). By the definition of a finite stabilization output-feedback controller, the spectrum of the system is finite, $|W_1(p,\lambda)| = w(p)$, where $w(p)$ is a polynomial. Consider the auxiliary system

$$\big(I_n - \Phi_0(\lambda_h)\big)\dot{\xi}(t) = \Phi(\lambda_h)\xi(t) + \Psi(\lambda_h)\bar{u}(t), \quad t > 0, \tag{A.2}$$

where $\Phi_0(\lambda) = \big(D(\lambda)\big)'$, $\Phi(\lambda) = \big(A(\lambda)\big)'$, $\Psi(\lambda) = \big(C(\lambda)\big)'$, and $\bar{u}$ is a piecewise continuous control input. The initial conditions for system (A.2) are chosen similarly to those of (3).

For system (A.2) we define the controller

$$\begin{aligned} \bar{u}(t) &= H_{11}(p_{_D}, \lambda_h)\xi(t) + H_{12}(p_{_D}, \lambda_h)\tilde{x}(t), \\ \dot{\tilde{x}}(t) &= H_{21}(p_{_D}, \lambda_h)\xi(t) + H_{22}(p_{_D}, \lambda_h)\tilde{x}(t), \end{aligned} \tag{A.3}$$

where $H_{i1}(p,\lambda) = \big(B(\lambda)U_{1i}(p,\lambda)\big)'$ and $H_{i2}(p,\lambda) = \big(U_{2i}(p,\lambda)\big)'$, $i = 1, 2$. Let $W_\xi(p,\lambda)$ denote the characteristic matrix of system (A.2), (A.3). It is easy to see that $W_\xi(p,\lambda) = \big(W_1(p,\lambda)\big)'$, so

$|W_\xi(p, e^{-ph})| = w(p)$. Thus, there exists a feedback law for system (A.2) such that the closed loop system has a finite (but not a priori given) spectrum, i.e., it is spectrally reducible. Therefore [15], the condition $\operatorname{rank}[I_n - \Phi_0(\lambda),\ \Psi(\lambda)] = n\ \forall \lambda \in \mathbb{C}$ holds, which is equivalent to (10). The proof of Lemma 1 is complete.

Proof of Statement 1. The characteristic matrix $W_1(p, e^{-ph})$ of system (1), (2), (34)–(36) is given by

$$W_1(p,\lambda) = \begin{bmatrix} W(p,\lambda) - B(\lambda)R_{00}(p,\lambda)C(\lambda) & -B(\lambda)R_{01}(p,\lambda) & -B(\lambda)R_{02}(p,\lambda) \\ -R_{10}(p,\lambda)C(\lambda) & pI_{n_1} - R_{11}(p,\lambda) & -R_{12}(p,\lambda) \\ -(K(\lambda)+\overline{B}(\lambda)R_{00}(p,\lambda))C(\lambda) & -\overline{B}(\lambda)R_{01}(p,\lambda) & pI_{n_2} - R_{22}(p,\lambda) - \overline{B}(\lambda)R_{02}(p,\lambda) \end{bmatrix}, \quad \text{(A.4)}$$

where $\lambda = e^{-ph}$.

We represent the variable x_2 in the relations (34)–(36) as a vector with two vector components: $x_2 = \operatorname{col}[x_{21}, x_{22}]$, where $x_{21} \in \mathbb{R}^n$ and $x_{22} \in \mathbb{R}^3$. Also, we partition the matrices $R_{i2}(p,\lambda)$, $i = \overline{1,2}$, and $K(\lambda)$ in (37) into blocks corresponding to the components x_{21} and x_{22} and write them in an expanded form:

$$\begin{gathered} R_{02}(p,\lambda) = [L_{00}(p,\lambda)\Pi_{11}(\lambda), 0_{r\times 3}],\ R_{12}(p,\lambda) = [L_{10}(p,\lambda)\Pi_{11}(\lambda), 0_{n_1\times 3}], \\ R_{22}(p,\lambda) = \begin{bmatrix} A(\lambda)\Pi_{11}(\lambda) + V_{i_0}(\lambda)\widetilde{C}(\lambda) & Q_{12}(p,\lambda) \\ Q_{21}(p,\lambda) & Q_{22}(p,\lambda) \end{bmatrix},\ K(\lambda) = \begin{bmatrix} K_0(\lambda) \\ -K_1(\lambda) \end{bmatrix}. \end{gathered} \quad \text{(A.5)}$$

Here, the blocks $Q_{12}(p,\lambda) \in \mathbb{R}^{n\times 3}[\lambda]$, $Q_{21}(p,\lambda) \in \mathbb{R}^{3\times n}[\lambda]$, and $Q_{22}(p,\lambda) \in \mathbb{R}^{3\times 3}[\lambda]$ correspond to the block partition of the matrix $Q(p,\lambda)$ in (29) (the first upper block of the matrix (29) is the matrix $A_V(\lambda)$ described by (22)), and $K_1(\lambda) = \operatorname{col}[1,0,0]\tilde{e}'_{i_0}C_y(\lambda)$ (27).

Remark 7. Below it will be necessary to write the matrices partitioned into blocks. To fit them on the page width, thus making the considerations more visual, we will occasionally omit arguments in the notation of matrix blocks. For example, entries like B and $L_{00}\Pi_{11}$ will indicate $B(\lambda)$ and $L_{00}(p,\lambda)\Pi_{11}(\lambda)$, respectively.

Using the block partition (A.5) and the definitions of the matrices $K_0(\lambda)$ (22) and $\overline{B}(\lambda)$ (26), we write the matrix (A.4) as

$$W_1(p,\lambda) = \begin{bmatrix} W + BL_{00}\Pi_{12}C & -BL_{01} & -BL_{00}\Pi_{11} & 0_{n\times 3} \\ L_{10}\Pi_{12}C & pI_{n_1} - L_{11} & -L_{10}\Pi_{11} & 0_{n_1\times 3} \\ BL_{00}\Pi_{12}C + (A\Pi_{12} + V_{i_0}C_y)C & -BL_{01} & pI_n - A\Pi_{11} - V_{i_0}\widetilde{C} - BL_{00}\Pi_{11} & -Q_{12} \\ K_1C & 0_{3\times n_1} & -Q_{21} & pI_3 - Q_{22} \end{bmatrix}. \quad \text{(A.6)}$$

In system (1), (2), (34)–(36), let us introduce a new variable ε as follows:

$$x_{21}(t) = (I_n - D(\lambda_h))x(t) + \varepsilon(t), \quad t \geqslant t_0. \quad \text{(A.7)}$$

The change of variables (A.7) can be defined by the formulas

$$\begin{bmatrix} x(t) \\ x_1(t), \\ x_{21}(t) \\ x_{22}(t) \end{bmatrix} = \Omega(\lambda_h) \begin{bmatrix} x(t) \\ x_1(t), \\ \varepsilon(t) \\ x_{22}(t) \end{bmatrix}, \quad \Omega(\lambda) = \begin{bmatrix} I_n & 0_{n\times n_1} & 0_{n\times n} & 0_{n\times 3} \\ 0_{n_1\times n} & I_{n_1} & 0_{n_1\times n} & 0_{n_1\times 3} \\ I_n - D(\lambda) & 0_{n\times n_1} & I_n & 0_{n\times 3} \\ 0_{3\times n} & 0_{3\times n_1} & 0_{3\times n} & I_3 \end{bmatrix}, \quad |\Omega(\lambda)| \equiv 1.$$

Due to these formulas, the matrix $W_1(p,\lambda)\Omega(\lambda)$ will be the characteristic matrix obtained after the system replacement, and $|W_1(p,\lambda)| = |W_1(p,\lambda)\Omega(\lambda)|$.

Further transformations of the matrix $W_1(p,\lambda)\Omega(\lambda)$ require some relations. Note preliminarily that the definition of the matrices $\Pi_{ij}(\lambda)$ implies

$$\Pi_{11}(\lambda)\big(I_n - D(\lambda)\big) - \Pi_{12}(\lambda)C(\lambda) = I_n. \tag{A.8}$$

Next, in the matrix (A.6), we add block no. (3,3) multiplied on the right by the matrix $\big(I_n - D(\lambda)\big)$ to block no. (3,1). Using formula (A.8), we have the following chain of equalities:

$$\begin{aligned}
&B(\lambda)L_{00}(p,\lambda)\Pi_{12}(\lambda)C(\lambda) + \big(A(\lambda)\Pi_{12}(\lambda) + V_{i_0}(\lambda)C_y(\lambda)\big)C(\lambda)\\
&+\Big(pI_n - A(\lambda)\Pi_{11}(\lambda) - V_{i_0}(\lambda)\widetilde{C}(\lambda) - B(\lambda)L_{00}(p,\lambda)\Pi_{11}(\lambda)\Big)\big(I_n - D(\lambda)\big)\\
&= B(\lambda)L_{00}(p,\lambda)\Pi_{12}(\lambda)C(\lambda) + A(\lambda)\Pi_{12}(\lambda)C(\lambda)\\
&+V_{i_0}(\lambda)\begin{bmatrix}\big(I_l + C(\lambda)\Pi_{12}(\lambda)\big)C(\lambda)\\ \big(I_n - D(\lambda)\big)\Pi_{12}(\lambda)C(\lambda)\end{bmatrix} + p\big(I_n - D(\lambda)\big)\\
&-A(\lambda)\Pi_{11}(\lambda)\big(I_n - D(\lambda)\big) - V_{i_0}(\lambda)\begin{bmatrix}C(\lambda)\Pi_{11}(\lambda)\big(I_n - D(\lambda)\big)\\ \Big(\big(I_n - D(\lambda)\big)\Pi_{11}(\lambda) - I_n\Big)\big(I_n - D(\lambda)\big)\end{bmatrix}\\
&-B(\lambda)L_{00}(p,\lambda)\Pi_{11}(\lambda)\big(I_n - D(\lambda)\big) = -B(\lambda)L_{00}(p,\lambda) + p\big(I_n - D(\lambda)\big) - A(\lambda)\\
&+V_{i_0}(\lambda)\begin{bmatrix}C(\lambda) + C(\lambda)\Big(\Pi_{12}(\lambda)C(\lambda) - \Pi_{11}(\lambda)\big(I_n - D(\lambda)\big)\Big)\\ \big(I_n - D(\lambda)\big)\Big(\Pi_{12}(\lambda)C(\lambda) - \Pi_{11}(\lambda)\big(I_n - D(\lambda)\big)\Big) + \big(I_n - D(\lambda)\big)\end{bmatrix}\\
&= W(p,\lambda) - B(\lambda)L_{00}(p,\lambda).
\end{aligned} \tag{A.9}$$

Then, in the matrix (A.6), we add the first row of block no. (4,3) multiplied on the right by the matrix $\big(I_n - D(\lambda)\big)$ to the first row of block no. (4,1). (Note that the remaining two lower rows of the above blocks are zero, which follows from (29) and the form of the matrix $K_1(\lambda)$.) Using the intermediate reasoning in the chain of equalities (A.9), we arrive at the relation

$$\begin{aligned}
&[1,0,0]K_1(\lambda)C(\lambda) - [1,0,0]Q_{21}(p,\lambda)\big(I_n - D(\lambda)\big)\\
&= \tilde{e}'_{i_0}\left(\begin{bmatrix}\big(I_l + C(\lambda)\Pi_{12}(\lambda)\big)C(\lambda)\\ \big(I_n - D(\lambda)\big)\Pi_{12}(\lambda)C(\lambda)\end{bmatrix} - \begin{bmatrix}C(\lambda)\Pi_{11}(\lambda)\big(I_n - D(\lambda)\big)\\ \Big(\big(I_n - D(\lambda)\big)\Pi_{11}(\lambda) - I_n\Big)\big(I_n - D(\lambda)\big)\end{bmatrix}\right) = 0.
\end{aligned} \tag{A.10}$$

Due to formula (A.8) and the relations (A.9) and (A.10),

$$W_1(p,\lambda)\Omega(\lambda) = \begin{bmatrix}W - BL_{00} & -BL_{01} & -BL_{00}\Pi_{11} & 0_{n\times 3}\\ -L_{10} & pI_{n_1} - L_{11} & -L_{10}\Pi_{11} & 0_{n_1\times 3}\\ W - BL_{00} & -BL_{01} & pI_n - A\Pi_{11} - V_{i_0}\widetilde{C} - BL_{00}\Pi_{11} & -Q_{12}\\ 0_{3\times n} & 0_{3\times n_1} & -Q_{21} & pI_3 - Q_{22}\end{bmatrix}.$$

In the matrix $W_1(p,\lambda)\Omega(\lambda)$, we multiply the first row of blocks by (-1) and add it to the third row, replacing the third row of blocks with the result. Let Ω_1 denote the matrix of this transformation. Obviously, $|\Omega_1| = 1$ and

$$\begin{aligned}
\Omega_1 W_1(p,\lambda)\Omega(\lambda) &= \begin{bmatrix}W - BL_{00} & -BL_{01} & -BL_{00}\Pi_{11} & 0_{n\times 3}\\ -L_{10} & pI_{n_1} - L_{11} & -L_{10}\Pi_{11} & 0_{n_1\times 3}\\ 0_{n\times n} & 0_{n\times n_1} & pI_n - A\Pi_{11} - V_{i_0}\widetilde{C} & -Q_{12}\\ 0_{3\times n} & 0_{3\times n_1} & -Q_{21} & pI_3 - Q_{22}\end{bmatrix}\\
&= \begin{bmatrix}W_0(p,\lambda) & \widetilde{W}(p,\lambda)\\ 0_{(n+1)\times(n+n_1)} & pI_{n+3} - Q(p,\lambda)\end{bmatrix},
\end{aligned} \tag{A.11}$$

where the block $\widetilde{W}(p,\lambda)$ is defined straightforwardly. The structure of the matrix (A.11) shows that the function $\operatorname{col}[\varepsilon, x_{22}]$ is defined by a system with the characteristic matrix $I_{n+3} - Q(p,\lambda)$ (i.e., by system (30), which is pointwise degenerate). Therefore, $e_i'\operatorname{col}[\varepsilon(t), x_{22}(t)] \equiv 0$, $t \geqslant t_0 + \tilde{t}_2$, $i = \overline{1, n+2}$. So, for $t \geqslant \bar{t}_4$, we have $\bar{t}_4 = t_0 + \tilde{t}_2 + \gamma_5 h$, where γ_5 is the maximum degree of the variable λ in the block $\widetilde{W}(p,\lambda)$, and the function $\operatorname{col}[x, x_1]$ is defined by a homogeneous system with the characteristic matrix (14), which is also pointwise degenerate. Hence, for $t_1 = \bar{t}_1 + \bar{t}_4$, where $\bar{t}_1$ is given by (12), the identities $\bar{e}_i'\operatorname{col}[x(t), x_1(t)] \equiv 0$, $t \geqslant t_1$, hold. In combination with (A.7), this result implies the pointwise degeneracy of system (1), (2), (34)–(36).

Due to the form of the matrix $\Omega_1 W_1(p,\lambda)\Omega(\lambda)$ in (A.11) and equalities (28) and (13), the eigenvalues of system (1), (2), (34)–(36) are determined by the roots of the polynomial $d_1(\lambda)d_0(\lambda)$. The proof of Proposition 1 is complete.

Proof of Lemma 2. Let us introduce the new variable $X(t) = \big(I_n - D(\lambda_h)\big)x(t)$, $t \geqslant 0$, in system (1). Then $x(t) = \Pi_D(\lambda_h)X(t)$, $t \geqslant h \deg_\lambda \Pi_D(\lambda)$, and the function $X(t)$ is defined by the delayed system

$$\dot{X}(t) = A(\lambda_h)\Pi_D(\lambda_h)X(t), \quad t > hm_0. \tag{A.12}$$

As is known, the smoothness of the solution of the delayed system (A.12) increases by one when increasing the time variable by the value $m_0 h$. Therefore, for the given number ρ_1 and $t \geqslant m_0 h + (\rho_1 - 1)m_0 h = \rho_1 m_0 h$, the function $X(t)$ is such that $X \in \widetilde{C}^{\rho_1}\big([\rho_1 m_0 h, +\infty), \mathbb{R}^n\big)$, and the desired conclusion follows. The proof of this lemma is complete.

Proof of Lemma 3. By condition (10), there exist [15; 25, p. 228] polynomial matrices $M_{ij}(\lambda)$ and $K_{ij}(\lambda)$ of appropriate dimensions such that

$$\begin{gathered}\begin{vmatrix} I_n - D(\lambda) - \lambda B(\lambda)M_{11}(\lambda) & -\lambda B(\lambda)M_{12}(\lambda) \\ -\lambda M_{21}(\lambda) & I_r - \lambda M_{22}(\lambda) \end{vmatrix} \equiv 1, \\ \begin{vmatrix} I_n - D(\lambda) - \lambda K_{11}(\lambda)C(\lambda) & -\lambda K_{12}(\lambda) \\ -\lambda K_{21}(\lambda)C(\lambda) & I_l - \lambda K_{22}(\lambda) \end{vmatrix} \equiv 1. \end{gathered} \tag{A.13}$$

We define the matrices

$$\widetilde{U}_{11}(\lambda) = 0_{r\times n}, \quad \widetilde{U}_{12}(\lambda) = \begin{bmatrix} \lambda M_{12}(\lambda), & \lambda M_{11}(\lambda), & 0_{n\times l} \end{bmatrix},$$

$$\widetilde{U}_{21}(\lambda) = \begin{bmatrix} 0_{(r\times n)} \\ -\lambda K_{11}(\lambda) \\ -\lambda K_{21}(\lambda) \end{bmatrix},$$

$$\widetilde{U}_{22}(\lambda) = \begin{bmatrix} \lambda M_{22}(\lambda) & \lambda M_{21}(\lambda) & 0_{r\times l} \\ \lambda B(\lambda)M_{12}(\lambda) & D(\lambda) + \lambda K_{11}(\lambda)C(\lambda) + \lambda B(\lambda)M_{11}(\lambda) & \lambda K_{12}(\lambda) \\ 0_{l\times r} & \lambda K_{21}(\lambda)C(\lambda) & \lambda K_{22}(\lambda) \end{bmatrix}.$$

Note that $\widetilde{U}_{ij}(0)$ are zero matrices. Let us denote

$$\Gamma(\lambda) = E\big(I_{2n+r+l} - \widetilde{D}(\lambda)\big)E^{-1}, \quad \text{where} \quad E = \begin{bmatrix} I_n & 0_{n\times r} & 0_{n\times n} & 0_{n\times l} \\ 0_{r\times n} & I_r & 0_{r\times n} & 0_{r\times l} \\ -I_n & 0_{n\times r} & I_n & 0_{n\times l} \\ 0_{l\times n} & 0_{l\times r} & 0_{l\times n} & I_l \end{bmatrix}.$$

Direct verification shows that

$$\Gamma(\lambda)=\begin{bmatrix} I_n-D(\lambda)-\lambda B(\lambda)M_{11}(\lambda) & -\lambda B(\lambda)M_{12}(\lambda) & -\lambda B(\lambda)M_{11}(\lambda) & 0_{n\times l} \\ -\lambda M_{21}(\lambda) & I_r-\lambda M_{22}(\lambda) & -\lambda M_{21}(\lambda) & 0_{r\times l} \\ 0_{n\times n} & 0_{n\times r} & I_n-D(\lambda)-\lambda K_{11}(\lambda)C(\lambda) & -\lambda K_{12}(\lambda) \\ 0_{l\times n} & 0_{l\times r} & -\lambda K_{21}(\lambda)C(\lambda) & I_l-\lambda K_{22}(\lambda) \end{bmatrix}.$$

In view of the identities (A.13), we conclude that $\big|\Gamma(\lambda)\big|\equiv 1$, and the relation (42) is immediate. The proof of this lemma is complete.

REFERENCES

1. Dolgii, Yu.F. and Surkov, P.G., *Matematicheskie modeli dinamicheskikh sistem s zapazdyvaniem* (Mathematical Models of Dynamic Systems with Delay), Yekaterinburg: Ural University, 2012. https://rucont.ru/efd/209395 (Accessed July 15, 2024.)
2. Glagolev, M.V., Sabrekov, A.F., and Goncharov, V.M., Delay Differential Equations as a Tool for Mathematical Modelling of Population Dynamic, *Environmental Dynamics and Global Climate Change*, 2018, vol. 9, no. 2, pp. 40–63. https://doi.org/10.17816/edgcc10483
3. Poloskov, I.E., *Metody analiza sistem s zapazdyvaniem* (Analysis Methods for Systems with Delay), Perm: Perm State National Research University, 2020. http://www.psu.ru/files/docs/science/books/mono/poloskov-metody-analiza-sistem.pdf
4. Krasovskii, N.N. and Osipov, Yu.S., On the Stabilization of Motions of a Plant with Delay in the Control System, *Izv. Akad. Nauk SSSR. Tekh. Kibern.*, 1963, no. 6, pp. 3–15.
5. Osipov, Yu.S., On the Stabilization of Controlled Systems with Delay, *Differ. Uravn.*, 1965, vol. 1, no. 5, pp. 606–618.
6. Pandolfi, L., Stabilization of Neutral Functional-Differential Equations, *J. Optim. Theory Appl.*, 1976, vol. 20, no. 2, pp. 191–204. https://doi.org/10.1007/BF01767451
7. Lu, W.S., Lee, E., and Zak, S., On the Stabilization of Linear Neutral Delay-Difference Systems, *IEEE Transact. Autom. Control.*, 1986, vol. 31, no. 1, pp. 65–67. https://doi.org/10.1109/TAC.1986.1104115
8. Rabah, R., Sklyar, G.M., and Rezounenko, A.V., On Pole Assignment and Stabilizability of Neutral Type Systems, in *Topics in Time-Delay Systems. Lecture Notes in Control and Inf. Sci.*, Berlin: Springer, 2009, vol. 388, pp. 85–93. https://doi.org/10.1007/978-3-642-02897-7_8
9. Dolgii, Yu.F. and Sesekin, A.N., Regularization Analysis of a Degenerate Problem of Impulsive Stabilization for a System with Time Delay, *Tr. Inst. Mat. Mekh. UrO RAN*, 2022, vol. 28, no. 1, pp. 74–95. https://doi.org/10.21538/0134-4889-2022-28-1-74-95
10. Hu, G.D. and Hu, R., A Frequency-Domain Method for Stabilization of Linear Neutral Delay Systems, *Syst. Control Lett.*, 2023, vol. 181, art. no. 105650. https://doi.org/10.1016/j.sysconle.2023.105650
11. Minyaev, S.I. and Fursov, A.S., Topological Approach to the Simultaneous Stabilization of Plants with Delay, *Diff. Equat.*, 2013, vol. 49, no. 11, pp. 1423–1431. https://doi.org/10.1134/S0012266113110098
12. Watanabe, K., Finite Spectrum Assignment and Observer for Multivariable Systems with Commensurate Delays, *IEEE Trans. Autom. Control*, 1986, vol. AC–31, no. 6, pp. 543–550. https://doi.org/10.1109/TAC.1986.1104336
13. Wang, Q.G., Lee, T.H., and Tan, K.K., *Finite Spectrum Assignment Controllers for Time Delay Systems*, Springer-Verlag, 1999. https://doi.org/10.1007/978-1-84628-531-8
14. Metel'skii, A.V., Spectral Reduction, Complete Damping, and Stabilization of a Delay System by a Single Controller, *Diff. Equat.*, 2013, vol. 49, no. 11, pp. 1405–1422. https://doi.org/10.1134/S0012266113110086
15. Khartovskii, V.E., Spectral Reduction of Linear Systems of the Neutral Type, *Diff. Equat.*, 2017, vol. 53, no. 3, pp. 366–381. https://doi.org/10.1134/S0012266117030089
16. Marchenko, V.M., Control of Systems with Aftereffect in Scales of Linear Controllers with Respect to the Type of Feedback, *Diff. Equat.*, 2011, vol. 47, no. 7, pp. 1014–1028. https://doi.org/10.1134/S0012266111070111

17. Metel'skii, A.V. and Khartovskii, V.E., Criteria for Modal Controllability of Linear Systems of Neutral Type, *Diff. Equat.*, 2016, vol. 52, no. 11, pp. 1453–1468. https://doi.org/10.1134/S0012266116110070
18. Khartovskii, V.E., Modal Controllability for Systems of Neutral Type in Classes of Differential-Difference Controllers, *Autom. Remote Control*, 2017, vol. 78, no. 11, pp. 1941–1954. https://doi.org/10.1134/S0005117917110017
19. Zaitsev, V. and Kim, I., Arbitrary Coefficient Assignment by Static Output Feedback for Linear Differential Equations with Non-Commensurate Lumped and Distributed Delays, *Mathematics*, 2021, no. 9, art. no. 2158. https://doi.org/10.3390/math9172158
20. Karpuk, V.V. and Metel'skii, A.V., Complete Calming and Stabilization of Linear Autonomous Systems with Delay, *J. Comput. Syst. Sci. Int.*, 2009, vol. 48, no. 6, pp. 863–872. https://doi.org/10.1134/S1064230709060033
21. Metel'skii, A.V., Urban, O.I., and Khartovskii, V.E., Damping of a Solution of Linear Autonomous Difference-Differential Systems with Many Delays Using Feedback, *J. Comput. Syst. Sci. Int.*, 2015, vol. 54, no. 2, pp. 202–211. https://doi.org/10.1134/S1064230715020100
22. Metel'skii, A.V., Khartovskii, V.E., and Urban, O.I., Solution Damping Controllers for Linear Systems of the Neutral Type, *Diff. Equat.*, 2016, vol. 52, no. 3, pp. 386–399. https://doi.org/10.1134/S0012266116030125
23. Fomichev, V.V., Sufficient Conditions for the Stabilization of Linear Dynamical Systems, *Diff. Equat.*, 2015, vol. 51, no. 11, pp. 1512–1517. https://doi.org/10.1134/S0012266115110129
24. Metel'skii, A.V., Complete and Finite-Time Stabilization of a Delay Differential System by Incomplete Output Feedback, *Diff. Equat.*, 2019, vol. 55, no. 12, pp. 1611–1629. https://doi.org/10.1134/S0012266119120085
25. Khartovskii, V.E., *Upravlenie lineinymi sistemami neitral'nogo tipa: kachestvennyi analiz i realizatsiya obratnykh svyazei* (Control of Linear Systems of Neutral Type: Qualitative Analysis and Feedback Implementation), Grodno: Grodno State University, 2022.
26. Khartovskii, V.E., Finite Stabilization and Finite Spectrum Assignment by a Single Controller Based on Incomplete Measurements for Linear Systems of the Neutral Type, *Diff. Equat.*, 2024, vol. 60, no. 5, pp. 655–676. https://doi.org/10.1134/S0012266124050094
27. Kharitonov, V.L., Prediction Based Control: Implementation Issue, *Differential Equations and Control Processes*, 2015, no. 4, pp. 51–65. URL: http://diffjournal.spbu.ru/pdf/kharitonov2.pdf
28. Mondie, S. and Mihiels, W., Finite Spectrum Assignment of Unstable Time-Delay Systems with a Safe Implementation, *IEEE Transact. Autom. Control*, 2003, vol. 48, no. 12, pp. 2207–2212. https://doi.org/10.1109/TAC.2003.820147
29. Kappel, F., Degenerate Difference-Differential Equations. Algebraic Theory, *Diff. Equat.*, 1977, vol. 24, no. 1, pp. 99–126.
30. Metel'skii, A.V. and Khartovskii, V.E., Finite Observer Design for Linear Systems of Neutral Type, *Autom. Remote Control*, 2019, vol. 80, no. 12, pp. 2152–2169. https://doi.org/10.1134/S0005117919120051
31. Metel'skii, A.V. and Khartovskii, V.E., Exact Reconstruction of the Solution for Linear Neutral Type Systems, *Diff. Equat.*, 2021, vol. 57, no. 2, pp. 251–271. https://doi.org/10.1134/S0012266121020130
32. Khartovskii, V.E. and Pavlovskaya, A.T., Complete Controllability and Controllability for Linear Autonomous Systems of Neutral Type, *Autom. Remote Control*, 2013, vol. 74, no. 5, pp. 769–784. https://doi.org/10.1134/S0005117913050032
33. Emel'yanov, S.V., Fomichev, V.V., and Fursov, A.S., Simultaneous Stabilization of Linear Dynamic Plants by the Variable-Structure Controller, *Autom. Remote Control*, 2012, vol. 73, no. 7, pp. 1126–1133. https://doi.org/10.1134/S0005117912070028

This paper was recommended for publication by S.A. Krasnova, a member of the Editorial Board

ISSN 0005-1179 (print), ISSN 1608-3032 (online), Automation and Remote Control, 2025, Vol. 86, No. 1, pp. 20–33.

NONLINEAR SYSTEMS

Lurie Equations and Equivalent Hamiltonian Systems

M. G. Yumagulov[*,a] **and L. S. Ibragimova**[*,b]

[*] *Ufa University of Science and Technology, Ufa, Russia*
e-mail: [a] *yum_mg@mail.ru,* [b] *lilibr@mail.ru*

Received April 5, 2024
Revised November 25, 2024
Accepted December 3, 2024

Abstract—This paper proposes new approaches to constructing equivalent Hamiltonian systems for linear and nonlinear Lurie equations (differential equations containing the derivatives of even orders only). The approaches are based on the transition from the linear part of the Lurie equation to the normal forms of the corresponding Hamiltonian systems, with a subsequent transformation of the resulting system. This scheme does not require complex and cumbersome transformations of the original equation. The effectiveness of the formulas derived is illustrated by examples.

Keywords: Lurie equation, Hamiltonian system, normal form, equivalence, observability.

DOI: 10.31857/S0005117925010022

1. INTRODUCTION

Consider the differential equation

$$L\left(\frac{d}{dt}\right)y = M\left(\frac{d}{dt}\right)f(y), \tag{1}$$

where

$$L(p) = p^{2n} + a_1 p^{2n-2} + a_2 p^{2n-4} + \ldots + a_{n-1}p^2 + a_n,$$
$$M(p) = b_0 p^{2m} + b_1 p^{2m-2} + \ldots + b_{m-1}p^2 + b_m,$$

are coprime polynomials ($0 \leqslant m < n$) and $f(y)$ is a scalar continuous function. Equation (1) describes the dynamics of a single-loop control system consisting of a linear link with the fractional-rational transfer function $W(p) = M(p)/L(p)$ and a nonlinear feedback with the characteristic $f(y)$; for example, see [1, 2]. Note that equations of the form (1) are often called *Lurie equations*.

The polynomials $L(p)$ and $M(p)$ contain degrees of even orders only. Differential equations of even orders arise in many problems of control theory, the theory of Hamiltonian systems, the theory of integrable equations, spectral theory, etc. In studies of such equations, an important direction is the problem of introducing a Hamiltonian structure to them. The availability of such a structure (as a consequence, the existence of first integrals and various types of symmetries) allows advancing significantly in the analysis of systems dynamics. The issues regarding the existence of a Hamiltonian structure for many types of differential equations and, accordingly, the construction of an equivalent Hamiltonian system for equations (1) in various problem statements were discussed in several research works, e.g., [2–9]. The problem statements below are close to those considered in [10, 11].

In this paper, we present new approaches to studying the above issues. The approaches are based on the transition from the linear part of the Lurie equation to the normal forms of the

corresponding Hamiltonian systems, with a subsequent transformation of the linear and nonlinear systems. The results obtained lead to effective algorithms for constructing the Hamiltonian of the system. The results can be applied to analyze the dynamics of systems described by differential equations of even orders as well as the stability and bifurcations of equilibria and periodic solutions of linear and nonlinear Lurie equations.

2. BACKGROUND

We recall some concepts of systems theory, control theory [1, 2, 7, 8], and the theory of Hamiltonian systems [3, 4].

2.1. The Equivalence of Systems

Let $\mathcal{A}$ and $\mathcal{B}$ be two systems described by the input-output-state equations. Assume that these systems have the same space $\mathcal{U}$ of inputs $u(t)$ and the same space $\mathcal{Y}$ of outputs $y(t)$. We denote by $\mathcal{S}$ and $\mathcal{T}$ the state spaces of systems $\mathcal{A}$ and $\mathcal{B}$, respectively.

Systems $\mathcal{A}$ and $\mathcal{B}$ are said to be *equivalent* if, for each state $\alpha \in \mathcal{S}$, there exists a state $\beta \in \mathcal{T}$ such that the outputs of systems $\mathcal{A}$ and $\mathcal{B}$ will coincide for the same inputs $u(t) \in \mathcal{U}$ and vice versa. In this case, we will write $\mathcal{A} \sim \mathcal{B}$.

2.2. On the Observability of Systems

Consider a dynamic system described by the equation

$$x' = Ax + \xi u(t), \quad y = (x(t), c), \tag{2}$$

where A is a square matrix of order n; ξ, $c \in R^n$ are fixed vectors; the symbol (x, c) indicates the inner product of vectors x and c from R^n. In this system, u, y, and x denote the input, output, and state, respectively.

Throughout this paper, vectors will be treated as column vectors unless they are explicitly stated to represent row vectors in a particular formula.

We define a square matrix of order n:

$$D = \begin{bmatrix} c \\ A^*c \\ (A^*)^2c \\ \vdots \\ (A^*)^{n-1}c \end{bmatrix}, \tag{3}$$

where A^* means the transpose of A and the vectors c, A^*c, $(A^*)^2c$, $\ldots$, $(A^*)^{n-1}c$ are row vectors. The matrix D is called the *observability matrix* of system (A.3). System (A.3) is said to be *observable* if $\det D \neq 0$.

2.3. On Hamiltonian Systems

An *autonomous Hamiltonian system* is a dynamic system described by the equation

$$x' = J\nabla H(x), \quad x \in R^{2n}, \tag{4}$$

where

$$J = \begin{bmatrix} 0 & I \\ -I & 0 \end{bmatrix}, \qquad \nabla H(x) = \left(\frac{\partial H}{\partial x_1}, \ldots, \frac{\partial H}{\partial x_{2n}}\right)^T, \tag{5}$$

0 and I stand for zero and identity matrices, respectively, of order n, and $H(x)$ is a scalar real smooth called the *Hamiltonian* of system (4).

A *linear autonomous Hamiltonian system* (LAHS) is a system of the form

$$\frac{dx}{dt} = JAx, \quad x \in R^{2n}, \tag{6}$$

where A is a real square symmetric matrix of order $2n$. The Hamiltonian of this system is given by

$$H(x) = \frac{1}{2}(Ax, x). \tag{7}$$

Below, the matrix JA participating in system (6) will be called the *Hamiltonian matrix*. Note its properties as follows:

G1) If the matrix JA has an eigenvalue λ, then the numbers $-\lambda$, $\overline{\lambda}$, and $-\overline{\lambda}$ are also eigenvalues of this matrix, with the same algebraic and geometric multiplicity and the same index.

G2) If the matrix JA has the eigenvalue $\lambda = 0$, then the algebraic multiplicity of this eigenvalue is an even number.

G3) The characteristic polynomial of the matrix JA contains degrees of even orders only.

Each Hamiltonian matrix belongs to one and only one equivalence class of symplectically similar matrices. In each such class, one representative, called the *normal form*, is often distinguished. The kind of the normal form is determined by the properties of the root subspaces of the matrix JA. We refer to [3, 9, 12, 13] for more details on the theory of normal forms and, in particular, the lists of normal forms.

A specific feature of normal forms is that different normal forms may correspond to a given set of eigenvalues with given multiplicities. As an illustration, consider fourth-order Hamiltonian matrices having two pairs of prime pure imaginary eigenvalues $\pm\omega_1 i$ and $\pm\omega_2 i$, where $\omega_1 > 0$ and $\omega_2 > 0$. In this case, there are two kinds of normal forms:

$$JA = \begin{bmatrix} 0 & 0 & \omega_1 & 0 \\ 0 & 0 & 0 & \sigma\omega_2 \\ -\omega_1 & 0 & 0 & 0 \\ 0 & -\sigma\omega_2 & 0 & 0 \end{bmatrix}, \quad \text{where} \quad \sigma = 1 \ \text{ or } \ \sigma = -1. \tag{8}$$

In the case $\sigma = 1$, the numbers $\omega_1 i$ and $\omega_2 i$ are called the *eigenvalues of the first kind*; in the case $\sigma = -1$, they are called the *eigenvalues of the first and second kind*, respectively. No symplectic transformations can reduce the normal form with $\sigma = 1$ to the normal form with $\sigma = -1$.

The above properties of Hamiltonian matrices determine many important qualitative characteristics of Hamiltonian systems (linear and nonlinear), such as strong stability properties, stability in the linear and nonlinear formulation, etc.; for example, see [9–15].

As will be shown below, due to this fact, the problem of constructing an equivalent Hamiltonian system for equation (1) may have qualitatively different solutions, namely, the resulting Hamiltonian systems (6) may have different normal forms.

3. THE LINEAR PROBLEM

3.1. The Standard Change of Variables

We discuss the problem of constructing an equivalent Hamiltonian system first for the linear equation

$$L\left(\frac{d}{dt}\right) y = 0. \tag{9}$$

With the standard change of variables

$$z_1 = y,\ z_2 = y',\ \ldots,\ z_{2n} = y^{(2n-1)}, \tag{10}$$

this equation is reduced to an equivalent system in the state space:

$$z' = A_0 z, \quad y = (z, c_0), \tag{11}$$

where z, c_0, $\gamma \in R^{2n}$, the symbol (z, c_0) indicates the inner product of vectors, and

$$A_0 = \begin{bmatrix} 0 & 1 & 0 & 0 & \ldots & 0 & 0 \\ 0 & 0 & 1 & 0 & \ldots & 0 & 0 \\ & & & & \ddots & & \\ 0 & 0 & 0 & 0 & \ldots & 0 & 1 \\ -a_n & 0 & -a_{n-1} & 0 & \ldots & -a_1 & 0 \end{bmatrix}, \quad c_0 = \begin{bmatrix} 1 \\ 0 \\ \vdots \\ 0 \\ 0 \end{bmatrix}. \tag{12}$$

System (11) is Hamiltonian only for $n = 1$, i.e., when equation (9) takes the simplest form $y'' + a_1 y = 0$. If $n \geqslant 2$, system (11) is no longer Hamiltonian. From this point onwards, we assume that $n \geqslant 2$.

3.2. Constructing the Hamiltonian System

Since the polynomial $L(p)$ contains degrees of even orders only, the roots of the equation $L(p) = 0$ have properties similar to properties G1 and G2 of Hamiltonian matrices. Therefore, the polynomial $L(p)$ with this set of roots can be assigned one or more normal forms with the same set of eigenvalues.

We propose the following construction scheme of an equivalent Hamiltonian system for equation (9).

At the first stage, the roots of the equation $L(p) = 0$ are used to determine possible normal forms of the desired Hamiltonian system. One of the corresponding Hamiltonian matrices JA is chosen.

The second stage is to define a nonzero vector $c \in R^{2n}$ and the Hamiltonian system

$$\frac{dx}{dt} = JAx, \quad y = (x(t), c). \tag{13}$$

Theorem 1. *Equation* (9) *and the Hamiltonian system* (13) *are equivalent iff system* (13) *is observable.*

This theorem can be supplemented by the following result. Let $\tilde{y} = \begin{bmatrix} y \\ y' \\ \vdots \\ y^{(2n-1)} \end{bmatrix}$, where $y^{(k)}$ denotes the kth-order derivative of the scalar function $y = y(t)$.

Theorem 2. *Assume that one of the possible normal forms of JA is chosen according to the properties of the roots of the equation $L(p) = 0$. Assume also that the vector c is appropriately chosen to make system* (13) *observable. Then the change of variables $x = D^{-1}\tilde{y}$, where D is the observability matrix of system* (13)*, reduces equation* (9) *to the equivalent Hamiltonian system* (13) *with the Hamiltonian* (7)*. In addition, the matrices A_0 and JA are related by the equality $A_0 = D(JA)D^{-1}$.*

The proofs of Theorems 1 and 2 and other main results are postponed to the Appendix.

Remark 1. According to Theorems 1 and 2, for equation (9), the problem of constructing an equivalent Hamiltonian system in normal form may have a nonunique solution. In other words, equation (9) can be reduced, via linear nondegenerate transformations, to qualitatively different Hamiltonian systems of the form (13) in the sense that the corresponding Hamiltonian matrices belong to different equivalence classes of symplectically similar matrices.

Note also that for equation (9), the problem of constructing an equivalent Hamiltonian system with a particular normal form may be unsolvable. This situation arises, e.g., when the equation $L(p) = 0$ has multiple roots. In this case, equation (9) may lead to such normal forms of Hamiltonian matrices for which the corresponding system is unobservable for any vector c.

3.3. A Linear Link with Two Degrees of Freedom

As an illustration, consider the fourth-order Lurie equation

$$y'''' + ay'' + by = 0, \tag{14}$$

where the real coefficients a and b satisfy the conditions

$$a > 0, \;\; b > 0, \;\; d = a^2 - 4b > 0. \tag{15}$$

In this case, all the four roots of the characteristic equation

$$\lambda^4 + a\lambda^2 + b = 0$$

are different and pure imaginary of the form $\pm i\omega_1$, $\pm i\omega_2$, where the numbers $\omega_1 > 0$ and $\omega_2 > 0$ satisfy the equation $\omega^4 - a\omega^2 + b = 0$, i.e.,

$$\omega_1^2 = \frac{a + \sqrt{d}}{2}, \quad \omega_2^2 = \frac{a - \sqrt{d}}{2}. \tag{16}$$

Now we discuss the construction of an equivalent Hamiltonian system for equation (14).

Let us utilize the above scheme. In the problem under consideration, equation (14) can be reduced to two different normal forms of the desired Hamiltonian system, namely, the matrix (8) for $\sigma = 1$ and $\sigma = -1$. With an appropriate choice of the vector $c \in R^4$, it is possible to obtain two qualitatively different LAHSs (13) with the normal form (8) of the matrix JA that are equivalent to equation (14) both for $\sigma = 1$ and for $\sigma = -1$.

To show this fact, let $c = (c_1, c_2, 0, 0)$ be some vector such that $c_1 c_2 \neq 0$. Then equation (14) can be reduced to the Hamiltonian system (13) via a linear nondegenerate transformation.

Indeed, to apply Theorem 1, we should establish the observability of system (13) with the normal form (8) of the matrix JA. We have

$$(JA)^* c = \begin{bmatrix} 0 \\ 0 \\ \omega_1 c_1 \\ \sigma\omega_2 c_2 \end{bmatrix}, \;\; (JA^*)^2 c = \begin{bmatrix} -\omega_1^2 c_1 \\ -\sigma\omega_2^2 c_2 \\ 0 \\ 0 \end{bmatrix}, \;\; (JA^*)^3 c = \begin{bmatrix} 0 \\ 0 \\ -\omega_1^3 c_1 \\ -\sigma\omega_2^3 c_2 \end{bmatrix}. \tag{17}$$

Hence, the matrix (3) takes the form

$$D(c) = \begin{bmatrix} c_1 & c_2 & 0 & 0 \\ 0 & 0 & \omega_1 c_1 & \sigma\omega_2 c_2 \\ -\omega_1^2 c_1 & -\sigma\omega_2^2 c_2 & 0 & 0 \\ 0 & 0 & -\omega_1^3 c_1 & -\sigma\omega_2^3 c_2 \end{bmatrix}, \tag{18}$$

and

$$\det D(c) = \begin{cases} -c_1^2 c_2^2 \omega_1 \omega_2 (\omega_1^2 - \omega_2^2)^2 & \text{if } \sigma = 1 \\ c_1^2 c_2^2 \omega_1 \omega_2 (\omega_1^4 - \omega_2^4) & \text{if } \sigma = -1. \end{cases}$$

This means that $\det D(c) \neq 0$ for $c_1 c_2 \neq 0$ and $\omega_1 \neq \omega_2$. Thus, the matrix $D(c)$ is nonsingular (reversible), and system (13) is observable accordingly. By Theorem 1, equation (14) and system (13) are equivalent. By Theorem 2, the change of variables $\tilde{y} = D(c)x$, where $\tilde{y} = \begin{bmatrix} y \\ y' \\ y'' \\ y''' \end{bmatrix}$, reduces system (13) to the scalar differential equation (14). The solutions $y(t)$ and $x(t)$ of equation (14) and system (13) are related by the equality $y(t) = c_1 x_1(t) + c_2 x_2(t)$.

Thus, an equivalent Hamiltonian system for the linear equation (14) has been constructed. Once again, we underline that equation (14) can be reduced to two different Hamiltonian representations (13) with the normal forms (8). Additional information about the object under study is required for a particular choice of the normal form.

EXAMPLE 1

The planar bounded circular three-body problem is one of the most interesting problems in celestial mechanics; for example, see [13, 16–18]. In the linear statement, the problem of investigating the motion of a small-mass body in the neighborhood of triangular libration points leads to the differential equation

$$y'''' + y'' + \frac{27}{4}\mu(1-\mu)y = 0. \tag{19}$$

Its characteristic equation has the form

$$\lambda^4 + \lambda^2 + \frac{27}{4}\mu(1-\mu) = 0. \tag{20}$$

Following the above scheme, we pass from equation (19) to an equivalent LAHS of the form (13). Let $\mu \in (0, \mu^*) \bigcup (1-\mu^*, 1)$, where $\mu^* = \frac{1}{2} - \frac{\sqrt{69}}{18} \approx 0.0385$. In this case, all the four roots of equation (20) are pure imaginary: $\lambda_{1,2} = \pm\omega_1(\mu)i$, $\lambda_{3,4} = \pm\omega_2(\mu)i$; here

$$\omega_1(\mu) = \sqrt{\frac{1}{2} - \frac{1}{2}\sqrt{1 - 27\mu(1-\mu)}}, \quad \omega_2(\mu) = \sqrt{\frac{1}{2} + \frac{1}{2}\sqrt{1 - 27\mu(1-\mu)}}.$$

Hence, there are two kinds of the normal forms (8). For a particular kind determined from certain considerations, we choose, e.g., the vector $c = (1, 1, 0, 0, 0)$. Using (17) and (18), we construct the matrix $D = D(c)$, which turns out to be nonsingular. Consequently, with the change of variables $\tilde{y} = D(c)x$, equation (19) can be reduced to an equivalent Hamiltonian system of the form (13), and their solutions $y(t)$ and $x(t)$ are related by the equality $y(t) = x_1(t) + x_2(t)$.

Note that according to the analysis of the original three-body problem statement [13], one should take $\sigma = -1$ in the normal form (8).

4. THE NONLINEAR PROBLEM

4.1. Main Results

Now we discuss the problem of constructing an equivalent Hamiltonian system for the nonlinear Lurie equation (1).

As in the linear problem, the first stage is to determine possible normal forms of the linear part of the desired Hamiltonian system using the roots of the equation $L(p) = 0$. And one of the corresponding Hamiltonian matrices JA is chosen.

At the second stage, it is necessary to define a nonzero vector $c \in R^{2n}$ and the linear Hamiltonian system (13). Assume that this system is observable. Let $D = D(c)$ be the corresponding observability matrix.

We define the vectors

$$\gamma = \begin{bmatrix} 0 \\ \gamma_2 \\ 0 \\ \gamma_4 \\ \vdots \\ 0 \\ \gamma_{2n} \end{bmatrix}, \quad \tilde{y} = \begin{bmatrix} y \\ y' \\ \vdots \\ y^{(2n-1)} \end{bmatrix}, \quad \tilde{f}(y) = \begin{bmatrix} f(y) \\ (f(y))' \\ (f(y))'' \\ \vdots \\ (f(y))^{(2n-3)} \end{bmatrix}, \tag{21}$$

where the t-derivatives $y^{(k)}$ and $(f(y))^{(k)}$ of given functions $y = y(t)$ and $f(y(t))$, respectively; the coordinates of the vector γ are given by

$$\begin{gathered} \gamma_2 = \gamma_4 = \ldots = \gamma_{2n-2m-2} = 0, \quad \gamma_{2n-2m} = b_0, \\ \gamma_{2n-2m+2} + \gamma_{2n-2m}a_1 = b_1, \ \ldots, \ \gamma_{2n} + \gamma_{2n-2}a_1 + \ldots + \gamma_{2n-2m}a_m = b_m. \end{gathered} \tag{22}$$

Also, we define a rectangular matrix of order $2n \times (2n-2)$:

$$T = \begin{bmatrix} 0 & 0 & 0 & 0 & \ldots & 0 & 0 \\ 0 & 0 & 0 & 0 & \ldots & 0 & 0 \\ \gamma_2 & 0 & 0 & 0 & \ldots & 0 & 0 \\ 0 & \gamma_2 & 0 & 0 & \ldots & 0 & 0 \\ & & & & \ddots & & \\ \gamma_{2n-2} & 0 & \gamma_{2n-4} & 0 & \ldots & 0 & 0 \\ 0 & \gamma_{2n-2} & 0 & \gamma_{2n-4} & \ldots & 0 & \gamma_2 \end{bmatrix}.$$

Lemma 1. *Assume that the linear system* (13) *is observable. Then the change of variables*

$$x = (D(c))^{-1}[\tilde{y} - T\tilde{f}(y)] \tag{23}$$

reduces equation (1) *to the system*

$$x' = JAx + \xi f(y), \quad y = (x(t), c), \tag{24}$$

where the matrix JA is the chosen normal form and $\xi = (D(c))^{-1}\gamma$.

Lemma 1 can be verified by direct calculation.

Note that equation (1) and system (24) are equivalent. However, the nonlinear system (24) obtained via the change (23) is not necessarily Hamiltonian.

Recall that the vector c is chosen only from the observability condition of the linear system (13). This provides much freedom when choosing the vector c. As it turns out, under some additional conditions imposed on the vector c, the nonlinear system (24) will be Hamiltonian. In particular, we have the following result.

Lemma 2. *Assume that the vector c is chosen based on two requirements:*

- *The linear system* (13) *is observable.*
- *For some real number* α,

$$\gamma = \alpha D(c) J c, \tag{25}$$

where $D(c)$ *is the observability matrix of system* (13), γ *is the vector* (21), *and* J *is the matrix* (5).

Then the change of variables (23) *reduces the nonlinear equation* (1) *to a Hamiltonian system of the form* (24) *with the Hamiltonian*

$$H(x) = \frac{1}{2}(Ax, x) + \alpha F((x, c)), \tag{26}$$

where $F(y)$ *is the primitive of the function* $f(y)$, *i.e.,* $F'(y) = f(y)$.

Remark 2. Equality (25) in expanded form comes to a system of n linear algebraic equations with the $2n$ unknowns

$$\alpha c_1^2,\ \alpha c_2^2,\ \ldots,\ \alpha c_{2n}^2$$

and the parameter α. These equations include the coefficients determining the kind of the chosen normal form. As a result, the system of equations (25) is solvable only for one choice of the normal form. In other words, in contrast to the linear problem, the nonlinear one has a uniquely determined kind of the normal form of the Hamiltonian system constructed. This fact will be proved below for systems with two degrees of freedom.

Thus, we have the following result.

Theorem 3. *Assume that a possible normal form* JA *is chosen in accordance with the properties of the roots of the equation* $L(p) = 0$. *Let the vector* c *be chosen so that:*

1) *The linear system* (13) *is observable.*
2) *Equality* (25) *holds for some* α.

Then the change of variables (23) *reduces equation* (1) *to the equivalent Hamiltonian system* (24) *with the Hamiltonian* (26), *and the kind of its normal form is uniquely determined.*

4.2. Equations with Two Degrees of Freedom

As a basic application, consider the fourth-order equation

$$L\left(\frac{d}{dt}\right) y = M\left(\frac{d}{dt}\right) f(y), \tag{27}$$

where

$$L(p) = p^4 + ap^2 + b, \quad M(p) = b_0 p^2 + b_2 \tag{28}$$

are coprime real polynomials and $f(y)$ is a scalar continuous function. Equations of the form (27) are often called *equations with two degrees of freedom*.

As in Section 3.3, by assumption, the coefficients a and b of the polynomial $L(p)$ satisfy (15). Hence, all the four roots of the polynomial $L(p)$ are pure imaginary of the form $\pm i\omega_1$, $\pm i\omega_2$, where the numbers $\omega_1 > 0$ and $\omega_2 > 0$ are given by (16). We will construct an equivalent Hamiltonian system for equation (27) using Theorem 3.

As noted in Section 3.3, two different normal forms of the desired Hamiltonian system correspond to the polynomial $L(p)$, namely, the matrices (8) for $\sigma = 1$ and $\sigma = -1$. By analogy with Section 3.3,

we choose a vector $c = (c_1, c_2, 0, 0, 0)$ such that $c_1 c_2 \neq 0$. In this case, the linear system (13) is observable.

It remains to ensure condition 2) of Theorem 3, i.e., choose the vector c so that equality (25) holds. In this equality, $D(c)$ is the matrix (18), and the four-dimensional vector γ is given by (21) and (22) with respect to equation (27):

$$\gamma = \begin{bmatrix} 0 \\ \gamma_2 \\ 0 \\ \gamma_4 \end{bmatrix} = \begin{bmatrix} 0 \\ b_0 \\ 0 \\ b_2 - ab_0 \end{bmatrix}.$$

Therefore, equality (25) comes to the system of two equations

$$\begin{cases} \alpha(\omega_1 c_1^2 + \sigma\omega_2 c_2^2) = -\gamma_2 \\ \alpha(\omega_1^3 c_1^2 + \sigma\omega_2^3 c_2^2) = \gamma_4 \end{cases}$$

with the unknowns αc_1^2 and αc_2^2. Hence, we obtain

$$\alpha c_1^2 = \frac{\omega_2^2\gamma_2 + \gamma_4}{\omega_1(\omega_1^2 - \omega_2^2)}, \quad \alpha c_2^2 = -\frac{\omega_1^2\gamma_2 + \gamma_4}{\sigma\omega_2(\omega_1^2 - \omega_2^2)}.$$

Due to the coprimeness of the polynomials (28),

$$(\omega_1^2\gamma_2 + \gamma_4)(\omega_2^2\gamma_2 + \gamma_4) \neq 0.$$

Therefore, $\alpha \neq 0$ and

$$\left(\frac{c_1}{c_2}\right)^2 = -\sigma\frac{\omega_2}{\omega_1}\kappa,$$

where

$$\kappa = \frac{\omega_2^2\gamma_2 + \gamma_4}{\omega_1^2\gamma_2 + \gamma_4}. \tag{29}$$

Thus, equation (25) is solvable only for $\sigma = 1$ (if $\kappa < 0$) or only for $\sigma = -1$ (if $\kappa > 0$).

Let $\kappa < 0$ ($\kappa > 0$). In this case, the following values can be taken as the solution of equation (25):

$$c_1 = 1, \quad c_2 = \sqrt{-\frac{\omega_1}{\kappa\omega_2}} \quad \left(c_2 = \sqrt{\frac{\omega_1}{\kappa\omega_2}}\right), \quad \alpha = \frac{\omega_2^2\gamma_2 + \gamma_4}{\omega_1(\omega_1^2 - \omega_2^2)}. \tag{30}$$

In other words, the following result has been established.

Theorem 4. *Assume that $\kappa < 0$ ($\kappa > 0$). Let the numbers α, c_1, and c_2 be given by* (30)*. Then the change of variables* (23) *reduces equation* (27) *to the equivalent Hamiltonian system* (24) *with the Hamiltonian* (26)*:*

$$H(x) = \frac{1}{2}(Ax, x) + \alpha F(x_1 c_1 + x_2 c_2),$$

where $F(y)$ is the primitive of the function $f(y)$, i.e., $F'(y) = f(y)$. In addition, the kind of the normal form (8) *is uniquely determined: $\sigma = 1$ in the case $\kappa < 0$ ($\sigma = -1$ in the case $\kappa > 0$).*

EXAMPLE 2

Consider equation (27) of the form

$$y'''' + 5y'' + 4y = (f(y))'' + 3f(y). \tag{31}$$

In other words, we have the polynomials (28) with $a = 5$, $b = 4$, $b_0 = 1$, and $b_2 = 3$. Then $\omega_1 = 2$ and $\omega_2 = 1$, and the vector γ is $\gamma = \begin{bmatrix} 0 \\ 1 \\ 0 \\ -2 \end{bmatrix}$, i.e., $\gamma_2 = 1$ and $\gamma_4 = -2$.

Formula (29) yields $\kappa = -1/2 < 0$. By Theorem 4, the kind of the normal form (8) is uniquely determined: $\sigma = 1$. Next, the values (30) are $c_1 = 1$, $c_2 = 2$, and $\alpha = -1/6$.

According to Theorem 4, the change of variables (23) with the matrix $D(c)$ (18), $\omega_1 = 2$, $\omega_2 = 1$, $\sigma = 1$, $c_1 = 1$, and $c_2 = 2$ reduces equation (31) to the equivalent Hamiltonian system (24) with the matrix JA (8) with $\omega_1 = 2$, $\omega_2 = 1$, $\sigma = 1$, and the vector $\xi = (D(c))^{-1}\gamma$ equal to $\xi = \begin{bmatrix} 0 \\ 0 \\ 1/6 \\ 1/3 \end{bmatrix}$.

The Hamiltonian of this system is

$$H(x) = \frac{2x_1^2 + x_2^2 + 2x_3^2 + x_4^2}{2} - \frac{1}{6}F(x_1 + 2x_2).$$

5. CONCLUSIONS

This paper has proposed new approaches to constructing equivalent Hamiltonian systems for linear and nonlinear Lurie equations (differential equations containing derivatives of even orders only). The approaches are based on the transition from the linear part of the Lurie equation to the normal forms of the corresponding Hamiltonian systems, with a subsequent transformation of the resulting system. This scheme does not require complex and cumbersome transformations of the original equation. It has been demonstrated that, in the linear case, the problem of constructing equivalent Hamiltonian systems can lead to qualitatively different systems. At the same time, for nonlinear systems, the above problem is uniquely solvable in a natural sense. The Appendix contains similar results in a general formulation (without requiring that the original equations contain derivatives of even orders only). The main results have been reduced to computational formulas and algorithms.

ACKNOWLEDGMENTS

The authors are grateful to Profs. E.M. Mukhamadiev and A.B. Nazimov for a useful discussion of the issues considered in this paper. This discussion took place in October 2022 in Ufa during the Ufa Autumn Mathematical School, the international conference sponsored by the Scientific and Educational Mathematical Center of the Volga Federal District and VinTekh LLC.

APPENDIX

Auxiliary Constructs

The proofs of the main theoretical results of this paper are based on the following auxiliary assertions of a general nature. They concern not only Hamiltonian systems and are of independent interest.

Consider a system described by the nth-order differential equation

$$L\left(\frac{d}{dt}\right)y = M\left(\frac{d}{dt}\right)u(t), \tag{A.1}$$

where

$$\begin{gathered} L(p) = p^n + a_1 p^{n-1} + \ldots + a_{n-1}p + a_n, \\ M(p) = b_0 p^m + b_1 p^{m-1} + \ldots + b_m \end{gathered} \tag{A.2}$$

are coprime real polynomials of degrees n and m $(n > m \geqslant 0)$.

For equation (A.1), it is required to construct an equivalent system described by the equations

$$x' = Ax + \xi u(t), \quad y = (x(t), c), \tag{A.3}$$

where A is a square matrix of order n, $\xi, c \in R^n$ are fixed vectors, and the symbol (x, c) indicates the inner product of vectors x and c from R^n. The inverse problem is to construct from system (A.3) an equivalent system described by the differential equation (A.1).

The simplest transition is from (A.1) to the equivalent system

$$z' = A_0 z + \gamma u(t), \quad y = (z(t), c_0), \tag{A.4}$$

where $c_0 = (1, 0, 0, \ldots, 0)$,

$$A_0 = \begin{bmatrix} 0 & 1 & 0 & \ldots & 0 & 0 \\ 0 & 0 & 1 & \ldots & 0 & 0 \\ & & & \ddots & & \\ 0 & 0 & 0 & \ldots & 0 & 1 \\ -a_n & -a_{n-1} & -a_{n-2} & \ldots & -a_2 & -a_1 \end{bmatrix}, \quad z = \begin{bmatrix} z_1 \\ z_2 \\ \vdots \\ z_n \end{bmatrix}, \quad \gamma = \begin{bmatrix} \gamma_1 \\ \gamma_2 \\ \vdots \\ \gamma_n \end{bmatrix},$$

and the coordinates of the vector γ are given by

$$\begin{gathered} \gamma_1 = \gamma_2 = \ldots = \gamma_{n-m-1} = 0, \quad \gamma_{n-m} = b_0, \quad \gamma_{n-m+1} + \gamma_{n-m}a_1 = b_1, \\ \ldots, \quad \gamma_n + \gamma_{n-1}a_1 + \ldots + \gamma_{n-m}a_m = b_m. \end{gathered} \tag{A.5}$$

Direct calculation shows that the transition from equation (A.1) to system (A.4) can be implemented via the change of variables $z = \tilde{y} - T\tilde{u}$, where

$$\tilde{y} = \begin{bmatrix} y \\ y' \\ \vdots \\ y^{(n-1)} \end{bmatrix}, \quad \tilde{u} = \begin{bmatrix} u \\ u' \\ \vdots \\ u^{(n-2)} \end{bmatrix}, \tag{A.6}$$

and the rectangular matrix T of dimensions $n \times (n-1)$ has the form

$$T = \begin{bmatrix} 0 & 0 & 0 & \ldots & 0 \\ \gamma_1 & 0 & 0 & \ldots & 0 \\ \gamma_2 & \gamma_1 & 0 & \ldots & 0 \\ & & & \ddots & \\ \gamma_{n-1} & \gamma_{n-2} & \gamma_{n-3} & \cdots & \gamma_1 \end{bmatrix}. \tag{A.7}$$

Similar problems arise for nonlinear systems. In them, the analog of equation (A.1) is a nonlinear feedback system described by

$$L\left(\frac{d}{dt}\right)y = M\left(\frac{d}{dt}\right)f(y),$$

where $L(p)$ and $M(p)$ are the polynomials (A.2) and $f(y)$ is a scalar continuous function. The analog of system (A.3) is the one described by

$$x' = Ax + \xi f(y), \quad y = (x(t), c).$$

Various issues related to these problems were discussed in many works. Let us emphasize the fundamental monograph [8] with a detailed analysis of basic concepts ("system," "equivalence," "transfer function", etc.) and, moreover, constructive methods for designing equivalent systems (within the linear theory).

To study the problems formulated here, we consider the following systems described by input-output-state equations:

- system $\mathcal{A}$ (A.1),
- system $\mathcal{B}$ described by the equations

$$x' = Ax + \xi u(t), \quad w = (x(t), c), \tag{A.8}$$

- system $\mathcal{C}$ described by the equations

$$z' = A_0 z + \gamma u(t), \quad v = (z(t), c_0). \tag{A.9}$$

Note that systems (A.8) and (A.9) are the same systems (A.3) and (A.4). They are presented in a new form only to avoid confusion with the notation of the outputs of the systems under consideration.

Let the input space of systems $\mathcal{A}$, $\mathcal{B}$, and $\mathcal{C}$ be the set C^m-smooth functions $u(t)$, and let their state space be the space R^n. For a given input $u(t)$ and a given initial state $\tilde{y}_0 = (y_0, y_1, \ldots, y_{n-1})$ (at the time $t = 0$), we define the output $y(t)$ of system $\mathcal{A}$ as the solution of the Cauchy problem

$$\begin{cases} L\left(\dfrac{d}{dt}\right)y = M\left(\dfrac{d}{dt}\right)u(t) \\ y(0) = y_0,\ y'(0) = y_1,\ \ldots, y^{(n-1)}(0) = y_{n-1}. \end{cases}$$

For a given input $u(t)$ and a given initial state $x_0 \in R^n$ (at the time $t = 0$), we define the output $w(t)$ of system $\mathcal{B}$ by the equality $w(t) = (x(t), c)$, where $x(t)$ is the solution of the Cauchy problem

$$\begin{cases} x' = Ax + \xi u(t) \\ x(0) = x_0. \end{cases}$$

The output $v(t)$ of system $\mathcal{C}$ is defined by analogy.

The following assertions are true.

Theorem 5. *Systems $\mathcal{A}$ and $\mathcal{C}$ are equivalent.*

Theorem 6. *Systems $\mathcal{B}$ and $\mathcal{C}$ are equivalent iff system $\mathcal{B}$ is observable, $A_0 = DAD^{-1}$, and $\gamma = D\xi$, where D denotes the observability matrix of system $\mathcal{B}$ and the vector γ consists of the coordinates* (A.5).

Assume that systems $\mathcal{B}$ and $\mathcal{C}$ are equivalent. Then system (A.4) *is reducible to system* (A.3) *via the nondegenerate change of variables $x = D^{-1}z$.*

Theorem 7. *Systems $\mathcal{A}$ and $\mathcal{B}$ are equivalent iff system $\mathcal{B}$ is observable, $A_0 = DAD^{-1}$, and $\gamma = D\xi$.*

Assume that systems $\mathcal{A}$ and $\mathcal{B}$ are equivalent. Then equation (A.1) *is reducible to system* (A.3) *via the change of variables*

$$x = D^{-1}(\tilde{y} - T\tilde{u}),$$

where the matrix T and the vectors $\tilde{y}$ and $\tilde{u}$ are given by (A.7) *and* (A.6)*, respectively.*

Theorem 5 is a well-known result; for example, see [2, 7, 8]. The validity of Theorem 7 follows from Theorems 5 and 6. Theorem 6 is established by standard methods of systems theory.

Proof of Theorem 1. *Necessity.* Let equation (9) and the Hamiltonian system (13) be equivalent. Then, by Theorem 7, system (13) is observable and the equality $A_0 = D(JA)D^{-1}$ holds with the matrix A_0 (12) and the observability matrix D of system (13).

Sufficiency. Let system (13) be observable. It is required to prove the equivalence of equation (9) and the Hamiltonian system (13). For this purpose, we show that the output $y(t) = (x(t), c)$ of system (13) is also that of equation (9) under an initial state y_0 such that $y_0 = (x(0), c)$ and, conversely, that each output $y(t)$ of equation (9) is also the output of system (13) under an initial state x_0 such that $y_0 = (x_0, c)$.

Let us restrict the considerations to the case $n = 2$ (i.e., system (13) is four-dimensional). Then equation (9) takes the form (14) and, therefore, $L(p) = p^4 + ap^2 + b$.

For the output $y(t) = (x(t), c)$ of system (13), we have

$$y' = (x', c) = (x, A^*c), \quad y'' = (x, (A^*)^2c), \quad y'''' = (x, (A^*)^4c).$$

Hence,

$$y'''' + ay'' + by = (x, (A^*)^4c) + (x, (A^*)^2c)a + (x, c)b = (x, [(A^*)^4 + a(A^*)^2 + bI]c) = 0,$$

since the matrix A (and, consequently, the transposed matrix A^*) satisfies its characteristic equation $p^4 + ap^2 + b = 0$. Thus, the function $y(t) = (x(t), c)$ is the solution of equation (9).

Now, let $y(t)$ be the output of equation (14); the corresponding initial state is $\tilde{y}_0 = (y_0, y_1, y_2, y_3)$. We determine the initial state x_0 of the four-dimensional system (13) from the system of equations

$$(x_0, c) = y_0, \quad (x_0, A^*c) = y_1, \quad (x_0, (A^*)^2c) = y_2, \quad (x_0, (A^*)^3c) = y_3$$

or (which is the same) from the equation $D(c)x_0 = \tilde{y}_0$. Due to the observability of system (13), this equation has the unique solution $x_0 = (D(c))^{-1}\tilde{y}_0$. Obviously, the output of system (13) under this initial state x_0 coincides with the function $y(t)$.

The proof of Theorem 1 is complete.

Proof of Theorem 2. This result is immediate from Theorem 7.

Proof of Lemma 2. According to Lemma 1, the change of variables (23) reduces equation (1) to system (24). To establish Lemma 2, it remains to show that the function (26) is the Hamiltonian of system (24), i.e., the validity of the relation

$$J\nabla H(x) = JAx + \xi f((c, x)).$$

Since $J\nabla H(x) = JAx + \alpha J\nabla F((x, c))$, we have to verify the equality

$$\alpha J\nabla F((x, c)) = \xi f((c, x)).$$

We have $\nabla F((x, c)) = f((c, x))c$, which yields $J\nabla F((x, c)) = f((c, x))Jc$. Thus, it is necessary to show $\alpha Jc = \xi$. In turn, this equality follows from (25) and the relation $\xi = D^{-1}\gamma$ (see Lemma 1).

The proof of Lemma 2 is complete.

REFERENCES

1. Leonov, G.A., *Teoriya upravleniya* (Control Theory), St. Petersburg: St. Peterburg University, 2006.
2. Voronov, A.A., *Vvedenie v dinamiku slozhnykh upravlyaemykh sistem* (Introduction to the Dynamics of Complex Controlled Systems), Moscow: Nauka, 1985.
3. Zhuravlev, V.F., Petrov, F.G., and Shunderyuk, M.M., *Izbrannye zadachi gamil'tonovoi mekhaniki* (Selected Problems of Hamiltonian Mechanics), Moscow: Lenand, 2015.
4. Meyer, K., Hall, G., and Offin, D., *Introduction to Hamiltonian Dynamical Systems and the N-Body Problem*, New York: Springer, 2009.
5. Krasnosel'skii, A.M., Lifshits, Je.A., and Sobolev, A.V., *Positive Linear Systems: The Method of Positive Operators*, Sigma Series in Applied Mathematics, vol. 5, Berlin: Hilderman Verlag, 1990.
6. Yumagulov, M.G., Ibragimova, L.S., and Belova, A.S., Investigation of the Problem on a Parametric Resonance in Lurie Systems with Weakly Oscillating Coefficients, *Autom. Remote Control*, 2022, vol. 83, no. 2, pp. 252–263.
7. Polyak, B.T., Khlebnikov, M.V., and Rapoport, L.B., *Matematicheskaya teoriya avtomaticheskogo upravleniya* (Mathematical Theory of Optimal Control), Moscow: LENAND, 2019.
8. Zadeh, L. and Desoer, Ch., *Linear System Theory: The State Space Approach*, New York: McGraw-Hill, 1963.
9. Bryuno, A.D., Normal Form of a Hamiltonian System with a Periodic Perturbation, *Preprint of Keldysh Inst. Appl. Math.*, Moscow, 2019, no. 057. https://doi.org/10.20948/prepr-2019-57
10. Krasnosel'skii, A.M. and Rachinskii, D.I., On Hamiltonian Nature of Lurie Systems, *Autom. Remote Control*, 2000, vol. 61, no. 8, pp. 1259–1262.
11. Krasnosel'skii, A.M. and Rachinskii, D.I., Existence of Continua of Cycles in Hamiltonian Control Systems, *Autom. Remote Control*, 2001, vol. 62, no. 2, pp. 227–235.
12. Chow, Sh.-N., Li, Ch., and Wang, D., *Normal Forms and Bifurcation of Planar Vector Fields*, Cambridge: Cambridge University Press, 1994.
13. Markeev, A.P., *Tochki libratsii v nebesnoi mekhanike i kosmodinamike* (Libration Points in Celestial Mechanics and Cosmodynamics), Moscow: Nauka, 1978.
14. Yakubovich, V.A. and Starzhinskii, V.M., *Lineinye differentsial'nye uravneniya s periodicheskimi koeffitsientami i ikh prilozheniya* (Linear Differential Equations with Periodic Coefficients and Their Applications), Moscow: Nauka, 1972.
15. Yumagulov, M.G., Ibragimova, L.S., and Belova, A.S., Perturbation Theory Methods in Problem of Parametric Resonance for Linear Periodic Hamiltonian Systems, *Ufa Math. J.*, 2021, vol. 13, no. 3, pp. 174–190.
16. Polyak, B.T. and Shalby, L.A., Minimum Fuel-Consumption Stabilization of a Spacecraft at the Lagrangian Points, *Autom. Remote Control*, 2019, vol. 80, no. 12, pp. 2217–2228.
17. Markeev, A.P., *Lineinye gamil'tonovy sistemy i nekotorye zadachi ob ustoichivosti dvizheniya sputnika otnositel'no tsentra mass* (Linear Hamiltonian Systems and Some Problems of Stability of Satellite Motion with Respect to the Center of Mass), Moscow–Izhevsk: Institute for Computer Studies, 2009.
18. Yumagulov, M.G., Belikova, O.N., and Isanbaeva, N.R., Bifurcation Near Boundaries of Regions of Stability of Libration Points in the Three-Body Problem, *Astron. Rep.*, 2018, vol. 62, no. 2, pp. 144–153.

This paper was recommended for publication by N.V. Kuznetsov, a member of the Editorial Board

ISSN 0005-1179 (print), ISSN 1608-3032 (online), Automation and Remote Control, 2025, Vol. 86, No. 1, pp. 34–47.

CONTROL IN TECHNICAL SYSTEMS

Approaches to Optimizing Guidance Methods to High-Speed Intensively Maneuvering Targets. Part II. Analyzing the Capabilities of Different Ways to Optimize Guidance Methods

V. S. Verba[*,a], **V. I. Merkulov**[*,b], **and V. P. Kharkov**[**,c]

[*] *JSC Concern Vega, Moscow, Russia*
[**] *LLC NPO NaukaSoft, Moscow, Russia*
e-mail: [a] *vvs.msk@gmail.com,* [b] *mvipost41@gmail.com,* [c] *charkovvp@rambler.ru*

Received March 20, 2024
Revised July 8, 2024
Accepted September 2, 2024

Abstract—Based on the requirements for optimization methods of high-speed aircraft interception systems (see part I of the study), different ways to optimize guidance methods are analyzed. The capabilities of the classical theory of optimal control, as well as its modifications with local optimization and local optimization by the minimum of quadratic-biquadratic performance functionals, are considered at the qualitative level within the concept of inverse dynamics problems. In addition, the ways to optimize the information support of all approaches are assessed.

Keywords: statistical theory of optimal control, local optimization, quadratic-biquadratic performance functional, inverse dynamics problem, adaptive analog-discrete filtering

DOI: 10.31857/S0005117925010031

1. INTRODUCTION

The military and technical perfection of guidance systems is largely determined by the ways to optimize control laws and their information support, representing the basis for their development. Currently, many optimization methods known match the requirements of an accurate and cost-efficient operation to different degrees [1]. Note those of the statistical theory of optimal control (STOC), which are used to design the best guidance systems jointly in terms of accuracy and control costs. These methods are based on the principle of minimizing quadratic performance functionals, which contain both control errors and energy costs of control implementation.

In this class of optimization ways, it is necessary to distinguish rather complex classical STOC methods, ensuring the optimality of guidance systems for the entire interception time [2–9], and simpler ones, ensuring their local optimality for each current time instant [2–4, 10–12].

In the practical development of complex technical systems for various purposes, design methods based on the concept of inverse dynamics problems (IDP) [13–18] are also used. Their peculiarity lies in the sufficiently simple consideration of different nonlinearities during the control design procedure.

Gradient methods are most widespread among the design ways neglecting the energy consumption of control signals [1, 19]. These methods optimize control laws in terms of different performance functionals having an extremum on the system operation interval.

Various modifications of Kalman filters are often used to optimize information systems [3, 4, 20–23].

In recent time, the so-called intelligent optimization methods based on neural network approaches [24, 25] have been gaining popularity in the design of systems operating under a priori uncertainty.

The analysis of the requirements for the optimization methods carried out in [26] demonstrated, first of all, the possibility of forming nonstationary guidance methods, the possibility of operation in a given domain of application conditions and constraints, and the possibility of implementation by the dynamic properties of the carrier and the capability of estimating the coordinates used in the guidance method. Note that the latter possibility can be assessed only based on the design results of particular guidance methods.

Practical ways to implement nonstationary guidance methods with the possibility of changing control and information priorities during flight, based on time-varying state models and coefficients of penalty matrices for accuracy and cost-efficient operation as functions of range and speed, were discussed in detail in [4].

The methods for designing guidance laws for high-speed aircraft (HSA) based on the classical STOC approach in the Letov–Kalman formulation and its local modification (with the mismatch between the dynamic properties of the target and the interceptor treated as disturbances) were also considered in [4].

Below, we qualitatively assess different ways to optimize guidance methods to HSA that match, to a greater or lesser extent, the requirements discussed in [26].

Note that the sections and formulas mentioned below have a double numbering system: the first digit corresponds to the part of the study whereas the second to the section or formula.

2. THE CLASSICAL OPTIMAL CONTROL THEORY IN THE LETOV–KALMAN FORMULATION: ANALYSIS OF CAPABILITIES

Consider the mathematical apparatus of the conventional statistical theory of optimal control [3–9] in its simplest form when applied to the problem under study. For an interceptor described by

$$\dot{\mathbf{x}}_{\text{int}}(t) = \mathbf{F}_{\text{int}}\mathbf{x}_{\text{int}}(t) + \mathbf{B}_{\text{int}}\mathbf{u}(t) + \boldsymbol{\xi}_{\text{int}}(t), \quad \mathbf{x}_{\text{int}}(0) = \mathbf{x}_{\text{int}0}, \tag{2.1}$$

intended for a target with a trajectory

$$\dot{\mathbf{x}}_{\text{tar}}(t) = \mathbf{F}_{\text{tar}}\mathbf{x}_{\text{tar}}(t) + \boldsymbol{\xi}_{\text{tar}}(t), \quad \mathbf{x}_{\text{tar}}(0) = \mathbf{x}_{\text{tar}0}, \tag{2.2}$$

under available measurements

$$\mathbf{z}(t) = \mathbf{H}\mathbf{x}(t) + \boldsymbol{\xi}_{\text{z}}(t), \quad \mathbf{x}(t) = \left[\mathbf{x}_{\text{tar}}^{\text{T}}(t) \quad \mathbf{x}_{\text{int}}^{\text{T}}(t)\right]^{\text{T}}, \tag{2.3}$$

this apparatus yields the optimal control law

$$\mathbf{u}(t) = \mathbf{K}^{-1}\mathbf{B}_{\text{int}}^{\text{T}}\mathbf{P}(t)[\hat{\mathbf{x}}_{\text{tar}}(t) - \hat{\mathbf{x}}_{\text{int}}(t)], \tag{2.4}$$

$$\dot{\mathbf{P}}(t) = -\mathbf{L} - \mathbf{F}_{\text{int}}^{\text{T}}\mathbf{P}(t) - \mathbf{P}(t)\mathbf{F}_{\text{int}} + \mathbf{P}(t)^{\text{T}}\mathbf{B}_{\text{int}}\mathbf{K}^{-1}\mathbf{B}_{\text{int}}^{\text{T}}\mathbf{P}(t), \quad \mathbf{P}(t_{\text{fin}}) = \mathbf{Q}, \tag{2.5}$$

in terms of the minimum value of the quadratic Letov–Kalman performance functional

$$I = M\left\{[\mathbf{x}_{\text{tar}}(t_{\text{fin}}) - \mathbf{x}_{\text{int}}(t_{\text{fin}})]^{\text{T}}\mathbf{Q}[\mathbf{x}_{\text{tar}}(t_{\text{fin}}) - \mathbf{x}_{\text{int}}(t_{\text{fin}})]\right.$$
$$\left. + \int_0^{t_{\text{fin}}} [\mathbf{x}_{\text{tar}}(t) - \mathbf{x}_{\text{int}}(t)]^{\text{T}}\mathbf{L}[\mathbf{x}_{\text{tar}}(t) - \mathbf{x}_{\text{int}}(t)]dt + \int_0^{t_{\text{fin}}} \mathbf{u}^{\text{T}}(t)\mathbf{K}\mathbf{u}(t)dt\right\}. \tag{2.6}$$

Here, $\mathbf{x}_{\text{int}}$ and $\mathbf{x}_{\text{tar}}$ are the n-dimensional vectors of interceptor and target states, respectively; $\mathbf{F}_{\text{int}}$ and $\mathbf{F}_{\text{tar}}$ are the internal connection matrices of the processes (2.1) and (2.2); $\mathbf{u}$ is the r-dimensional control vector ($r \leqslant n$); $\mathbf{B}_{\text{int}}$ is the control efficiency matrix; $\mathbf{z}$ is the m-dimensional measurement vector ($m \leqslant 2n$); $\mathbf{H}$ is the connection matrix of (2.1) and (2.2) with (2.3); $\mathbf{P}$ is a symmetric matrix defining the current weight of the control errors; t and t_{fin} are the current and final control time, respectively; $\mathbf{Q}$ and $\mathbf{L}$ are nonnegative definite penalty matrices for the final and current control accuracy, respectively; $\mathbf{K}$ is a positive definite penalty matrix for control signals; $\boldsymbol{\xi}_{\text{int}}$, $\boldsymbol{\xi}_{\text{tar}}$, and $\boldsymbol{\xi}_{\text{z}}$ are the vectors of centered Gaussian noises of the state and measurement vectors, respectively; finally, $\hat{\mathbf{x}}_{\text{int}}$ and $\hat{\mathbf{x}}_{\text{tar}}$ are the vectors of the optimal estimates of the processes (2.1) and (2.2), respectively.

Note that the minimized functional (2.6) includes three terms. The first, terminal, defines the system accuracy at the final time instant of control; the second, the integral accuracy over the entire control time; and the third, the energy consumption of control signals. Minimizing the performance functional (2.6), the control law (2.4), (2.5) is jointly the best in terms of accuracy and cost efficiency, which is an undoubted advantage.

Direct analysis of (2.1)–(2.5) leads to several general conclusions.

1. The control law (2.4), (2.5) depends on the system state $\hat{\mathbf{x}}_{\text{int}}$ and $\hat{\mathbf{x}}_{\text{tar}}$, its capability to perceive control signals (determined by the matrix $\mathbf{B}_{\text{int}}$), the penalties $\mathbf{K}$ for control signals, and the weight matrix $\mathbf{P}$. The larger the control penalty is, the smaller the signals $\mathbf{u}$ will be (accordingly, the more cost-efficient the system will be but the less accurate). The latter is due to that small values of $\mathbf{u}$ cause small values of $\dot{\mathbf{x}}_{\text{int}}$ in (2.1), and consequently small targeted changes of $\mathbf{x}_{\text{int}}$. If system (2.1) perceives the control signals $\mathbf{u}$ well (the matrix $\mathbf{B}_{\text{int}}$ has large coefficients), then it is reasonable to make them large: in this case, there will be large values of $\dot{\mathbf{x}}_{\text{int}}$ and the system will quickly change its state $\mathbf{x}_{\text{int}}$. If the coefficients of the matrix $\mathbf{B}_{\text{int}}$ are small, then large control signals should not be used, as it will result in unreasonably high energy consumption with very little gain in accuracy.

2. In (2.4), the coefficients of the matrix $\mathbf{P}$ aggregately describe the current accuracy and cost efficiency penalties determined by the matrices $\mathbf{L}$ and $\mathbf{K}$, the deterministic connections, and the efficiency of the control signals conditioned by the matrices $\mathbf{F}_{\text{int}}$ and $\mathbf{B}_{\text{int}}$. The impact of deterministic connections is manifested in that a change in the penalty l_{ii} for the operation accuracy on some coordinate x_i causes a change in the accuracy on other coordinates functionally connected with x_i. The corresponding changes in the matrix $\mathbf{P}$ lead to changes in control signals and, consequently, in the system's efficiency.

3. The peculiarity of (2.4), (2.5) is that the coefficients of the matrix (2.5) are calculated in inverse time from t_{fin} to t when solving the Riccati equation, while in (2.4) they are used in direct time. Note that, due to the number of equations in (2.5) to be solved for determining the matrix $\mathbf{P}$, the control formation complexity significantly exceeds that of the optimized system (2.1). Moreover, even a slight increase in the dimension of (2.1) leads to excessively many equations to be solved when calculating the matrix $\mathbf{P}$. (The number of the equations is n^2.) This phenomenon, called the curse of dimensionality and characteristic of many optimal systems, restrains the application of optimal control algorithms for high-dimensional complex systems. However, for time-invariant systems, the matrix $\mathbf{P}$, defined only by a priori information, can be obtained in advance. Accordingly, the coefficients $\mathbf{K}^{-1}\mathbf{B}_{\text{int}}^{\text{T}}\mathbf{P}(t)$ for (2.4), whose number is defined by the dimension $r \times n$, can also be calculated in advance. Hence, the procedure of using (2.4), (2.5) becomes somewhat simpler in practice.

4. Assigning different penalties $\mathbf{L}$ and $\mathbf{Q}$ to the current and final accuracy allows implementing different errors at different operation stages of the interception system, thereby ensuring the desired accuracy at the end of control under very low current energy costs.

For the problem of designing a guidance method to HSA with the apparatus (2.1)–(2.6), we draw the following conclusions:

- By adjusting the form the matrices $\mathbf{Q}$, $\mathbf{L}$, and $\mathbf{K}$, using the representation of their elements as a function of the state coordinates, it is possible to form a time-varying guidance law [4] with the redistribution of control functions depending on the value of the state coordinates with a significant complication of the calculation procedure of (2.5).
- The linear dependence of (2.4) on the control errors ($\Delta\mathbf{x} = \mathbf{x}_{\text{tar}} - \mathbf{x}_{\text{int}}$) does not provide an enhanced role for control to withdraw from the stability loss bounds.
- To implement (2.4), (2.5), the guidance time should be known, which is practically impossible.
- When linear (linearized) state models are used, the control law (2.4), (2.5) ensures acceptable universality of the guidance method, implementing stable operation in a wide range of application conditions [3].
- The need to solve the high-dimensional two-point boundary value problem due to resolving equation (2.5) in reverse time from t_{fin} to t, while the control law (2.4) is formed in direct time from t to t_{fin}, significantly complicates the control design procedure.
- In the law (2.4), the dependence of the control signal on the dynamic properties of the interceptor ($\mathbf{F}_{\text{int}}$) is considered in a complex way when solving (2.5), which makes it difficult to predict its significance in interception problems.
- The capability to form all the optimal estimates $\hat{\mathbf{x}}_{\text{int}}$ and $\hat{\mathbf{x}}_{\text{tar}}$, required to implement (2.4), is determined by the observability condition [3], see Section 6. The fulfillment of this condition depends on the internal connections of (2.1), (2.2) and the set of measurement sensors in (2.3).

In conclusion, we underline that the classical optimal control theory in the Letov–Kalman formulation does not satisfy all the requirements for implementing the guidance method to HSA.

The most challenging obstacles to optimizing interception methods using this method are the need to know the guidance time and the complexity of solving the two-point boundary value problem.

3. LOCAL OPTIMIZATION METHODS BY THE MINIMUM OF QUADRATIC PERFORMANCE FUNCTIONALS: ANALYSIS OF CAPABILITIES

It seems more promising to use local optimization methods that minimize performance functionals for each current time instant without requiring knowledge of the guidance time. Then it is possible to generate control without solving the complex two-point boundary value problem, which significantly simplifies the control design procedure. Moreover, within this approach, various disturbances affecting the interceptor can be quite simply considered directly in the control law without expanding the state vector. In this case, for an interceptor described by

$$\dot{\mathbf{x}}_{\text{int}}(t) = \mathbf{F}_{\text{int}}\mathbf{x}_{\text{int}}(t) + \mathbf{B}_{\text{int}}\mathbf{u}(t) + \mathbf{s}_{\text{int}}(t) + \boldsymbol{\xi}_{\text{int}}(t), \quad \mathbf{x}_{\text{int}}(0) = \mathbf{x}_{\text{int}0}, \tag{3.1}$$

intended for an HSA with the trajectory (2.2) under the available measurements (2.3), the local optimization method [3] yields the optimal control law

$$\mathbf{u}(t) = \mathbf{K}^{-1}\mathbf{B}_{\text{int}}^{\text{T}}\left[\mathbf{Q}(\hat{\mathbf{x}}_{\text{tar}}(t) - \hat{\mathbf{x}}_{\text{int}}(t)) - \mathbf{G}\hat{\mathbf{s}}_{\text{int}}(t)\right], \tag{3.2}$$

in terms of the minimum value of the performance functional

$$I = M\left\{[\mathbf{x}_{\text{tar}}(t) - \mathbf{x}_{\text{int}}(t)]^{\text{T}}\mathbf{Q}[\mathbf{x}_{\text{tar}}(t) - \mathbf{x}_{\text{int}}(t)] \right.$$
$$\left. + 2[\mathbf{x}_{\text{tar}}(t) - \mathbf{x}_{\text{int}}(t)]^{\text{T}}\mathbf{G}\mathbf{s}_{\text{int}}(t) + \mathbf{s}_{\text{int}}^{\text{T}}(t)\mathbf{Q}\mathbf{s}_{\text{int}}(t) + \int_0^t \mathbf{u}^{\text{T}}(t)\mathbf{K}\mathbf{u}(t)dt\right\}. \tag{3.3}$$

Here, $\mathbf{s}_{\text{int}}$ and $\hat{\mathbf{s}}_{\text{int}}$ are the n-dimensional vectors of the measured disturbances affecting the interceptor and their optimal estimates, respectively; $\mathbf{G}$ is a nonnegative matrix defining the weight of disturbances in the control law (3.2).

For the problem of designing a guidance method to HSA [26], the analysis of (3.1)–(3.3) leads to the following conclusions:

1. Using the coefficients of the matrices $\mathbf{Q}$ and $\mathbf{G}$ as functions of the state coordinates (the range and approach speed), it is possible to generate control laws [4] with rather easily assigned instants of, first, changing control priorities during guidance and surveillance trajectory control [4] and, second, adjusting the effects of disturbances on different interception trajectory sections.

2. The method has high implementability due to the following features:

- the capability to optimize the guidance system for a particular carrier by forming additional correction signals that compensate for its inertia;
- the capability to consider a wide range of natural and virtual disturbances [3] in the form of mismatches between the dynamic properties of the target and interceptor, the prediction of the target's spatial position compensating for the carrier's inertia, the approach of the state coordinates to acceptable stability loss bounds, etc.;
- the simplicity of control signals formation for each current time instant (there is no need to know the guidance time and solve the complex two-point boundary value problem).

The capability of estimating all state coordinates used in the guidance method can be determined only by the results of designing particular control laws.

3. The method possesses high universality, characterized by the capability to design stable guidance methods in a wide field of application conditions, including those not corresponding to the models underlying the design procedure [4].

4. The method does not guarantee withdrawal from the stability loss bounds due to the linear dependence of (3.2) on the control errors.

4. LOCAL OPTIMIZATION METHODS BY THE MINIMUM OF QUADRATIC-BIQUADRATIC PERFORMANCE FUNCTIONALS: ANALYSIS OF CAPABILITIES

According to the capabilities of guidance design schemes with local optimization methods by the minimum of conventional quadratic performance functionals [4] (see the above analysis), the problems of withdrawing the carrier from stability loss bounds and using the derivatives of the line-of-sight (LoS) angle rate in control laws are still challenging, which significantly complicates their information support procedure.

Both problems can be solved by applying guidance methods with a nonlinear (cubic) dependence on the control errors generated during the local minimization of quadratic-biquadratic performance functionals [3, 27].

In the elementary case, for the interceptor (2.1) intended for a target with the trajectory (2.2) under the available measurements (2.3), this approach yields the optimal control law

$$\mathbf{u}(t) = \mathbf{K}^{-1}\mathbf{B}_{\text{int}}^{\mathrm{T}}\left\{\mathbf{Q} + 2\left[\Delta\hat{\mathbf{x}}(t)\Delta\hat{\mathbf{x}}(t)^{\mathrm{T}}\mathbf{R}\right]\right\}\Delta\hat{\mathbf{x}}(t), \quad \Delta\hat{\mathbf{x}}(t) = \hat{\mathbf{x}}_{\text{tar}}(t) - \hat{\mathbf{x}}_{\text{int}}(t), \tag{4.1}$$

in terms of the minimum value of the performance functional

$$I = M\left\{\Delta\mathbf{x}(t)^{\mathrm{T}}\mathbf{Q}\Delta\mathbf{x}(t) + \mathbf{x}(t)^{\mathrm{T}}\left[\Delta\mathbf{x}(t)\Delta\mathbf{x}(t)^{\mathrm{T}}\mathbf{R}\right]\Delta\mathbf{x}(t) + \int_0^t \mathbf{u}^{\mathrm{T}}(t)\mathbf{K}\mathbf{u}(t)dt\right\}. \tag{4.2}$$

Direct analysis of (4.1) brings to the following conclusions.

1. The control signal consists of two parts: the first

$$\mathbf{K}^{-1}\mathbf{B}_{\text{int}}^{\text{T}}\mathbf{Q}\Delta\hat{\mathbf{x}}(t) \tag{4.3}$$

determines its linear component whereas the second

$$2\mathbf{K}^{-1}\mathbf{B}_{\text{int}}^{\text{T}}\left[\Delta\hat{\mathbf{x}}(t)\Delta\hat{\mathbf{x}}(t)^{\text{T}}\mathbf{R}\right]\Delta\hat{\mathbf{x}}(t) \tag{4.4}$$

the cubic component. In addition to the terms proportional to Δx_i^3 $(i = \overline{1,n})$, formula (4.4) contains the combined terms $\Delta x_i^2\Delta x_j$ and $\Delta x_i\Delta x_j^2$ $(i = \overline{1,n},\ j = \overline{1,n},\ i \neq j)$.

2. The relationships between (4.3) and (4.4) depend on the coefficients of the matrices $\mathbf{Q}$ and $\mathbf{R}$ and, moreover, on the relationship between the control errors Δx_i and Δx_j.

For small errors $(\Delta x_i \to 0)$, the cubic component has almost no effect on the control signal and guidance accuracy, ensuring the high sensitivity of (4.1) to small errors.

Under large values of Δx_i, the cubic component becomes predominant, accelerating the handling of dangerous control errors.

The resulting control laws [4, 27] do not require estimating the derivatives of the LoS angle rate; the role of such estimates is played, to some extent, by the terms $\Delta x_i^2\Delta x_j$ and $\Delta x_i\Delta x_j^2$.

3. By manipulating the particular composition of the coefficients in the matrices $\left[\Delta\mathbf{x}(t)\Delta\mathbf{x}(t)^{\text{T}}\right]$ and $\mathbf{R}$, one can obtain different control laws with different sets of the combinational components.

4. Using the local optimization method by the performance functional (4.2) allows preserving all its advantages discussed in Section 3.

According to the analysis results [3–9], the mathematical apparatus of the local version of the statistical theory of optimal control with minimizing quadratic-biquadratic performance functionals is preferable to satisfy the set of requirements listed in [26]. This apparatus implements a wide range of control laws jointly the best in terms of accuracy and control costs.

5. INVERSE DYNAMICS PROBLEMS

There exists an entire class of control problems in which the control design procedure cannot be reduced to minimizing a certain rigorously defined performance functional. In particular, the matter concerns control problems with a natural global criterion reflecting, correctly and completely, the problem content. Here, the control objective is often to maintain definite relations between certain components of the state vector of plants. These relations usually describe the normal operation conditions of the plant or the nature of its transients.

Recently, control design methods based on the concept of inverse dynamics problems (IDP) have become widespread to solve such problems [13, 14]. The problem of implementing some model reference trajectory of a controlled system was among the first research works that underlined the development of the IDP method [15]. There are several known techniques and methods for solving control problems based on this method [16–18]. As was demonstrated in [18], the structural properties of control algorithms for linear systems are completely identical to those of the algorithms obtained by the classical analytical design theory with quadratic performance functionals.

Consider the IDP method to determine whether it meets the requirements for control design methods in guidance problems [26].

Let the mathematical model of a controlled observable dynamic system be described by a differential operator

$$\dot{\mathbf{x}}_{\text{int}}(t) = \mathbf{f}(\mathbf{x}_{\text{int}}(t), \mathbf{u}(t), \mathbf{a}(t), \mathbf{s}_{\text{int}}(t), t), \tag{5.1}$$

where $\mathbf{x}_{\text{int}}(t) = [x_{\text{int}1}(t), \ldots, x_{\text{int}n}(t)]^{\text{T}}$ denotes the n-dimensional state vector of the system;

$\mathbf{a}(t) = [a_1(t), \ldots, a_p(t)]^{\text{T}}$ is the p-dimensional vector of parameters;

$\mathbf{u}(t) = [u_1(t), \ldots, u_r(t)]^{\text{T}}$ stands for the r-dimensional vector of control functions;

$\mathbf{s}_{\text{int}}(t) = [s_{\text{int}1}(t), \ldots, s_{\text{int}n}(t)]^{\text{T}}$ is the n-dimensional vector of controlled exogenous disturbances representing a given time-varying function from the space L_2.

By assumption, the vector function $\mathbf{f}(\mathbf{x}_{\text{int}}(t), \mathbf{u}(t), \mathbf{a}(t), \mathbf{s}_{\text{int}}(t), t)$ is continuous and differentiable with respect to all the variables $\mathbf{x}_{\text{int}}, \mathbf{u}, \mathbf{a}, \mathbf{s}_{\text{int}}$.

It is required to find a control law $\mathbf{u}(t)$ optimizing the performance functional

$$I = \int_{t_0}^{t} L(\mathbf{x}_{\text{int}}(t), \mathbf{x}_{\text{tar}}(t), \mathbf{u}(t), \mathbf{s}_{\text{int}}(t), t)dt, \tag{5.2}$$

where $L(\mathbf{x}_{\text{int}}(t), \mathbf{x}_{\text{tar}}(t), \mathbf{u}(t), \mathbf{s}_{\text{int}}(t), t)$ is a scalar nonnegative function. The terminal time t (control termination) can be given or arbitrary. The coordinates $\mathbf{x}_{\text{int}}(t)$ and $\mathbf{x}_{\text{tar}}(t)$ must satisfy some hypersurface constraints [16]:

$$\mathbf{C}(\mathbf{x}_{\text{int}}, \mathbf{x}_{\text{tar}}) = 0. \tag{5.3}$$

If the relation (5.3) fails as the result of disturbances or nonzero initial conditions, the controlled object, due to its inertia, will tend to this hypersurface according to the expression

$$\lim_{t\to\infty} \mathbf{C}(\mathbf{x}_{\text{int}}, \mathbf{x}_{\text{tar}}) = 0. \tag{5.4}$$

In formulas (5.3) and (5.4), the function $\mathbf{C}(\mathbf{x}_{\text{int}}, \mathbf{x}_{\text{tar}})$ is an r-dimensional vector function with a continuous derivative with respect to its arguments and ∞ indicates the transient time of the plant.

In the general case, the law of vanishing of the function $\mathbf{C}(\mathbf{x}_{\text{int}}, \mathbf{x}_{\text{tar}})$ in (5.4) can be considered the solution of the equation

$$\boldsymbol{\psi}_1 \left[\lambda_i, \dot{\mathbf{C}}(\mathbf{x}_{\text{int}}, \mathbf{x}_{\text{tar}}), \ddot{\mathbf{C}}(\mathbf{x}_{\text{int}}, \mathbf{x}_{\text{tar}}), \ldots, \mathbf{C}^{(k)}(\mathbf{x}_{\text{int}}, \mathbf{x}_{\text{tar}})\right] = \boldsymbol{\psi}_2 \left[\beta, \dot{\mathbf{C}}(\mathbf{x}_{\text{int}}, \mathbf{x}_{\text{tar}})\right], \quad i = \overline{1,k}, \tag{5.5}$$

where λ_i and β are arbitrary constant numbers making the solution of (5.5) stable; i corresponds to the number of the constant coefficient specifying the weight of the kth derivative of the constraint (5.3) or (5.4); finally, $\boldsymbol{\psi}_1[\bullet]$ and $\boldsymbol{\psi}_2[\bullet]$ are r-dimensional (generally nonlinear) vector functions. However, in many engineering applications, the functions $\boldsymbol{\psi}_1[\bullet]$ and $\boldsymbol{\psi}_2[\bullet]$ in equation (5.5) can be described by the relations

$$\begin{aligned} \boldsymbol{\psi}_1[\bullet] &= \mathbf{C}^{(k)}(\mathbf{x}_{\text{int}}, \mathbf{x}_{\text{tar}}) + \lambda_{k-1}\mathbf{C}^{(k-1)}(\mathbf{x}_{\text{int}}, \mathbf{x}_{\text{tar}}) + \ldots + \lambda_1\dot{\mathbf{C}}(\mathbf{x}_{\text{int}}, \mathbf{x}_{\text{tar}}), \\ \boldsymbol{\psi}_2[\bullet] &= \beta_0\mathbf{C}(\mathbf{x}_{\text{int}}, \mathbf{x}_{\text{tar}}) \quad \text{or} \quad \boldsymbol{\psi}_2[\bullet] = \beta_0\mathbf{C}(\mathbf{x}_{\text{int}}, \mathbf{x}_{\text{tar}}) + \beta_2\mathbf{C}^3(\mathbf{x}_{\text{int}}, \mathbf{x}_{\text{tar}}). \end{aligned} \tag{5.6}$$

The coordinates of the n-dimensional vector $\mathbf{x}_{\text{tar}}(t)$ by their physical nature either coincide with the vector $\mathbf{x}_{\text{int}}(t)$ or represent some combination of its components.

The control $\mathbf{u}(t)$ must be defined as a function of the state coordinates of system (5.1) and the coordinates of the desired trajectory. The interception problem can be represented as the collection of two motions in the horizontal and vertical planes. Therefore, we consider the application of the control design method in a single plane under a single (scalar) control signal.

Scalar control action

The exogenous disturbance $\mathbf{s}_{\text{int}}(t)$ in (5.1) is a given time-varying function, and all its components are controlled.

Consider the case when system (5.1) can be written as the system of linear equations

$$\dot{\mathbf{x}}(t) = \mathbf{F}\mathbf{x}(t) + \mathbf{B}u(t) + \mathbf{s}_{\text{int}}(t), \tag{5.7}$$

where $\mathbf{F} = \|f_{ij}\|$ is a square matrix of dimensions $n \times n$ with known elements; $\mathbf{B}$ is the column vector of control coefficients in each system equation; the exogenous disturbance $\mathbf{s}_{\text{int}}(t)$ is a given time-varying function, and all its components are controlled; finally, $u(t)$ is the scalar control action.

Note that the number of controlled coordinates of the vector $\mathbf{x}(t)$ in the steady-state mode (hence, the dimension of the vector $\mathbf{C}(\mathbf{x}_{\text{int}}, \mathbf{x}_{\text{tar}})$) is determined by the dimension of the control vector. Then, without loss of generality, system (5.7) can be supposed equivalent to the scalar differential equation

$$\dot{x}^{(n)}_{\text{int}1}(t) + \sum_{i=0}^{n-1} \alpha_i x^{(i)}_{\text{int}1}(t) = \sum_{j=0}^{r} b_j u^{(j)}(t) + \sum_{l=0}^{n} k_l s_{\text{int}l}(t), \tag{5.8}$$

where $x_1(t)$ is the output coordinate of system (5.7); k_l is the weight of the disturbances $s_{\text{int}l}$.

For the sake of definiteness, let the function $\mathbf{C}(\mathbf{x}_{\text{int}}, \mathbf{x}_{\text{tar}})$ have the form

$$\mathbf{C}(\mathbf{x}_{\text{int}}, \mathbf{x}_{\text{tar}}) = x_{\text{int}1}(t) - x_{\text{tar}1}(t). \tag{5.9}$$

The solution of this problem will be found from the condition that $\mathbf{C}(\mathbf{x}_{\text{int}}, \mathbf{x}_{\text{tar}})$ vanishes according to some law:

$$\lim_{t\to\infty} \mathbf{C}(\mathbf{x}_{\text{int}}, \mathbf{x}_{\text{tar}}) = 0.$$

Moreover, the law $\mathbf{C}(\mathbf{x}_{\text{int}}, \mathbf{x}_{\text{tar}})$ can be defined by any differential operator, e.g., (5.6):

$$\mathbf{C}^{(n)}(\mathbf{x}_{\text{int}}, \mathbf{x}_{\text{tar}}) + \lambda_{n-1} \times \mathbf{C}^{(n-1)}(\mathbf{x}_{\text{int}}, \mathbf{x}_{\text{tar}}) + \ldots + \lambda_0 \times \mathbf{C}(\mathbf{x}_{\text{int}}, \mathbf{x}_{\text{tar}}) = 0, \tag{5.10}$$

where λ_j, $j = 0, 1, \ldots, n-1$, are any positive numbers making system (5.6) stable.

Substituting (5.8) into (5.10) yields the following rth-order differential equation for $u(t)$:

$$b_r u^{(r)}(t) + b_{r-1} u^{(r-1)}(t) + \ldots + b_0 u(t) = z(t), \tag{5.11}$$

where $z(t) = \sum_{i=0}^{n-1} \alpha_i x^{(i)}_{\text{int}1}(t) - \sum_{j=0}^{n-1} \lambda_j (x_{\text{int}1} - x_{\text{tar}1}) + x^{(n)}_{\text{tar}1}(t) - \sum_{l=0}^{n} k_l s_{\text{int}l}(t)$.

The most interesting case is when the components of the vector $\mathbf{B}$ in equation (5.7) equal zero, except the last one. Then the control action satisfying (5.11) is given by

$$\begin{aligned} u(t) = b_0^{-1} &\left[-\sum_{j=0}^{n-1} \lambda_j x^{(j)}_{\text{int}1}(t) + \sum_{i=0}^{n-1} \alpha_i x^{(i)}_{\text{int}1}(t) + \sum_{j=0}^{n-1} \lambda_j x^{(j)}_{\text{tar}1}(t) \right] \\ &- b_0^{-1} \left[\sum_{l=0}^{n} k_l s_{\text{int}l}(t) - x^{(n)}_{\text{tar}1}(t) \right]. \end{aligned} \tag{5.12}$$

In this expression, $\lambda_n = 1$.

Consider in detail the peculiarities of the controlled process under the control action given by equation (5.11) or (5.12). Let the parameters α_j, $j = 0, 1, \ldots, n-1$, and b_i, $i = 0, 1, \ldots, r$, of system (5.7) be known exactly; then the controlled process satisfies the equation

$$x^{(n)}_{\text{int}1}(t) + \sum_{j=0}^{n-1} \lambda_j x^{(j)}_{\text{int}1}(t) = \lambda_0 x_{\text{int}1}(t) + \sum_{j=0}^{n-1} \lambda_j x^{(j)}_{\text{tar}1}(t). \tag{5.13}$$

In matrix form, it can be written as

$$\dot{\mathbf{x}}_{\text{int}}(t) = \mathbf{A}_\lambda \mathbf{x}(t) + \mathbf{B}_\lambda \mathbf{x}_{\text{tar}}(t). \tag{5.14}$$

Due to (5.13) and (5.14), the properties of the controlled process are uniquely determined by the coefficients λ_j regardless of the properties of the original system. The reason is that $\mathbf{A}_\lambda$ represents a Frobenius matrix with the last row defined by the coefficients $\lambda_j,\ j = 0, 1, \ldots, n-1$.

The unknown coefficients $\lambda_j,\ j = 0, 1, \ldots, n-1$, are obtained from the necessary conditions for the optimality of the performance functional (5.2).

Note in conclusion that the control $u(t)$ designed by this method is a function of the state coordinates $\mathbf{x}_{\text{int}}$ and $\mathbf{x}_{\text{tar}}$ and the parameters $\lambda_j,\ j = 0, 1, \ldots, n-1$. In addition, for the nonlinear system, the mathematical model of the controlled process is also described by equation (5.14), i.e., the equation of the desired process.

The analysis of this control design method as applied to HSA interception shows the following:

— First, it allows assessing the possibility of forming control laws for both fixed and current guidance time.

— Second, the IDP method allows designing both linear and nonlinear laws by using different functions: $\boldsymbol{\psi}_2[\bullet] = \beta_0 \mathbf{C}(\mathbf{x}_{\text{int}}, \mathbf{x}_{\text{tar}})$ for linear control and $\boldsymbol{\psi}_2[\bullet] = \beta_0 \mathbf{C}(\mathbf{x}_{\text{int}}, \mathbf{x}_{\text{tar}}) + \beta_2 \mathbf{C}^3(\mathbf{x}_{\text{int}}, \mathbf{x}_{\text{tar}})$ for linear cubic control. As a result, the carrier is withdrawn from stability loss bounds.

— Third, the control laws can be either time-invariant or time-varying, which is determined by the mathematical models (5.1)–(5.7) and the type of target maneuvering, stemming from the control laws (5.11) and (5.12).

— Fourth, in view of (5.14), the closed-loop control system has the required properties regardless of the control law: it is described by a linear differential equation and provides the achievable requirements for stability, overshoot, and robustness to a priori errors of no more than 30%.

The method implements target interception in a given fixed time if the interception trajectory is represented as a straight line and an arc with a known radius.

In addition, the control laws designed by the IDP method require reasonable computational resources for their real-time implementation.

6. ANALYSIS OF CAPABILITIES TO OPTIMIZE THE INFORMATION SUPPORT OF GUIDANCE METHODS

Information support, which reduces estimating the relative and absolute motion coordinates of the target and interceptor motion in guidance methods, is a prerequisite of their implementation [26]. According to the review of guidance methods [2, 4, 27], it is generally required to obtain the following estimates in each control plane: range, approach speed, target's relative bearing, target's LoS angle rate, and its derivatives.

The necessary conditions determining the capability of forming these estimates are given by the observability criterion [2, 3] based on the relationships between the original state models (2.1), (2.2), and (2.3). As applied to linear systems, this criterion has the form

$$\operatorname{rank}\left[\mathbf{H}^{\mathrm{T}} \left| \mathbf{F}^{\mathrm{T}}\mathbf{H}^{\mathrm{T}} \right| \left(\mathbf{F}^{\mathrm{T}}\right)^2 \mathbf{H}^{\mathrm{T}} \left| \ldots \right| \left(\mathbf{F}^{\mathrm{T}}\right)^{N-1} \mathbf{H}^{\mathrm{T}} \right] = N = 2n, \tag{6.1}$$

where $\mathbf{F}$ is the dynamic matrix of the generalized state vector used in (2.3).

The physical meaning of (6.1) is that N independent equations with N unknowns can be obtained based on (2.1), (2.2), and (2.3) to relate the measurements to the estimates uniquely.

In the applied sense, along with establishing the very capability of designing filtering algorithms, the criterion (6.1) allows determining the set of measurement sensors to estimate the state vector. In addition, due to (6.1), the zero derivatives of the state vector should at least be measured to solve this problem [4]. As applied to the guidance problem, the range and relative bearing of the target should at least be measured.

Note that different state coordinates contribute differently to the guidance errors. As demonstrated by the studies [2, 28], the estimation errors of angular coordinates affect the homing accuracy by an order of magnitude or more than the estimation errors of the range and its derivatives.

Various approaches to selecting the information support optimization procedure are possible, depending on the antenna system.

The first approach is based on adaptive analog-discrete filtering algorithms.

The second involves multistage filtering.

The third one is to transform input signals in order to optimize the use of a given mechanically controlled antenna actuator.

The fourth approach is based on tracking systems with a nonlinear dependence on tracking errors that optimizes them by the minimum of a local quadratic-biquadratic performance functional. For details, see Section 4.

The theoretical foundations of these approaches, as well as particular estimation algorithms and research results concerning their effectiveness, were discussed in detail in [3, 4, 28].

There exist three reasons for using analog-discrete filtering:

— the necessity to generate a trajectory control signal for the interceptor continuously;

— the discrete and non-simultaneous arrival of measurements generated by sensors of various physical nature (e.g., radars and airborne signal systems) at the estimation algorithm;

— the unavailability of the state models reflecting adequately the complex spatial maneuvers of HSA, which predetermines the divergence of traditional Kalman filters and the necessity to apply different adaptation schemes.

Analog-discrete filtering includes extrapolation carried out with a small step τ, approaching the analog prediction by accuracy and providing a continuous control signal formation mode of the carrier, and correction carried out with a sufficiently large interval $T \gg \tau$ at the arrival instants of measurements.

In the general case, for processes described by

$$\mathbf{x}(k) = \mathbf{\Phi}(k, k-1)\mathbf{x}(k-1) + \boldsymbol{\xi}_x(k-1) \tag{6.2}$$

under available measurements

$$\mathbf{z}(k) = \mathbf{Q}_z \left[\mathbf{H}(k)\mathbf{x}(k) + \xi_z(k)\right], \tag{6.3}$$

$$\mathbf{Q}_z(k) = \begin{cases} \mathbf{E} & \text{for } k = nT/\tau,\ n = 1, 2, 3, \dots \\ 0 & \text{for } k \neq nT/\tau, \end{cases}$$

adaptive analog-discrete filtering algorithms [3] yield the estimates

$$\hat{\mathbf{x}}(k) = \mathbf{x}_{\mathrm{e}}(k) + \mathbf{K}_{\mathrm{fa}}(k)\Delta\mathbf{z}(k), \quad \hat{\mathbf{x}}(0) = \mathbf{x}_0, \tag{6.4}$$

$$\Delta\mathbf{z}(k) = \mathbf{z}(k) - \mathbf{Q}_z(k)\mathbf{H}(k)\mathbf{x}_{\mathrm{e}}(k), \tag{6.5}$$

$$\mathbf{x}_{\mathrm{e}}(k) = \mathbf{\Phi}(k, k-1)\hat{\mathbf{x}}(k-1) + \mathbf{u}_{\mathrm{fin}}(k), \tag{6.6}$$

$$\mathbf{u}_{\text{fin}}(k) = \begin{cases} \begin{cases} \mathbf{f}_{\text{pr}}(\Delta\mathbf{z}(k)) & \text{for } k = nT/\tau \text{ if the adaptive correction} \\ & \text{of the prediction results is used} \\ 0 & \text{for } k \neq nT/\tau \end{cases} \\ 0 \quad \text{if the prediction results are not corrected,} \end{cases} \tag{6.7}$$

$$\mathbf{K}_{\text{fa}}(k) = \mathbf{Q}_{\text{int}}(k)\mathbf{D}(k)\mathbf{H}^{\text{T}}(k)\mathbf{D}_z^{-1}(k), \tag{6.8}$$

$$\mathbf{Q}_{\text{int}}(k) = \begin{cases} \begin{cases} \mathbf{f}_{\text{int}}(\Delta\mathbf{z}(k)) & \text{for } k = nT/\tau \text{ if the adaptive correction} \\ & \text{of the residual gains is used} \\ \mathbf{E} & \text{for } k \neq nT/\tau \end{cases} \\ \mathbf{E} \quad \text{if the residual gains are not corrected,} \end{cases} \tag{6.9}$$

$$\mathbf{D}(k) = \begin{cases} [\mathbf{E} - \mathbf{K}_{\text{fa}}(k)\mathbf{H}(k)]\mathbf{D}_{\text{e}}(k) & \text{for } k = nT/\tau \\ \mathbf{D}_{\text{e}}(k) & \text{for } k \neq nT/\tau, \end{cases} \quad \mathbf{D}(0) = \mathbf{D}_0, \tag{6.10}$$

$$\mathbf{D}_{\text{e}}(k) = \mathbf{\Phi}(k, k-1)\mathbf{D}(k-1)\mathbf{\Phi}^{\text{T}}(k, k-1) + \mathbf{D}_x(k-1). \tag{6.11}$$

Here, $\mathbf{\Phi}$ is the internal connection matrix of (6.2); $\mathbf{Q}_z(k)$ is the matrix of measurement arrival signs; $\mathbf{D}_x$ is the variance matrix of the state noises $\boldsymbol{\xi}_x$ of (6.2); $\mathbf{D}_z$ is the variance matrix of the measurement noises $\boldsymbol{\xi}_z$ of (6.3); $\mathbf{D}$ is the matrix of estimation errors; $\mathbf{u}_{\text{fin}}$ is the prediction correction determined by analyzing the residual $\mathbf{f}_{\text{pr}}(\Delta\mathbf{z}(k))$; $\mathbf{Q}_{\text{int}}$ is the matrix of weights used to correct the residual gain automatically by analyzing $\mathbf{f}_{\text{int}}(\Delta\mathbf{z}(k))$; finally, $\mathbf{E}$ denotes an identity matrix of appropriate dimensions.

The difference between (6.3)–(6.11) and the typical Kalman algorithm lies in two features as follows. The first is that the state extrapolation (6.6) and the computation of the covariance matrix of the prediction errors (6.11) are carried out with a small interval τ whereas the measurements (6.3) and the correction of the estimates $\hat{\mathbf{x}}$ (6.4) with a large interval $T \gg \tau$. Moreover, the second feature predetermines the possibility of using many adaptation techniques and non-simultaneously arriving measurements.

Formulas (6.2)–(6.11) present the two most efficient methods for preventing the divergence of the filtering algorithm (6.3), (6.4) in the case of intensively maneuvering HSA. The first method is based on forming the adaptive prediction correction (6.7); the second one involves the correction (6.9) of the residual gain (6.8). The preference for one of these adaptation schemes depends on the dimension of the target motion model and the set of measurement sensors.

The procedures for calculating the corrections (6.7) and (6.9), including the case of non-simultaneously arriving measurements, were considered in detail in [3].

Note that in the intervals between the arrival of the measurements (6.3), the interceptor control signal is generated based on the prediction results (6.6) for $\mathbf{u}_{\text{fin}} = 0$. During this time, the prediction error is accumulated due to the mismatch between the HSA real flight and its model (6.2). Two operations are executed when the measurements (6.3) from any sensor arrive at the instants corresponding to $n = 1, 2, 3, \ldots$.

The first operation is to calculate the adaptive corrections (6.7) of the prediction (6.6) by changing the residual (6.5) or the correction (6.9) that tunes its weight; the calculation rules were described in [3, 28].

The second operation is intended to generate the estimate (6.4) under the adaptation method selected. In this case, the real estimation accuracy is somewhat worse than the potential one (6.10), (6.11), but the estimates are stable for HSA with complex maneuvers.

In addition to the adaptive prediction correction (6.7) or the correction (6.9) of the residual gain, discussed in [4], a rather effective filtering method is to identify the parameters $\mathbf{\Phi}(k, k-1)$ (6.2)

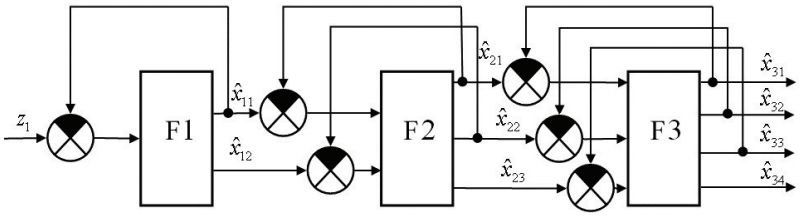

The functional diagram of the three-stage filter of the fourth order.

of the original state model. However, while providing an efficient adaptation of the model to the application conditions, this method has significantly higher computational costs [28].

Estimating the range, approach speed, and its derivatives from the independent measurements of range (the delay time of reflected signals) and speed (the Doppler frequency) is not difficult. At the same time, a rather complex problem is to estimate relative bearing, LoS angle rate, and its derivatives from the measurements of angles only.

Here, one of the simplest solutions is multistage filtering [4]. The measurements are supplied to the input of a multistage filter. It represents a set of serially connected filters of ascending dimension ($n \geqslant 2$) in which a current filter generates estimates used in the next filter as measurements. As a result, the number of feedback loops increases, thereby improving the stability and accuracy of the derivatives estimates.

The operation principles of this method are explained on the example of a three-stage filter of the fourth order and one measurement sensor. Its functional diagram is presented in the figure with the following notations: F1 is the filter's first stage, which forms the estimates $\hat{x}_{11}$ and $\hat{x}_{12}$ from the measurement z_1 and passes them to the second stage as measurements; F2 is the filter's second stage, which forms the estimates $\hat{x}_{21}, \hat{x}_{22}$, and $\hat{x}_{23}$ and passes them to the third stage as measurements; F3 is the filter's third stage, which forms the estimates $\hat{x}_{31}, \hat{x}_{32}, \hat{x}_{33}$, and $\hat{x}_{34}$ and passes them to the user.

The effectiveness of the multistage filtering method was validated in [4], where the angle and its derivatives up to the fourth order were stably estimated as an illustrative example with a single measurement sensor.

7. CONCLUSIONS

The material presented in this paper leads to the following findings.

The requirements for ways to optimize guidance methods to HSA [26], including the need to design time-varying control laws in a given area of application conditions under current constraints and implementability conditions, and the results of previous studies have been considered as a basis to assess the capabilities of various optimization methods for designing interceptor's control laws.

In particular, the following approaches have been assessed:

- the classical optimal control theory in the Letov–Kalman formulation;
- local optimization methods, including those with real and virtual disturbances;
- local optimization by quadratic-biquadratic performance functionals;
- the concept of inverse dynamics problems;
- ways to provide the information support of guidance methods designed.

According to the comparative analysis results, the local optimization method by the minimum of quadratic-biquadratic performance functionals and the method based on inverse dynamics problems have the best capabilities according to the set of requirements.

In future papers, we will assess the capabilities of gradient-based optimization and the so-called intelligent control methods.

In addition, examples of designing particular guidance methods within the most appropriate optimization approaches will be presented.

In conclusion, an important aspect should be emphasized. When several optimization methods are used, the problem of a qualified choice of the best result arises inevitably. In the simplest case, this choice is made by comparing performance and survivability indicators. The so-called foresight concept [29] can be adopted for a more justified choice. This concept allows automating the choice of the best alternative based on many heterogeneous tactical, economic, and technological attributes.

REFERENCES

1. Verba, V.S., Kapustyan, S.G., Merkulov, V.I., and Kharkov, V.P., Optimisation of Radio-Electronic Control Systems. Synthesis of Optimal Control, *Information-Measuring and Control Systems*, 2012, no. 12, pp. 3–16; 2013, no. 3, pp. 3–18; 2013, no. 11, pp. 3–21.
2. *Aviatsionnye sistemy radioupravleniya* (Aircraft Radio Control Systems), Merkulov, V.I., Ed., Moscow: Zhukovsky Air Force Engineering Academy, 2008.
3. Merkulov, V.I. and Verba, V.S., *Sintez i analiz aviatsionnykh radioelektronnykh sistem upravleniya. Kniga 1* (Design and Analysis of Aircraft Radioelectronic Control Systems. Book 1), Moscow: Radiotekhnika, 2023.
4. Merkulov, V.I. and Verba, V.S., *Sintez i analiz aviatsionnykh radioelektronnykh sistem upravleniya. Kniga 2* (Design and Analysis of Aircraft Radioelectronic Control Systems. Book 2), Moscow: Radiotekhnika, 2023.
5. Roitenberg, Ya.N., *Avtomaticheskoe upravlenie* (Automatic Control), Moscow: Nauka, 1992.
6. Sage, A.P. and White, Ch.C., *Optimum Systems Control*, Prentice-Hall, 1977.
7. Chernous'ko, F.L. and Kolmanovskii, V.B., *Optimal'noe upravlenie pri sluchainykh vozmushcheniyakh* (Optimal Control under Random Perturbations), Moscow: Nauka, 1978.
8. Afanas'ev, V.N., Kolmanovskii, V.B., and Nosov, V.R., *Matematicheskaya teoriya konstruirovaniya sistem upravleniya* (Mathematical Theory of Control Systems Design), Moscow: Vysshaya Shkola, 1998.
9. Krasovskii, A.A., *Sistemy avtomaticheskogo upravleniya poletom i ikh analiticheskoe konstruirovanie* (Automatic Flight Control Systems and Their Analytical Design), Moscow: Nauka, 1973.
10. Galyaev, A.A., Lysenko, P.V., and Rubinovich, E.Y., Optimal Stochastic Control in the Interception Problem of a Randomly Tracking Vehicle, *Mathematics*, 2021, vol. 9, no. 19, art. no. 2386.
11. An, JY., Lee, CH., and Tahk, MJ., A Collision Geometry-Based Guidance Law for Course-Correction-Projectile, *Int. J. Aeronaut. Space Sci.*, 2019, vol. 20, no. 2, pp. 442–458.
12. Su, W., Li, K., and Chen, L., Coverage-Based Cooperative Guidance Strategy against Highly Maneuvering Target, *Aerospace Science and Technology*, 2017, vol. 71, pp. 147–155.
13. Krut'ko, P.D., *Obratnye zadachi dinamiki upravlyaemykh sistem. Lineinye modeli* (Inverse Dynamics Problems of Controlled Systems. Linear Models), Moscow: Nauka, 1987.
14. Krut'ko, P.D., *Obratnye zadachi dinamiki upravlyaemykh sistem. Nelineinye modeli* (Inverse Dynamics Problems of Controlled Systems. Nonlinear Models), Moscow: Nauka, 1988.
15. Petrov, B.N., Krut'ko, P.D., and Popov, E.P., Construction of Control Algorithms as an Inverse Problem of Dynamics, *Dokl. Akad. Nauk SSSR*, 1979, vol. 247, no. 5, pp. 1078–1081.
16. Kharkov, V.P., Structural-Parametric Control Design for Dynamic Systems, *Izv. Akad. Nauk SSSR. Tekh. Kibern.*, 1991, no. 2.
17. Kharkov, V.P., Adaptive Control of Dynamic Systems Based on Inverse Dynamics Problems, Izv. Ross. Akad. Nauk. Teor. Sist. Upravlen., 1994, no. 4.

18. Merkulov, V.I. and Kharkov, V.P., Synthesis of Control Law of Interception High-Speed & Highly Maneuverable Air Targets, *Information-measuring and Control Systems*, 2017, no. 10, pp. 3–8.

19. *Uglomernye dvukhpozitsionnye passivnye sistemy radiomonitoringa vozdushnogo bazirovaniya* (Angle-Measured Two-Position Passive Airborne Radio Monitoring Systems), Verba, V.S., Ed., Moscow: Radiotekhnika, 2022.

20. Merkulov, V.I., Verba V.S., and Il'chuk, A.R., *Avtomaticheskoe soprovozhdenie tselei v RLS integrirovannykh aviatsionnykh kompleksov. Tom 1* (Automatic Radar Target Tracking in Integrated Aviation Complexes. Vol. 1), Verba, V.S., Ed., Moscow: Radiotekhnika, 2018.

21. Song, F., Li, Y., Cheng, W., et al., An Improved Kalman Filter Based on Long Short-Memory Recurrent Neural Network for Nonlinear Radar Target Tracking, *Wireless Communications and Mobile Computing*, 2022, no. 7, pp. 1–10.

22. Prokhorov, M.B. and Saul'ev, V.K., The Kalman–Bucy Method of Optimal Filtering and Its Generalizations, *Journal of Soviet Mathematics*, 1979, vol. 12, no. 3, pp. 354–380.

23. Kuzovkov, N.T., Karabanov, S.V., and Salychev, O.S., *Neprerыvnye i diskretnye sistemy upravleniya i metody identifikatsii* (Continuous and Discrete Control Systems and Identification Methods), Moscow: Mashinostroenie, 1978.

24. Fedunov, B.E., *Bortovye intellektual'nye sistemy takticheskogo urovnya dlya antropotsentricheskikh ob"ektov* (Onboard Intelligent Tactical-Level Systems for Anthropocentric Objects), Moscow: DeLibri, 2018.

25. Vasil'ev, V.I. and Il'yasov, B.G., *Intellektual'nye sistemy upravleniya. Teoriya i praktika* (Intelligent Control Systems. Theory and Practice), Moscow: Radiotekhnika, 2009.

26. Verba, V.S. and Merkulov, V.I., Approaches to Optimizing Guidance Methods to High-Speed Intensively Maneuvering Targets. Part I. Justifying Requirements for Ways to Optimize Guidance Methods, *Autom. Remote Control*, 2024, vol. 85, no. 11, pp. 1108–1112.

27. Merkulov, V.I., Non-stationary Guidance Algorithms, *Aerospace Defense Herald*, 2020, vol. 1, pp. 30–43.

28. *Avtomaticheskoe soprovozhdenie tselei v RLS integrirovannykh aviatsionnykh kompleksov. Tom 2* (Automatic Radar Target Tracking in Integrated Aviation Complexes. Vol. 2), Verba, V.S., Ed., Moscow: Radiotekhnika, 2018.

29. Antsev, G.V., Gaenko, V.P., and Sarychev, V.A., Foresight as a Methodology of Conceptual Analysis Pre-Research Forecasting and Evaluation of Development Directions (Options) Technically Complex System Objects, *Achievements of Modern Radioelectronics*, 2022, vol. 76, no. 11, pp. 25–39.

This paper was recommended for publication by A.A. Galyaev, a member of the Editorial Board

ISSN 0005-1179 (print), ISSN 1608-3032 (online), Automation and Remote Control, 2025, Vol. 86, No. 1, pp. 48–60.

CONTROL IN TECHNICAL SYSTEMS

Hardware-in-the-Loop Simulation of Control System for Vertical Plasma Position in KTM Tokamak

A. E. Konkov[*,a], V. I. Kruzhkov[*,b], E. A. Pavlova[*,c], P. S. Korenev[*,d], B. Zh. Chektybayev[,e], S. V. Kotov[**,f], D. B. Zarva[**,g], and A. A. Zhaksybayeva[**,h]**

[*] *Trapeznikov Institute of Control Sciences, Russian Academy of Sciences, Moscow, Russia*
[**] *The Institute of Atomic Energy of the National Nuclear Center, Kurchatov, Republic of Kazakhstan*
e-mail: [a] konkov@ipu.ru, [b] kruzhkov@ipu.ru, [c] pavlova@physics.msu.ru, [d] pkorenev@ipu.ru, [e] chektybaev@nnc.kz, [f] ksvlondon@mail.ru, [g] zarva@nnc.kz, [h] zhaksybaeva@nnc.kz

Received July 11, 2024
Revised September 13, 2024
Accepted September 20, 2024

Abstract—The article is devoted to the development of a digital control system for the unstable vertical plasma position in the KTM tokamak. A controller with fixed parameters was synthesized using an array of plant models. The synthesized controller ensures the desired control performance and robust stability margins simultaneously for two plant models with varying parameters. A robust stability analysis was carried out. The performance of the system was verified through hardware-in-the-loop (HIL) simulation using a complete nonlinear model of the voltage inverter, taking into account its maximum current and voltage limitations.

Keywords: tokamak, KTM, hardware-in-the-loop simulation, robust controller, LMI

DOI: 10.31857/S0005117925010048

1. INTRODUCTION

Control systems for the vertical plasma position are critically important for the operation of modern D-shaped tokamaks, where the plasma is elongated vertically in the poloidal cross-section [1–4]. The vertical position of the plasma in such tokamaks is inherently unstable, so a feedback control system is employed to provide plasma discharges. The vertical plasma position is controlled via a magnetic field generated by the current in the horizontal field coil (HFC) [5]. The vertical plasma position control system must ensure the stability of the plasma's vertical position and achieve the desired scenario for the vertical plasma position throughout the discharge.

The KTM tokamak (Kazakhstan Tokamak for Material testing) [6, 7] is located in Kurchatov, Kazakhstan. In addition to the HFC, the tokamak uses six poloidal field (PF) coils, a central solenoid (CS) for induction of the plasma current, a toroidal field coil, and a passive stabilization coil for the plasma position. Figure 1 shows the coil arrangement of the KTM tokamak.

The plasma in the tokamak is a non-stationary control plant; in particular, the dynamics of the vertical plasma position can change significantly during a discharge and may vary strongly in discharges with different scenarios. Previously, in [8], models of vertical plasma displacement were calculated for several shots, a control system for the HFC current was synthesized, and estimates of the controllability region for the vertical plasma position were obtained. A new HFC power supply, implemented as a voltage inverter operating in pulse-width modulation (PWM) mode, is planned for commissioning at the KTM tokamak. The goal of this work is to develop and perform hardware-in-the-loop simulation of a digital control system for the vertical plasma position with the new power supply. A static controller is synthesized to provide acceptable control quality and the necessary robust stability margins for the closed-loop control system under two different plasma discharge scenarios.

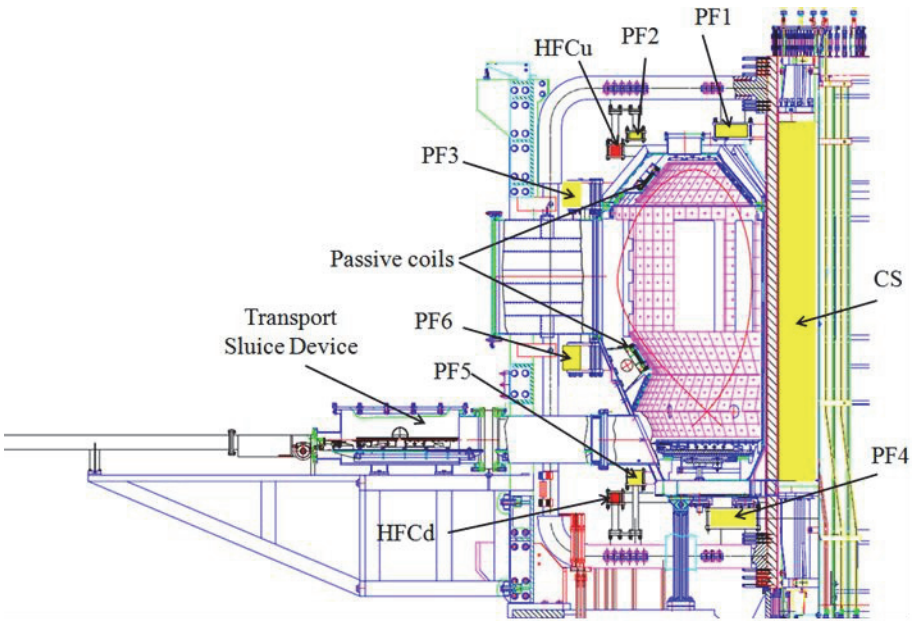

Fig. 1. Cross-section of the KTM tokamak.

Hardware-in-the-loop simulation [9] is an important stage before implementing the developed control system in experimental practice. In this method, the controller operates on real equipment that is functionally identical to what will be used in practice. With sufficiently accurate modeling of the controlled plant, hardware-in-the-loop simulation can guarantee the operability of the developed control system's and reduces implementation costs. This work proposes a methodology for conducting hardware-in-the-loop simulation of a cascade control system for the vertical plasma position and presents its results under various operating modes.

The problem statement, the structural diagram of the synthesized control system, and the description of the plasma models used are provided in Section 2. Section 3 describes the synthesis of the cascade control system for the vertical plasma position. Section 4 presents the analysis of the robust stability margins of the synthesized system in terms of gain and delay. Section 5 includes the results of hardware-in-the-loop simulation of the synthesized control system in normal and extreme operating conditions, enabling the verification of results obtained in Sections 3 and 4. The conclusion summarizes the main findings. The appendix compares the digital control system synthesized directly on the discrete plant model with the discretized system tuned on the continuous model, assuming the same tuning method is used for both, this is the justification for the choice of the control system synthesis method.

2. PROBLEM STATEMENT

The structural scheme of the digital cascade control system for the vertical plasma position in the KTM tokamak is shown in Fig. 2, where Z_{ref} is the reference for the vertical plasma position, Z is the vertical plasma position, $e_Z = Z_{ref} - Z$ is the vertical plasma position error, $I_{HFC\ ref}$ is the reference for the HFC current, I_{HFC} is the HFC current, $e_{I_{HFC}} = I_{HFC\ ref} - I_{HFC}$ is the HFC current error, U_{HFC} is the HFC voltage, and u_{PWM} is the control signal.

The actuator in the control system is a power supply for the HFC, implemented as a voltage inverter operating in PWM mode with the following parameters: three voltage levels $[-1, 0, 1]$ kV; power of 2 MW, corresponding to a maximum current of ± 2 kA; and a PWM frequency of 1 kHz. The voltage inverter consists of an H-bridge and a PWM controller, which converts the control

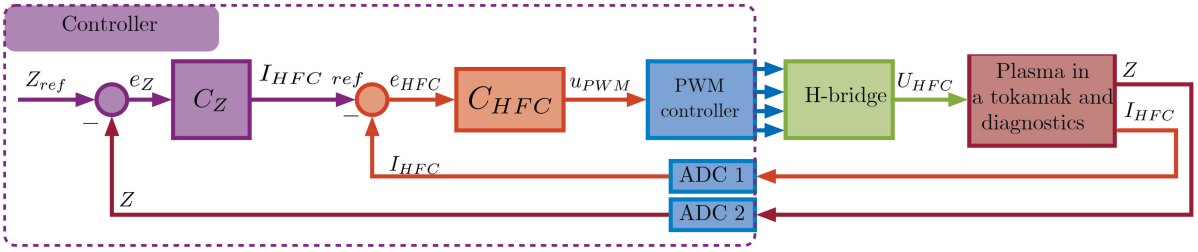

Fig. 2. Block scheme of the digital cascade control system for plasma vertical position in KTM with a voltage inverter in PWM mode.

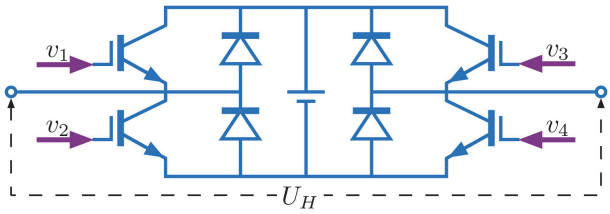

Fig. 3. Schematic diagram of an H-bridge with a DC voltage source.

signal u_{PWM} into pulse sequences v_{1-4} that control the H-bridge transistor gates (Fig. 3). There is no digital-to-analog converter (DAC) in the control system; instead, the PWM controller, as part of the digital control device, directly drives the gates of transistors via optocouplers with its digital outputs v_{1-4}.

The HFC comprises two sections connected in a series-opposing configuration. The voltage and current in the HFC are related by

$$L\dot{I}_{HFC}(t) + RI_{HFC}(t) = U_{HFC}(t),$$

where $R = 212$ mΩ is the HFC resistance, and $L = 17$ mH is the HFC inductance. The discrete transfer function of the HFC is

$$P_{HFC}(z) = \frac{R^{-1}\bigl(1 - \exp(-T_sR/L)\bigr)}{z - \exp(-T_sR/L)}, \quad I_{HFC}(z) = P_{HFC}(z)U_{HFC}(z), \tag{1}$$

where z is the Z-transform variable, and $T_s = 1$ ms is the sampling time.

Models of vertical plasma displacement in the KTM tokamak [8] were obtained from experimental data for two of the most typical plasma shots with a plasma current of 500 kA from the last experimental campaign [10]: shot no. 5121 with an elongation (the ratio of vertical to horizontal plasma diameters) of 1.4 and a normal duration, and shot no. 5126 with an elongation of 1.6 and a short plasma confinement time. These models are represented as linear state-space models with time-varying parameters in discrete time:

$$\begin{cases} x(T_sk + T_s) = A(T_sk)x(T_sk) + B(T_sk)u(T_sk) \\ y(T_sk) = C(T_sk)x(T_sk), \end{cases}$$

where $x = \left[I_{PF}^{\mathrm{T}}\ I_{VV}^{\mathrm{T}}\ I_P\right]^{\mathrm{T}} \in \mathbb{R}^{24\times1}$ is the state vector, $I_{PF} \in \mathbb{R}^{8\times1}$ is the vector of currents in the poloidal field coils (including I_{HFC}), $I_{VV} \in \mathbb{R}^{15\times1}$ are the currents in the vacuum vessel and passive structures, I_P is the plasma current, $u = U_{HFC}$ is the input, and $y = [Z\ I_{HFC}]^{\mathrm{T}}$ is the output vector.

For each vertical plasma displacement model, the set of matrices $\{A, B, C\}$ was calculated with a sampling time of $T_s = 1$ ms:

(1) Model of shot no. 5121 – for 1001 time points from 2.50 to 3.50 s;

(2) Model of shot no. 5126 – for 61 time points from 2.44 to 2.50 s.

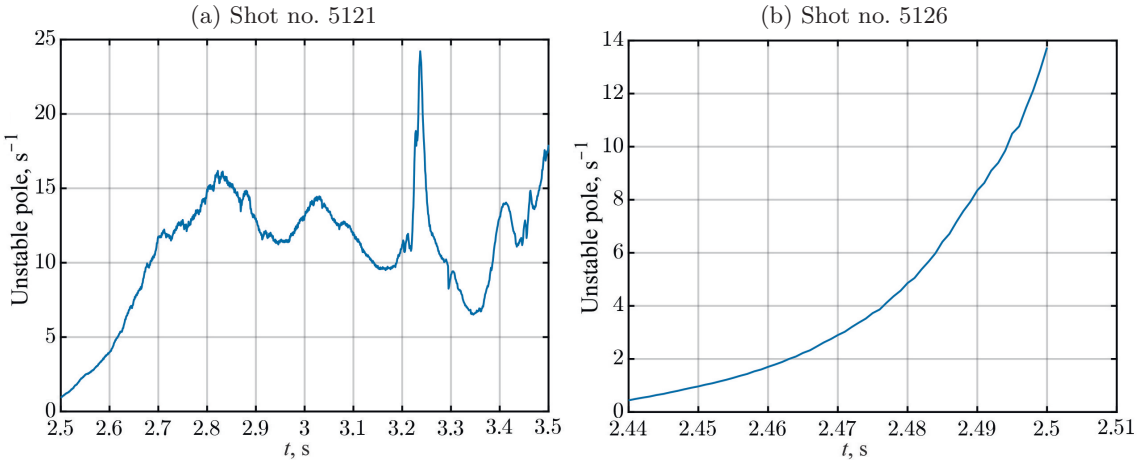

Fig. 4. Change in the magnitude of the single unstable pole of the plasma vertical motion models during the shot.

Both models have one unstable pole that varies significantly during the shot, as shown in Fig. 4. For controller synthesis, an array of discrete transfer functions was computed:

$$P_n(z) = C_n(zI - A_n)^{-1}B_n, \tag{2}$$

where the index n denotes the time point for which the model matrices were calculated: $A_n = A(T_s n)$, $B_n = B(T_s n)$, and $C_n = C(T_s n)$.

The controller must ensure that the control system has the necessary robust stability margin to provide acceptable control quality simultaneously for both vertical plasma displacement models with time-varying parameters. The control system must also have a sufficient phase stability margin to maintain stability when a transport delay of up to 10 ms (10 sampling steps of 1 ms each) is introduced into the feedback loop, which is the upper limit of possible delays in the data acquisition, processing, and transmission system of the KTM tokamak. The delay is modeled by incorporating a discrete transfer function z^{-10} into the feedback loop.

3. CASCADE CONTROL SYSTEM SYNTHESIS

The controllers in both control cascades were synthesized using the method described in [11], which allows for the synthesis of a discrete controller based on a set of discrete plant models and performs loop shaping of the open-loop transfer function. The synthesis is carried out using linear matrix inequalities through a convex-concave procedure. An alternative approach is discussed in the Appendix, where the controller is synthesized based on the continuous-time model of the plant, and then the controller is discretized.

First, the inner current control loop for the HFC is synthesized based on the model (1). The linear model of the voltage inverter was obtained by identifying the serial connection of the HFC and the voltage inverter using the approach described in [12]. As a result, a PI-controller was synthesized with the discrete transfer function

$$C_{HFC}(z) = K_{P_{HFC}} + K_{I_{HFC}}\frac{T_s z}{z-1}, \quad u_{PWM}(z) = C_Z(z)e_{HFC}(z), \tag{3}$$

where $K_{P_{HFC}} = 0.004$ V/A and $K_{I_{HFC}} = 0.15$ V/(A × s). The output of the controller, u_{PWM}, is limited to the range ±1 V, which is determined by the parameters of the PWM controller. The synthesized current control system for the HFC provides the fastest possible performance subject to the limitations of the power supply, which allows the current rise rate in the HFC to reach $U_{\max}/L = 58.8$ kA/s. This control system was used in [8] to estimate the controllability region of the vertical plasma position.

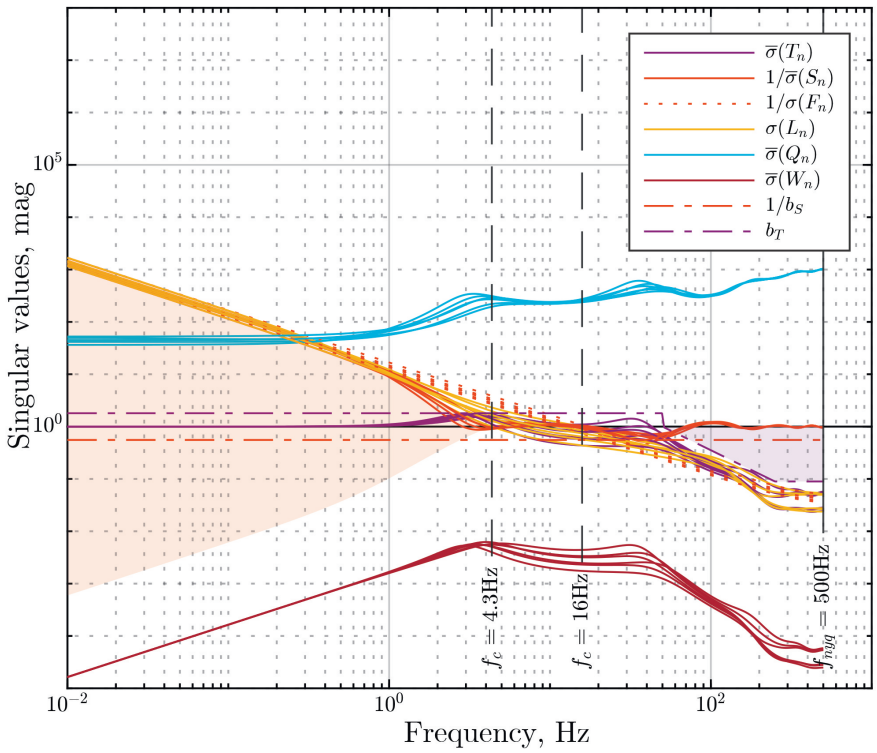

Fig. 5. Bode plot of the transfer functions of the plasma vertical position control system.

The synthesis of the outer control loop was performed on the set of discrete transfer functions of the inner loop: $Z(z) = G_n(z)I_{HFC\ ref}(z)$,

$$G_n(z) = P_n(z)A(z)C_{HFC}(z)\Big(I + P_n(z)A(z)C_{HFC}(z)\Big)^{-1}, \tag{4}$$

where $A(z) = U_{\max} z^{-T_{PWM}/T_s}$ is the linear model of the voltage inverter, $U_{\max} = 1$ kV, $T_{PWM}/T_s = 1$, and n is the index from (2). Thus, one controller will meet the given quality and robust stability criteria simultaneously for both models with variable parameters. As a result, a PID-controller was synthesized with the discrete transfer function

$$C_Z(z) = K_{P_Z} + K_{I_Z}\frac{T_s z}{z-1} + K_{D_Z}\frac{z-1}{T_s z}, \quad I_{HFC\ ref}(z) = C_{I_{HFC}}(z)e_Z(z), \tag{5}$$

where $K_{P_Z} = 245.3276$ A/m, $K_{I_Z} = 3.831$ kA/(m×s), $K_{D_Z} = 0.366$ (A×s)/m. The output $I_{HFC\ ref}$ of the controller, is limited to the range ±2 kA.

The Anti-Windup approach [13] was implemented during the synthesis of the controller to prevent saturation of the controller's output signal and the subsequent internal instability in the control system. In both controllers, a clamping mechanism is used, whereby integration is stopped when the signal at the controller output is outside the set range, and the output and input of the integrator have the same sign.

Figure 5 shows the results of controller synthesis using the method from [11], including the specified shaping functions and singular values of the discrete transfer functions of the synthesized system with models for the time points [3.229; 3.299; 3.449] s from shot model no. 5121 and [2.479; 2.489; 2.5] s from shot model no. 5126.

The open-loop transfer function array is given by

$$L_n(z) = G_n(z)C_Z(z), \quad Z(z) = L_n(z)e_Z(z), \tag{6}$$

where $G_n(z)$ is the array of inner loop transfer functions from (4), and $C_Z(z)$ is the transfer function of the controller (5). The sensitivity function array is given by

$$S_n(z) = \Big(I + L_n(z)\Big)^{-1}, \quad e_Z(z) = S_n(z)Z_{ref}(z),$$

the array of complementary sensitivity functions is

$$T_n(z) = L_n(z)S_n(z), \quad Z(z) = S_n(z)Z_{ref}(z),$$

the array of static and low-frequency sensitivity functions is

$$F_n(z) = \Big(G_n(1)K_{I_Z}T_s\Big)^{-1}(z-1), \text{ for small } \omega, \ z = \exp(j\omega T_s),$$

the array of Q-parameters is

$$Q_n(z) = C_Z(z)S_n(z), \quad I_{HFC\ ref}(z) = Q_n(z)Z_{ref}(z)$$

and the array of transfer functions from external input disturbance to $e_Z(z)$ is

$$W_n(z) = -S_n(z)G_n(z).$$

The specified shaping functions b_S and b_T limit the arrays of transfer functions $S_n(z)$ and $T_n(z)$ over the entire frequency range, ensuring the required robustness and quality margins for the closed-loop control system.

4. ROBUST STABILITY ANALYSIS OF THE PLASMA POSITION CONTROL CASCADE

To calculate the robust stability margins of the closed-loop system, the open-loop transfer function array (6) was used. Figure 6 shows the gain margins, and Fig. 7 shows the delay margins.

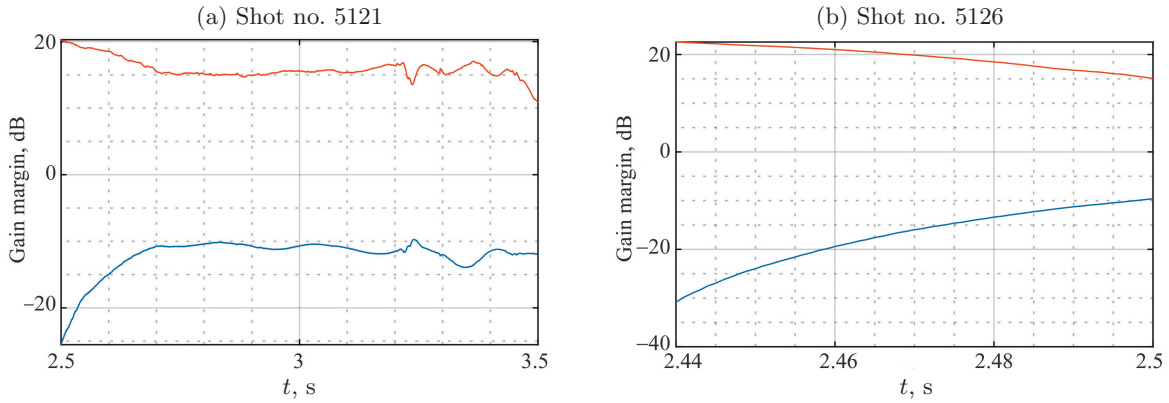

Fig. 6. Gain margin of the linear closed-loop control system.

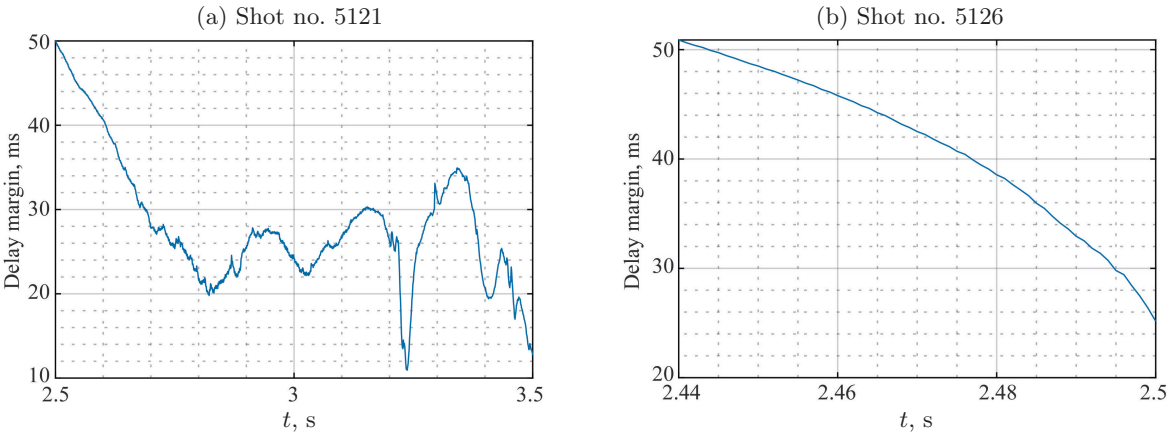

Fig. 7. Delay margin of the linear closed-loop control system.

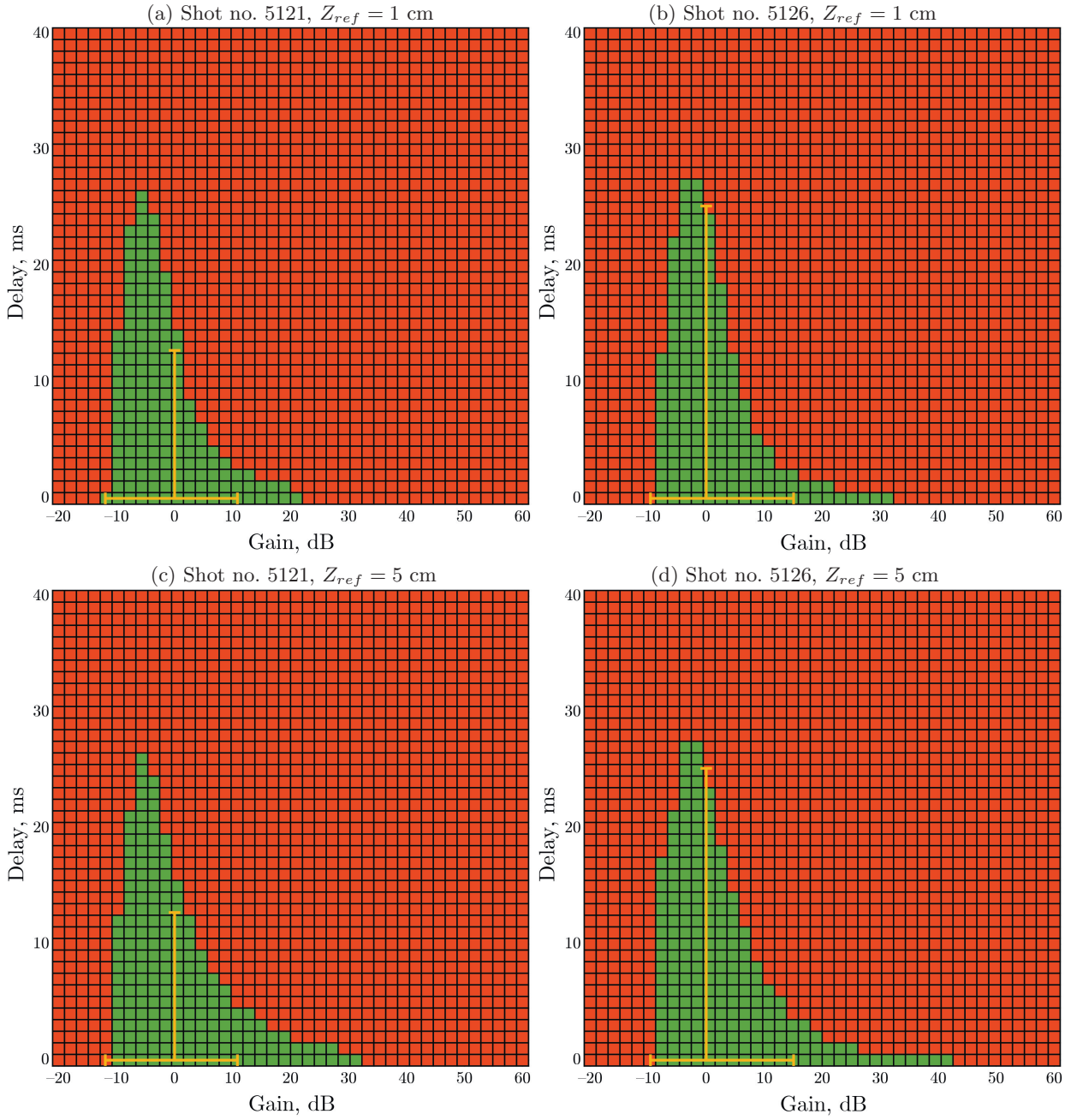

Fig. 8. Robust stability diagram of the nonlinear control system.

The delay margin T_M was calculated using the formula [14]:

$$T_M = \frac{\phi_M}{\omega_c}\frac{\pi}{180^\circ},$$

where ϕ_M is the phase margin, and ω_c is the gain crossover frequency (the frequency at which the open-loop gain first reaches the value 1). In the worst-case scenario, which occurs at the end of both shots, the synthesized control system has a satisfactory gain margin of ±10 dB (Fig. 6). The delay margin (Fig. 7) also exceeds the required 10 ms throughout both shots.

Figure 8 shows the stability diagrams of the nonlinear control system with the full model of the voltage inverter and the plasma vertical displacement model with variable parameters.

The delay and gain in the plasma vertical position feedback loop were varied. The nonlinear system has a limited controllability region, so the larger the reference input Z_{ref}, the smaller its robustness margins. Green indicates situations where the system is asymptotically stable, red indicates instability, and yellow shows the robustness margins of the linear model in the worst-case scenario (Figs. 6 and 7).

5. HARDWARE-IN-THE-LOOP SIMULATION

Hardware-in-the-loop simulation of the digital control system was conducted on the real-time test bed [15] at the Trapeznikov Institute of Control Sciences of RAS on two real-time target machines (RTTM). The structural scheme of the control system for hardware-in-the-loop simulation is shown in Fig. 9.

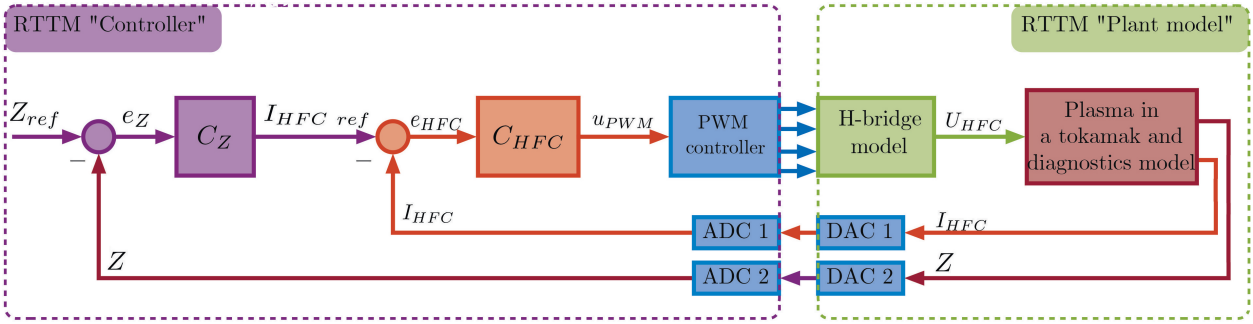

Fig. 9. Block diagram of the digital cascade control system for plasma vertical position in KTM during Hardware-in-the-loop simulation.

The digital controller is implemented on the RTTM "Controller," where, in addition to the controllers of both cascades, there is a PWM controller. This approach eliminates the need for using a DAC, which enhances the system's reliability and performance since the control signal u_{PWM} is not converted to analog. It is not necessary to spend time converting the signal to the DAC, also there is no need to ensure electromagnetic compatibility in the transmission line for the analog signal u_{PWM}, and the cost of implementing the PWM controller in analog form is reduced

On the RTTM "Plant model" is the model of vertical plasma displacement and the H-bridge model with a constant voltage source implemented in Simscape Electrical. The sampling time for the controllers is 1 ms, while the sampling time for the PWM controller, the H-bridge, and the vertical plasma displacement model is 100 μs. The sampling times differ by a factor of 10 to allow the PWM duty cycle to be 10%. If the control system implementation requires even smaller PWM duty cycle, the PWM controller can be implemented on an FPGA.

The concept of hardware-in-the-loop simulation of control systems assumes that part of the system is real, while the other part is represented by a model. In this case, all components of the controller are implemented on the RTTM "Controller." To make the controller functionally analogous to the one that will be used in the real control system (Fig. 2), there are two DACs at the output of the RTTM "Plant model."

5.1. Control System Simulation in Normal Operating Conditions

The results of hardware-in-the-loop simulation of the synthesized system in normal operating condition with a reference for the vertical plasma position of 5 cm are shown in Fig. 10. In addition to the transient process of the vertical plasma position and electrical signals from the power supply

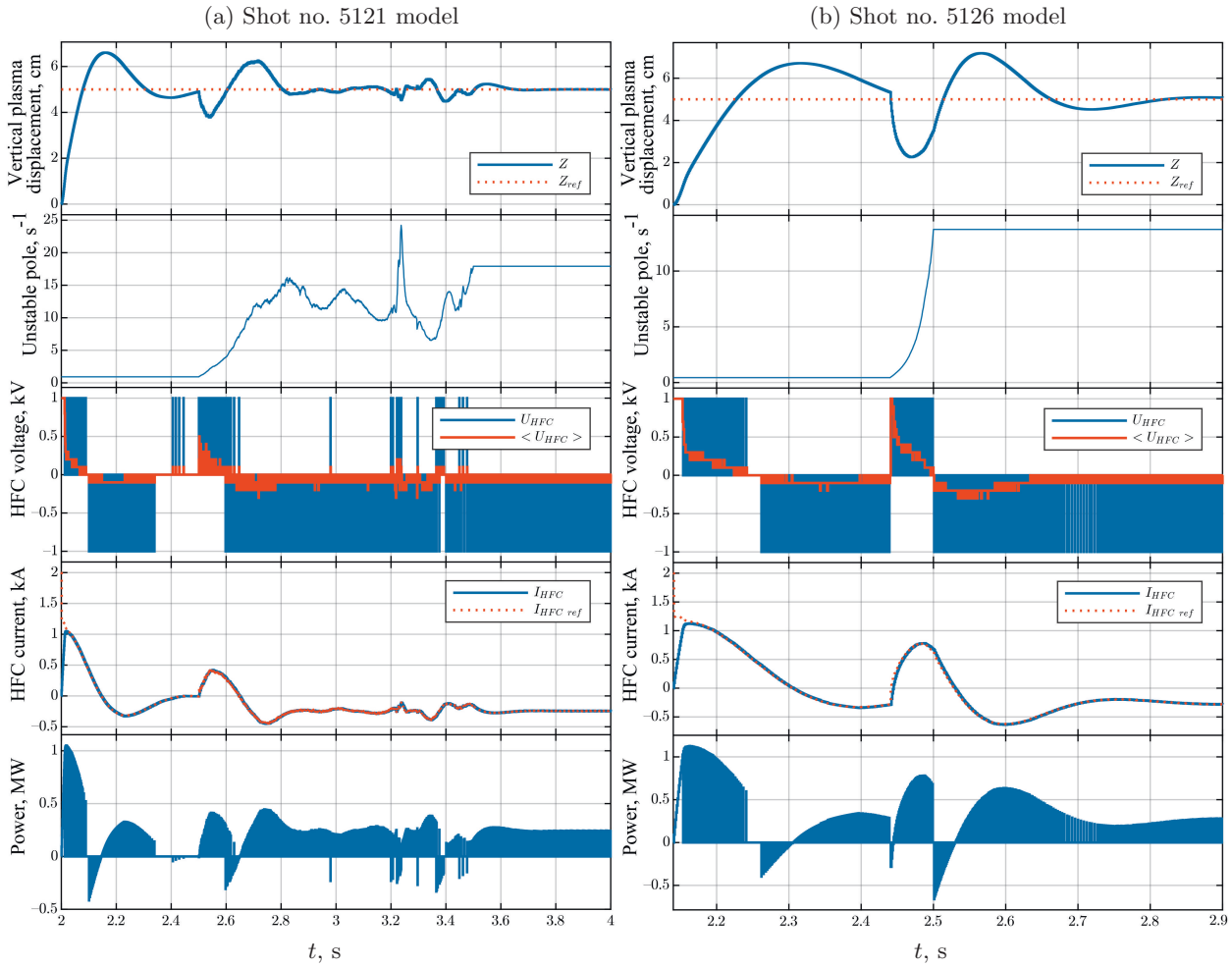

Fig. 10. Simulation of the plasma vertical position control system in KTM. The reference displacement is $Z_{ref} = 5$ cm.

(voltage, current, and power), the change in the unstable pole of the model for each shot is shown. The synthesized controller provides acceptable control quality for both vertical plasma displacement models. The required power of the voltage inverter does not exceed 1.2 MW, with a maximum possible power of 2 MW.

5.2. Control System Simulation in Extreme Operating Conditions

Figure 11 shows the results of hardware-in-the-loop simulation with the maximum vertical plasma displacement, at which the closed-loop system remains stable and provides acceptable control quality, and Fig. 12 shows the results for the maximum possible delay in the feedback loop for vertical plasma displacement. A plasma displacement of more than 10 cm vertically in the tokamak KTM is not required in practice, as this would cause the plasma separatrix to collide with the tokamak limiter. Therefore, the synthesized control system allows the control of vertical plasma position in the KTM tokamak over the entire possible range. In both cases, the delay exceeds the required 10 ms.

In [8], the upper bound of the vertical plasma position controllability region was calculated. For shot no. 5121 it is 23 cm, and for shot no. 5126 it is 26 cm. The actual controllability region for shot no. 5121 is 4 cm larger than the previously estimated value, which is explained by the fact

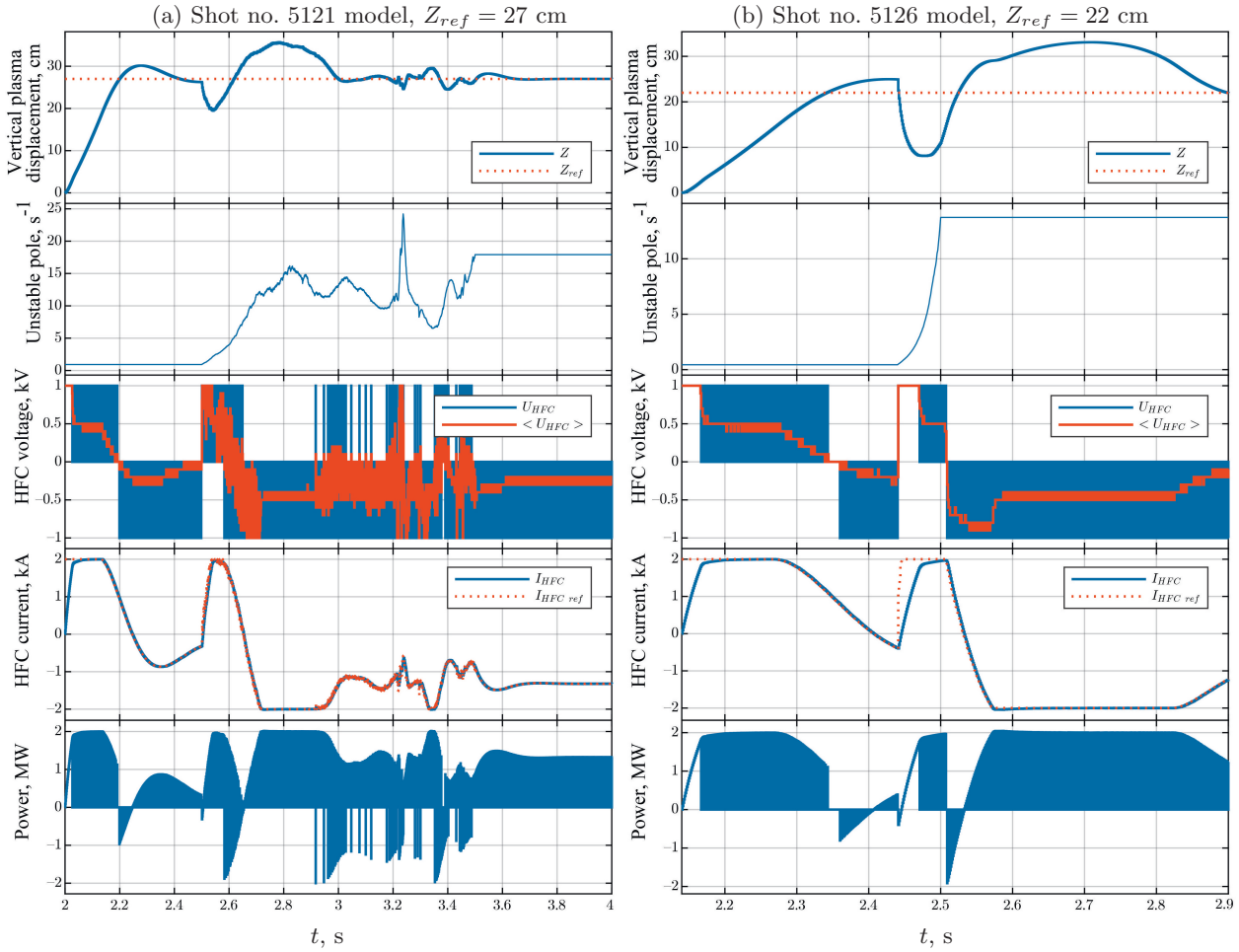

Fig. 11. Simulation of the plasma vertical position control system in KTM. The reference displacement is $Z_{ref} = 5$ cm.

that [8] used a model for one time point of the shot with the highest value of the unstable pole, which is not at the end of the shot, and any potential instability does not have time to develop. This also explains why the maximum delay of 14 ms (Fig. 12a) exceeds the minimum delay margin (Fig. 7a).

6. CONCLUSION

The operability of the control system has been demonstrated through hardware-in-the-loop simulation on two models of vertical plasma displacement, calculated based on experimental data from discharges with different scenarios. The full model of the voltage inverter in PWM mode, accounting for power limitations, was used in the simulation. With sufficient verification of the models used, the hardware-in-the-loop simulation guarantees the functionality of the control system when implemented in practical experiments.

The maximum possible vertical plasma displacement in the synthesized system with a voltage inverter in PWM mode is 27 cm for shot model no. 5121 and 22 cm for shot model no. 5126, which exceeds the actual required range of 10 cm. The maximum possible transport delay in the feedback loop for vertical plasma position, at which stability and acceptable control quality are maintained, is 14 ms for shot model no. 5121 and 23 ms for shot model no. 5126, which also exceeds the required value of 10 ms.

This work used a robust approach, where one controller is synthesized to meet the control quality and robust stability margin criteria simultaneously for multiple models of vertical plasma

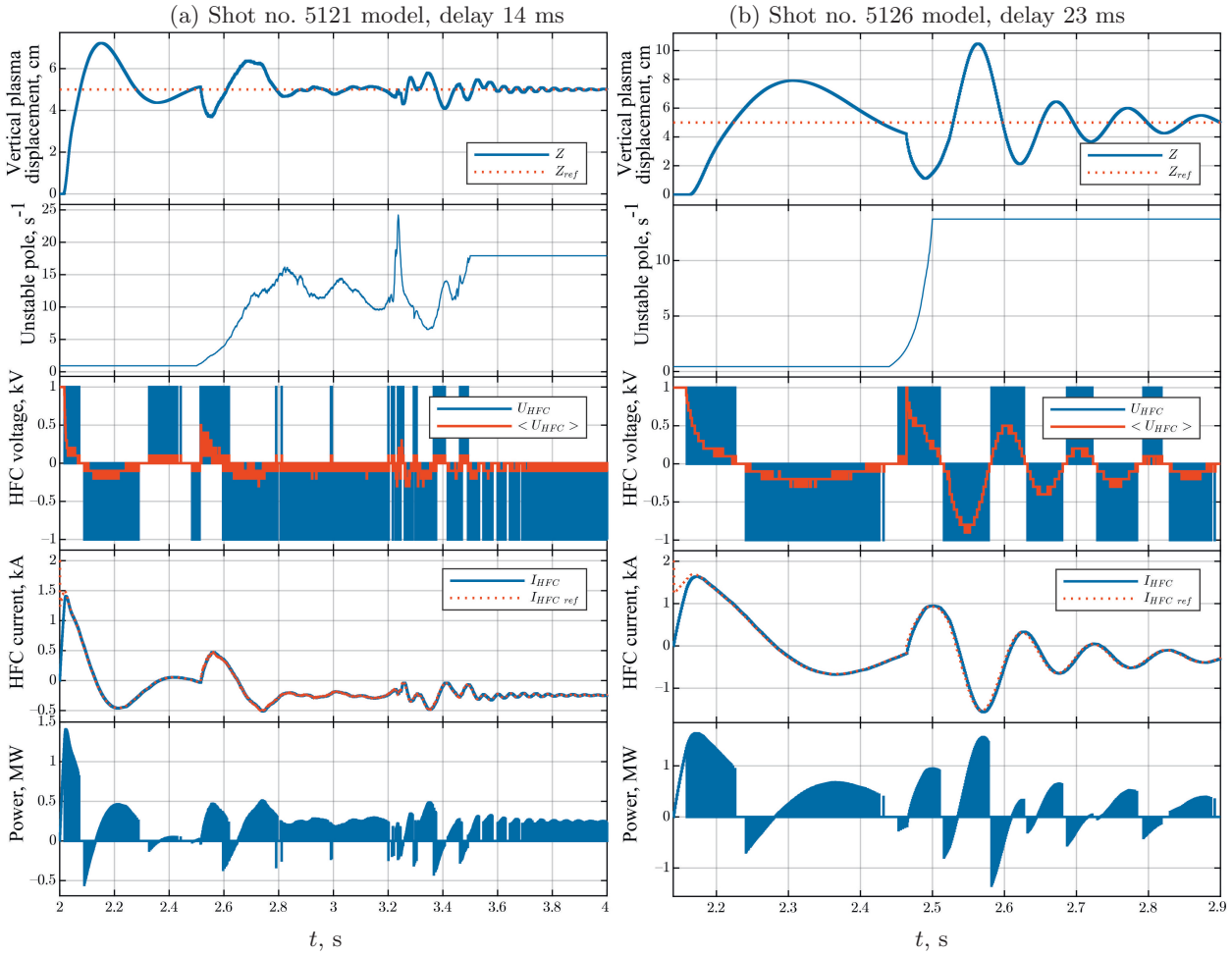

Fig. 12. Simulation of the plasma vertical position control system in KTM with the maximum possible delay in the feedback loop.

displacement. An alternative adaptive approach is possible, where the controller is tuned for a specific scenario or its parameters change during the discharge. The adaptive approach allows for better control quality since, in the case of the robust approach, the control quality is limited by the "worst-case" plant model. In this task, the robust approach is preferred over the adaptive one, as it does not require retuning the controller when the plasma discharge scenario changes.

FUNDING

This work was supported by the Russian Science Foundation project (no. 21-79-20180), as well as by the scientific and technical program IRN no. BR23891779 "Scientific-technical support of experimental research at the Kazakhstan material-testing KTM tokamak" under the program-targeted funding of the Ministry of Energy of the Republic of Kazakhstan.

APPENDIX

COMPARISON OF THE DIGITAL CONTROL SYSTEM WITH DISCRETIZED ANALOG CONTROL SYSTEM

The synthesis method [11] allows for the synthesis of both discrete and continuous control systems. A common approach is to apply a discretized controller in a digital control system. For example, in [16–19], continuous controllers were synthesized for plasma control in a tokamak. To demonstrate the drawbacks of this approach, the following comparison is made.

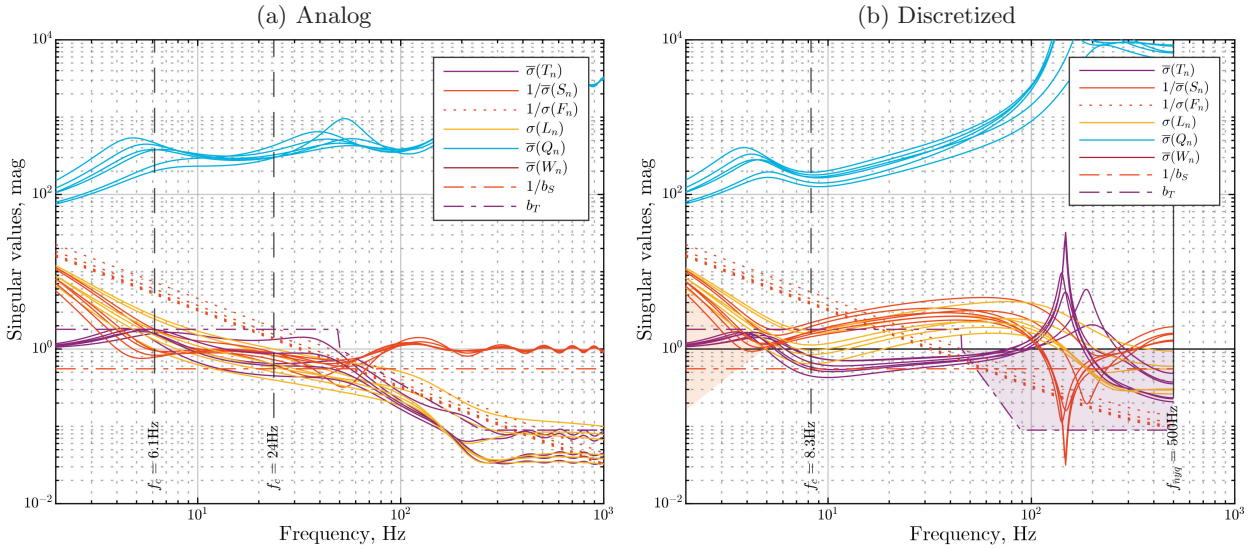

Fig. 13. Bode plot of the transfer functions of the analog and discretized plasma vertical position control system.

Figure 13a shows the result of synthesizing a continuous controller on the plant model in continuous time with the same shaping functions that were used for synthesizing the discrete controller in Section 3. The shaping functions in the synthesis method [11] define the control quality and the robustness margins of the closed-loop system, so the synthesized analog control system has approximately the same control quality and robustness margins as the digital system obtained earlier in Section 3.

The synthesized analog PID controller is given by the transfer function

$$\hat{C}_Z(s) = \hat{K}_{P_Z} + \hat{K}_{I_Z}\frac{1}{s} + \hat{K}_{D_Z}\frac{s}{\tau s + 1},$$

where $\hat{K}_{P_Z} = 266.9$ A/m, $\hat{K}_{I_Z} = 10.3$ kA/(m×s), $\hat{K}_{D_Z} = 0.53$ (A×s)/m, $\tau = 100$ μs, s – Laplace transform variable. After discretizing this controller using the ZOH method, the frequency response of the transfer functions of the discretized system was computed (Fig. 13b). The discretized control system is unstable.

In [20], it is shown that discretization may have little effect on the degradation of control quality and robustness margins, provided the closed-loop bandwidth is at least 30 times smaller than the sampling frequency. The closed-loop bandwidth of the control system varies depending on the shot time from 10 to 79 Hz, which means that the sampling time $T_s = 1$ ms is almost 2.5 times larger than needed to preserve control quality during discretization. Moreover, the plant model is not minimum-phase since it contains delay elements, which also contributes to the loss of stability of the control system during discretization.

REFERENCES

1. Mitrishkin, Y.V., Korenev, P.S., Prokhorov, A.A., et al., Plasma Control in Tokamaks. Part 1. Controlled thermonuclear fusion problem. Tokamaks. Components of control systems, *Advanc. Syst. Sci. Appl.*, 2018, vol. 18, no. 2, pp. 26–52.
2. Mitrishkin, Y.V., Kartsev, N.M., Pavlova, E.A., et al., Plasma Control in Tokamaks. Part 2. Magnetic plasma control systems, *Advanc. Syst. Sci. Appl.*, 2018, vol. 18, no. 3, pp. 39–78.
3. Mitrishkin, Y.V., Kartsev, N.M., Konkov, A.E., et al., Plasma Control in Tokamaks. Part 3.1. Plasma Magnetic Control Systems in ITER, *Advanc. Syst. Sci. Appl.*, 2020, vol. 20, no. 2, pp. 82–97.

4. Mitrishkin, Y.V., Kartsev, N.M., Konkov, A.E., et al., Plasma Control in Tokamaks. Part 3.2. Simulation and Realization of Plasma Control Systems in ITER and Constructions of DEMO, *Advanc. Syst. Sci. Appl.*, 2020, vol. 20, no. 3, pp. 136–152.

5. Ariola, M. and Pironti, A., *Magnetic Control of Tokamak Plasmas*, Springer International Publishing, 2016.

6. Korotkov, V.A., Azizov, E.A., Cherepnin, Yu.S., et al., Kazakhstan Tokamak for Material Testing Conceptual Design and Basic Parameters, *Fusion Engineering and Design*, 2001, vol. 56, pp. 831–835.

7. Zarva, D.B., Deriglazov, A.A., Batyrbekov, E.G., et al., Electrical Power Supply Complex of the Pulse Power System of the KTM Tokamak, *VANT. Ser. Termoyadernyi sintez*, 2018, vol. 41, no. 2, pp. 59–70.

8. Korenev, P.S., Konkov, A.E., Chektibaev, B.Zh., et al., Estimation of the Controllability Region of the Vertical Plasma Position in the KTM Tokamak with the HFC Coil, *VANT. Ser. Termoyadernyi sintez*, 2024, vol. 47, no. 3.

9. Mihalic, F., Truntic, M., and Hren, A., Hardware-in-the-Loop Simulations: A Historical Overview of Engineering Challenges, *Electronics*, 2022, vol. 11, p. 2462.

10. Batyrbekov, E.G., Tajibaeva, I.L., Baklanov, V.V., et al., Research in the field of controlled thermonuclear fusion in the Republic of Kazakhstan, *VANT. Ser. Termoyadernyi sintez*, 2024, vol. 47, no. 2, pp. 15–22.

11. Konkov, A.E. and Mitrishkin, Y.V., Synthesis Methodology for Discrete MIMO PID Controller with Loop Shaping on LTV Plant Model via Iterated LMI Restrictions, *Mathematics*, MDPI Publ., 2024, vol. 12, no. 6, p. 810.

12. Konkov, A.E. and Mitrishkin, Y.V., Comparison Study of Power Supplies in Real-Time Robust Control Systems of Vertical Plasma Position in Tokamak, *IFAC-PapersOnLine*, 2022, vol. 55, no. 9, pp. 327–332.

13. Grimm, G., Hatfield, J., Postlethwaite, I., et al., Antiwindup for stable linear systems with input saturation: An LMI-based synthesis, *IEEE Trans. Automat. Contr.*, 2003, vol. 48, no. 9, pp. 1509–1525.

14. Astrom, K. and Hagglund, T., *Advanced PID control*, ISA-The Instrumentation, Systems, and Automation Society, 2006.

15. Mitrishkin, Y.V., Konkov, A.E., and Korenev, P.S., Real-time Digital Simulation Testbed for Plasma Control in Tokamaks, *Materials of the XVI International Conference on Stability and Oscillations of Nonlinear Control Systems (Piatnitski Conference)*, 2022, pp. 286–289.

16. Mitrishkin, Y.V., Pavlova, E.A., Kuznetsov, E.A., and Gaydamaka, K.I., Continuous, Saturation, and Discontinuous Tokamak Plasma Vertical Position Control Systems, *Fusion Engineering and Design*, 2016, vol. 108, pp. 35–47.

17. Mitrishkin, Y.V., Prokhorov, A.A., Korenev, P.S., and Patrov, M.I., Hierarchical Robust Switching Control Method with the Improved Moving Filaments Equilibrium Reconstruction Code in the Feedback for Tokamak Plasma Shape, *Fusion Engineering and Design*, 2019, vol. 138, pp. 138–150.

18. Kruzhkov, V.I., Tuning of the Plasma Position Control System and Poloidal Currents in the Globus-M2 Tokamak and Its Implementation on the Real-Time Testbed, *Proceedings of the 17th All-Russian School-Conference of Young Scientists "Control of Large Systems"* (UBS'2021, Moscow), Moscow–Zvenigorod: Institute of Control Sciences named after V.A. Trapeznikov RAS, 2021, pp. 704–710.

19. Mitrishkin, Y.V., Korenev, P.S., Konkov, A.E., Kartsev, N.M., and Smirnov, I.S., New Horizontal and Vertical Field Coils with Optimised Location for Robust Decentralized Plasma Position Control in the IGNITOR Tokamak, *Fusion Engineering and Design*, 2022, vol. 174, p. 112993.

20. Franklin, G., Powell, J.D., and Workman, M.L., *Digital Control of Dynamic Systems*, Ellis-Kagle Press, 1997.

This paper was recommended for publication by N.N. Bakhtadze, a member of the Editorial Board

ISSN 0005-1179 (print), ISSN 1608-3032 (online), Automation and Remote Control, 2025, Vol. 86, No. 1, pp. 61–73.

On Guaranteed Estimate of Deviations from the Target Set in a Control Problem under Reinforcement Learning

I. A. Chistiakov

Lomonosov Moscow State University, Faculty of Computational Mathematics and Cybernetics, Moscow, Russia

e-mail: chistyakov.ivan@yahoo.com

Received August 29, 2024

Revised October 14, 2024

Accepted October 29, 2024

Abstract—We consider a target control problem of a special form, in which a system of differential equations includes nonlinear terms depending on state variables. We show that reinforcement learning algorithms such as Proximal Policy Optimization (PPO) can be used to find an inexact feedback solution. The chosen strategy is further approximated with a piecewise affine control. Based on the dynamic programming method, an inner estimate of the solvability set is calculated, as well as a corresponding a priori estimate of the distance between a final trajectory point and the target set. To do this, we examine an auxiliary problem for a piecewise linear system with noise and calculate a piecewise quadratic function as an approximate solution of the Hamilton–Jacobi–Bellman equation.

Keywords: nonlinear dynamics, dynamic programming, comparison principle, linearization, piecewise quadratic value function, reinforcement learning, PPO algorithm, solvability set

DOI: 10.31857/S0005117925010055

1. INTRODUCTION

We consider a target control problem for a nonlinear system of differential equations on a fixed finite time interval. This problem is closely related to construction of the solvability set containing all starting positions from which the control synthesis problem can be solved. To approximate this set, one may use various methods based on analysis of the corresponding differential inclusion [1–3] or depending on the Hamilton–Jacobi–Bellman (HJB) equation [4–7]. These approaches are applicable to a wide class of nonlinear systems, yet they require large computational costs. Recently, algorithms based on machine learning have also been developed, making it possible to approximate solution of the HJB equation with a neural network [8, 9] or to search for the control function directly [10]. However, the latter do not provide any guaranteed estimates.

This paper proposes to reduce computational complexity of solving the HJB equation by searching for an approximate solution in the class of piecewise quadratic functions defined on a set of simplices. We develop the ideas introduced in [11–13] and present a method based on piecewise linearization of the right-hand side of differential equations, considering an auxiliary control problem for a system with piecewise linear dynamics and bounded noise (linearization error). The comparison principle [14, 15] allows us to derive equations for the coefficients of the sought-for value function, whose zero sublevel set is an internal estimate of the solvability set of the original nonlinear system.

The search for an approximate HJB solution using the above-mentioned method is accompanied by construction of a suboptimal control strategy. Previously, a control strategy was proposed in the form of continuous piecewise affine function [13], determined by values at the vertices of the partition

simplices. In this case, the values at the vertices should be chosen in such a way as to minimize the derivative of the value function along the trajectory. However, since the constructed estimate of the value function is not smooth, it is required to use additional heuristics, which increase the error of the method. In this paper, we demonstrate that results of other algorithms can also be used as controls at the vertices. In particular, we propose using reinforcement learning [16, 17]. If control values are chosen based on the output of a neural network model, the resulting estimate of the value function can take smaller values at the initial time moment. Therefore, it would a priori guarantee reaching a smaller neighborhood of the target set.

Note that reinforcement learning algorithms also imply construction of a value function, which is an estimate of the resulting benefit from each possible position (in this case, we are talking about the distance to the target set at the final moment of time), or its analogues. But even with a well-chosen control, such an estimate is not reliable and may be inaccurate. At the same time, the approach indicated in this paper allows any predetermined control strategy to be approximated by a piecewise affine function, for which the resulting estimate will be guaranteed. This can be especially useful in case of additional interference, when calculation of trajectories for different initial points is not sufficient to estimate all possible variants of the system's behavior.

2. PROBLEM STATEMENT

We consider a system of nonlinear differential equations

$$\dot{x} = \mathbf{f}(t,x) + \mathbf{g}(t,x)u, \quad t \in [t_0, t_1],\ x \in \Omega, \tag{1}$$

where $\Omega \in \mathbb{R}^{n_x}$ is a compact set, large enough to contain all the trajectories of (1) for any $t \in [t_0, t_1]$; we assume that the boundary of Ω is a polyhedron. The nonlinear vector function $\mathbf{f}(t,x)$ and the matrix function $\mathbf{g}(t,x) \in \mathbb{R}^{n_x \times n_u}$ are continuous in t and twice continuously differentiable with respect to x. The interval $[t_0, t_1]$ is fixed. At every moment of time, the control vector u must belong to a compact convex set $\mathcal{P}$:

$$u \in \mathcal{P} \subset \mathbb{R}^{n_u}. \tag{2}$$

The main problem is to construct a continuous feedback control in the form $u = u(t,x)$, which steers the system (1) from a given point x_0 at time t_0 to the smallest possible neighborhood of a compact target set $\mathcal{X}_1 \subset \Omega$ at time t_1. Let $u(\cdot)$ denote feedback control. Thus,

$$x(t_1; t_0, x_0)|_{u(\cdot)} \in \mathcal{X}_1 + B_\varepsilon(0)$$

must hold, where $x(t_1; t_0, x_0)|_{u(\cdot)}$ is the final point of a trajectory that started at time t_0 from the point x_0, closed by control $u(\cdot)$; $B_\varepsilon(0)$ is a ball of radius ε centered at zero, and the value of $\varepsilon \geqslant 0$ must be minimized. We also assume that the target set is representable as $\mathcal{X}_1 = \{x \in \Omega \colon \phi_{\mathcal{X}_1}(x) \leqslant 0\}$, where $\phi_{\mathcal{X}_1}(x)$ is a twice differentiable function.

In addition, it is required to construct *the solvability set* $\mathcal{W}(t, t_1, \mathcal{X}_1)$ [15], that is, the set of all vectors $x \in \Omega$, for each of which there is a control $u(\cdot)$, satisfying the constraint (2) and transferring the system from position $\{t, x\}$ ($t \in [t_0, t_1]$) to the target set: $x(t_1; t, x)|_{u(\cdot)} \in \mathcal{X}_1$. However, since the task of constructing the exact solvability set is difficult, we limit ourselves to searching for internal estimates of this set.

3. SYSTEM WITH PIECEWISE LINEAR DYNAMICS

Let *n-dimensional simplex* [20] with vertices $x_1, x_2, \ldots, x_{n+1} \in \mathbb{R}^n$ be the set

$$S^n = \left\{ \alpha_1 x_1 + \alpha_2 x_2 + \ldots + \alpha_{n+1} x_{n+1} : \alpha_i \geqslant 0,\ \sum_{i=1}^{n+1} \alpha_i = 1 \right\},$$

where the vectors $x_2 - x_1, \ldots, x_{n+1} - x_1$ are linearly independent. In this case, a vector of *barycentric coordinates* $\alpha(x) = (\alpha_1, \ldots, \alpha_{n+1})^T$ uniquely defines the position of any point x inside the simplex. In addition, there is a matrix $\tilde{H}$ [11] such that the barycentric coordinates $\alpha(x)$ are linearly expressed in terms of x: $\alpha = \tilde{H} \times (x^T, 1)^T$.

Consider some partition of the Ω set into N simplices $\Omega^{(i)}$ such that any two simplices do not intersect or intersect only along any of their common faces of dimension smaller than n_x. In practice, having an arbitrary set of vertices, one may implement such partition using Delaunay triangulation [21, 22], which is efficiently computed by constructing a convex hull of points in $(n_x + 1)$-dimensional space [23].

The superscript (i) further denotes correspondence of a vector, matrix, or function to the simplex $\Omega^{(i)}$. In particular, vertices of a simplex are denoted as $g_1^{(i)}, \ldots, g_{n_x+1}^{(i)} \in \mathbb{R}^{n_x}$, $i = \overline{1, N}$. Note that each vertex can belong to several simplices.

In [11–13], a method was proposed to construct a continuous piecewise affine approximation of the system (1), which substantially uses a partition of the Ω set into simplices. The matrices $A^{(i)}$, $B^{(i)}$ and vectors $f^{(i)}$ are selected in such a way that the following representation is valid for all $u \in \mathcal{P}$:

$$\mathbf{f}(t,x) + \mathbf{g}(t,x)u = A^{(i)}(t)x + B^{(i)}(t)u + f^{(i)}(t) + v^{(i)}(t,x,u), \quad x \in \Omega^{(i)}, \tag{3}$$

where $v^{(i)}$ is a local linearization error. This error is bounded and there is an estimate for it based on decomposition of the functions $\mathbf{f}(t,x)$ and $\mathbf{g}(t,x)$ according to the Taylor's formula. Moreover, this estimate is independent of particular values $x \in \Omega^{(i)}$ and $u \in \mathcal{P}$. Thus, all possible values of $v^{(i)}$ can be bounded with some ellipsoid $\mathcal{Q}^{(i)}(t)$:

$$\mathcal{Q}^{(i)}(t) = \mathcal{E}(0, Q^{(i)}(t)) = \{x \in \mathbb{R}^{n_x} : \ \langle x, (Q^{(i)})^{-1}x\rangle \leqslant 1\}, \quad Q^{(i)} = (Q^{(i)})^T > 0. \tag{4}$$

Remark 1. If system (1) additionally contains an additive term in the form of unknown bounded function (interference), then it can also be taken into account during piecewise linearization by scaling the ellipsoids $\mathcal{Q}^{(i)}(t)$ and shifting their centers.

It is convenient to consider the extended variable space, where a vector $\tilde{x}$ is obtained by adding an auxiliary component with a fixed value equal to one: $\tilde{x} = (x^T, 1)^T$. Then, based on (3), we can write the following piecewise linear system of differential equations with autonomous switching [24, pp. 5–9] in the extended space of variables:

$$\dot{\tilde{x}} = \tilde{A}^{(i)}(t)\tilde{x} + \tilde{B}^{(i)}(t)u + \tilde{C}v^{(i)}, \quad \tilde{x} \in \Omega^{(i)} \times \{1\}, \ t \in [t_0, t_1], \tag{5}$$

$$\tilde{A}^{(i)}(t) = \begin{bmatrix} A^{(i)}(t) & f^{(i)}(t) \\ \mathbb{O}_{1\times n_x} & 0 \end{bmatrix}, \quad \tilde{B}^{(i)}(t) = \begin{bmatrix} B^{(i)}(t) \\ \mathbb{O}_{1\times n_u} \end{bmatrix}, \quad \tilde{C} = \begin{bmatrix} \mathbb{I}_{n_x\times n_x} \\ \mathbb{O}_{1\times n_x} \end{bmatrix},$$

where $v^{(i)}$ is interpreted as interference. We will call an interference acceptable if it is a measurable function of time and it satisfies the constraint $v^{(i)}(t) \in \mathcal{Q}^{(i)}(t)$ at each time moment. The index $i = i(x(t))$ in formula (5) is a function of system state at time t, however, for the sake of brevity, we omit the arguments of this function.

4. VALUE FUNCTION

4.1. General Background

Consider an auxiliary value function

$$\bar{V}(t,x) = \min_{u(\cdot)} \{\phi_{\mathcal{X}_1}(x(t_1)) : \ x(t) = x\}, \tag{6}$$

where $x(\cdot)$ is a trajectory of the nonlinear system (1), starting at the initial position and closed by a fixed feedback control $u(\cdot)$. Using the value function, the solvability set is constructed [15] as

$$\mathcal{W}(t,t_1,\mathcal{X}_1)=\left\{x\in\Omega:\ \bar{V}(t,x)\leqslant 0\right\}. \tag{7}$$

Along with (7), consider a formula for the neighborhood of the solvability set:

$$\mathcal{W}_\varepsilon(t,t_1,\mathcal{X}_1)=\left\{x\in\Omega:\ \bar{V}(t,x)\leqslant \varepsilon\right\},$$
$$\mathcal{W}_\varepsilon(t,t_1,\mathcal{X}_1)=\left\{x\in\Omega\mid \exists u(\cdot):\ \phi_{\mathcal{X}_1}(x(t_1;t,x)|_{u(\cdot)})\leqslant\varepsilon\right\}.$$

At any point of differentiability (t,x), where $t<t_1,\ x\in\Omega$, the function $\bar{V}(t,x)$ satisfies the backward Hamilton–Jacobi–Bellman equation

$$\min_{u\in\mathcal{P}}\bar{V}'(t,x;(1,(\mathbf{f}(t,x)+\mathbf{g}(t,x)u)^T)^T)=0, \tag{8}$$

where $\bar{V}'(t,x;\ell)$ is the derivative of the function $\bar{V}(t,x)$ at the point (t,x) in the direction $\ell\in\mathbb{R}^{n_x+1}$. At the final moment of time, the equality $\bar{V}(t_1,x)=\phi_{\mathcal{X}_1}(x)$ holds. The function $\bar{V}(t,x)$ can be non-differentiable, and hence the solution of (8) must be recognized in a generalized sense [25]. Nevertheless, we can replace the solution $\bar{V}(t,x)$ with such a piecewise quadratic function that equation (8) would be fulfilled approximately. This function will be further found based on consideration of piecewise linear system (5).

4.2. Piecewise Quadratic Function

At each vertex $g_l^{(i)}$ of each simplex $\Omega^{(i)}$, consider a function $\langle k_l^{(i)}(t),\tilde{x}\rangle$, which is affine in x. For each $t\in[t_0,t_1]$, the vector $k_l^{(i)}\in\mathbb{R}^{n_x+1}$ is a vector of unknown coefficients. Then, for each simplex $\Omega^{(i)}$, we can define a matrix of parameters, whose structure corresponds to the set of vertices $g_1^{(i)},\dots,g_{n_x+1}^{(i)}$:

$$K^{(i)}(t)=\left[k_1^{(i)}(t),\dots,k_{n_x+1}^{(i)}(t)\right]\in\mathbb{R}^{(n_x+1)\times(n_x+1)}.$$

Consider a piecewise quadratic function

$$V^{(i)}(t,\tilde{x})=\langle\tilde{x},K^{(i)}(t)\tilde{H}^{(i)}\tilde{x}\rangle,\quad \tilde{x}=(x^T,1)^T,\quad x\in\Omega^{(i)}. \tag{9}$$

Equation (9) corresponds to interpolation of the considered affine functions:

$$V^{(i)}(t,\tilde{x})=\langle\tilde{x},K^{(i)}(t)\tilde{H}^{(i)}\tilde{x}\rangle=\langle(K^{(i)}(t))^T\tilde{x},\alpha^{(i)}(x)\rangle=\sum_{l=1}^{n_x+1}\alpha_l^{(i)}(x)\langle k_l^{(i)}(t),\tilde{x}\rangle.$$

Since the function (9) is defined for the extended space of variables $\tilde{x}=(x^T,1)^T$, an arbitrary piecewise quadratic function defined on a set of simplices can be represented in such form.

We will use piecewise affine controls of the form

$$u(t,x)=Y^{(i)}(t)\tilde{H}^{(i)}\tilde{x}=\sum_{k=1}^{n_x+1}\alpha_k^{(i)}(x)y_k^{(i)}(t)\in\mathbb{R}^{n_u}, \tag{10}$$

where the matrix $Y^{(i)}(t)\in\mathbb{R}^{n_u\times(n_x+1)}$ consists of column vectors $y_k^{(i)}(t)\in\mathcal{P}$ that are the control values at the vertices of $\Omega^{(i)}$. Those values will be chosen later. Note that the values of $y_k^{(i)}(t)$ corresponding to the same vertex in different simplices will coincide, hence the control function $u(t,x)$ is continuous in x. Due to convexity of $\mathcal{P}$, the condition $u(t,x)\in\mathcal{P}$ is satisfied.

Consider the derivative of $V^{(i)}(t,\tilde{x})$ in the direction $\ell=(\ell_t,\ell_x)\in\mathbb{R}^{n_x+2}$:

$$\frac{dV^{(i)}}{d\ell}=\ell_t\langle\tilde{x},\dot{K}^{(i)}\tilde{H}^{(i)}\tilde{x}\rangle+\langle\ell_x,[K^{(i)}\tilde{H}^{(i)}+(\tilde{H}^{(i)})^T(K^{(i)})^T]\tilde{x}\rangle. \tag{11}$$

It was proved in [13] that the following estimate holds for $\ell=(\ell_t,\ell_x)^T$, where $\ell_t=1$, $\ell_x=\tilde{A}^{(i)}\tilde{x}+\tilde{B}^{(i)}u+\tilde{C}v^{(i)}$:

$$\frac{dV^{(i)}}{d\ell}(t,\tilde{x})\leqslant\langle\tilde{x},[\dot{K}^{(i)}+Z^{(i)}]\tilde{H}^{(i)}\tilde{x}\rangle. \tag{12}$$

The matrix $Z^{(i)}$ is known and can be expressed in terms of coefficients $K^{(i)}(t)$, coefficients $\tilde{A}^{(i)}(t)$, $\tilde{B}^{(i)}(t)$, $\tilde{C}$ of the piecewise linear system (5), and matrices $Y^{(i)}(t)$ that define control values at the vertices of $\Omega^{(i)}$. The obtained estimate is valid for any acceptable interference $v^{(i)}\in\mathcal{Q}^{(i)}(t)$.

Making $\dot{K}^{(i)}+Z^{(i)}$ to be zero matrix, we obtain the system of matrix differential equations which describes evolution of $V^{(i)}(t,\tilde{x})$ over time.

$$\dot{K}^{(i)}(t)+Z^{(i)}(t)=0,\quad t\in[t_0,t_1],\ i=\overline{1,N}. \tag{13}$$

Then it follows from (12)–(13) that along any trajectory of the system (5) the derivative of the function will not increase in each simplex $\Omega^{(i)}$. Next, we will show how to modify equations (13) so that the resulting function $V^{(i)}(t,\tilde{x})$ would be continuous, and therefore the derivative would not grow even when passing through the simplex boundaries. This can be used to construct a guaranteed a priori estimate for trajectory's end point deviation from the target set.

4.3. Boundary Conditions

To solve (13), one has to set boundary conditions at the final time moment $t=t_1$. In turn, it is necessary to construct a piecewise quadratic upper bound for the function $\phi_{\mathcal{X}_1}$. Based on representation (9), matrices $K^{(i)}(t_1)$ can be defined. In particular, if the boundary of the set $\mathcal{X}_1$ is a second-order hypersurface, then the representation $\phi_{\mathcal{X}_1}(x)=\langle\tilde{x},\hat{K}\tilde{x}\rangle$ is valid for some matrix $\hat{K}=\hat{K}^T$. Thus, let the parameter values of $V^{(i)}(t_1,\tilde{x})$ be equal to

$$K^{(i)}(t_1)=\hat{K}\times(\tilde{H}^{(i)})^{-1} \tag{14}$$

in each simplex. In general, for any twice differentiable function $\phi_{\mathcal{X}_1}$, it is possible to construct a piecewise affine upper bound [12], which is a special case of piecewise quadratic function and thus leads to conditions similar to (14). The function $V^{(i)}(t,\tilde{x})$ will be continuous in x over the entire set $\Omega\times\{1\}$ at time $t=t_1$.

4.4. Function Smoothing

Note that solution $V^{(i)}(t,x)$ (9) of the Cauchy problem (13)–(14) can be discontinuous at the boundaries of simplices. Each column of $K^{(i)}(t)$ defines the coefficients of the piecewise affine function $\langle k_l^{(i)}(t),\tilde{x}\rangle$ at some vertex g_l. However, generally speaking, each such point is a vertex of several simplices at once. Since matrices $Z^{(i)}$ in (11) are constructed independently for each simplex, the values of the derivatives $\dot{k}_l^{(i)}(t)$ are determined by several incompatible conditions.

Thus, the estimate (11) needs to be modified, so that the resulting function $V^{(i)}(t,x)$ would be continuous. We propose an alternative way to calculate the matrices $Z^{(i)}$ rather than in [13].

Instead of (13), consider a differential equation for each column of the matrix $K^{(i)}$:

$$\dot{k}_l^{(i)}(t)+z_l^{(i)}(t)=0,\quad t\in[t_0,t_1],\ i=\overline{1,N},\ l=\overline{1,n_x+1}, \tag{15}$$

where $z_l^{(i)}$ is the corresponding column of the matrix $Z^{(i)}$. Hence the estimate (12) can be rewritten in the form

$$\frac{dV^{(i)}}{d\ell}(t,\tilde{x}) \leqslant \langle \tilde{x}, [\dot{K}^{(i)} + Z^{(i)}]\tilde{H}^{(i)}\tilde{x}\rangle = \langle \tilde{x}, \dot{K}^{(i)}\tilde{H}^{(i)}\tilde{x}\rangle + \langle \tilde{x}, Z^{(i)}\tilde{H}^{(i)}\tilde{x}\rangle$$
$$\leqslant \langle \tilde{x}, \dot{K}^{(i)}\tilde{H}^{(i)}\tilde{x}\rangle + \langle \tilde{x}, Z^{(i)}\alpha^{(i)}(x)\rangle = \langle \tilde{x}, \dot{K}^{(i)}\tilde{H}^{(i)}\tilde{x}\rangle + \sum_{l=1}^{n_x+1} \alpha_l^{(i)}(x)\langle \tilde{x}, z_l^{(i)}\rangle. \tag{16}$$

For any fixed $t \in [t_0, t_1]$ and each vertex $g_l^{(i)}$, consider an auxiliary linear programming problem with respect to a new unknown vector $\hat{z}_l^{(i)}$:

$$\begin{cases} \langle \hat{z}_l^{(i)}, \tilde{g}_l^{(i)}\rangle \to \min \\ \langle \hat{z}_l^{(i)}, \tilde{g}_k^{(j)}\rangle \geqslant \langle z_{\nu(i,l,j)}^{(j)}, \tilde{g}_k^{(j)}\rangle \quad \forall j: \ g_l^{(i)} \in \Omega^{(i)} \cap \Omega^{(j)}, \ k = \overline{1, n_x+1}, \end{cases} \tag{17}$$

where $\nu(i,l,j)$ denotes a local index of a vertex $g_l^{(i)} \in \Omega^{(i)} \cap \Omega^{(j)}$ in the simplex $\Omega^{(j)}$.

Using solutions $\hat{z}_l^{(i)}$, we obtain matrices $\hat{Z}^{(i)}$ in a similar way. Given conditions of the problem (17) and linearity of the functions under consideration, we can continue the inequality (16):

$$\frac{dV^{(i)}}{d\ell}(t,\tilde{x}) \leqslant \langle \tilde{x}, [\dot{K}^{(i)} + Z^{(i)}]\tilde{H}^{(i)}\tilde{x}\rangle \leqslant \langle \tilde{x}, \dot{K}^{(i)}\tilde{H}^{(i)}\tilde{x}\rangle + \sum_{l=1}^{n_x+1} \alpha_l^{(i)}(x)\langle \tilde{x}, z_l^{(i)}\rangle$$
$$\leqslant \langle \tilde{x}, \dot{K}^{(i)}\tilde{H}^{(i)}\tilde{x}\rangle + \sum_{l=1}^{n_x+1} \alpha_l^{(i)}(x)\langle \tilde{x}, \hat{z}_l^{(i)}\rangle = \langle \tilde{x}, [\dot{K}^{(i)} + \hat{Z}^{(i)}]\tilde{H}^{(i)}\tilde{x}\rangle.$$

Note that solutions of the problems (17) corresponding to the same vertex in different simplices $\Omega^{(i)}$ will coincide (if the linear programming problem admits several solutions, they can be chosen the same). Hence, the piecewise-defined value function (9) obtained by solving the Cauchy problem

$$\begin{cases} \dot{K}^{(i)} + \hat{Z}^{(i)} = 0, & i = \overline{1, N}, \quad t \in [t_0, t_1] \\ K^{(i)}(t_1) = \hat{K} \times (\tilde{H}^{(i)})^{-1}, & i = \overline{1, N}, \end{cases} \tag{18}$$

will be continuous in $(t, \tilde{x})$ throughout the entire domain. The objective function in (17) corresponds to the values $V^{(i)}(t, \tilde{x})$ at the simplex vertices, and thus it tends to reduce function values at these points.

5. CONTROL SELECTION

Before solving the problem (18), we need to determine the controls $y_k^{(i)}$ from (10) at the vertices of simplices in order to construct matrices $\hat{Z}^{(i)}$ based on these values. In the previous works [11–13], they were chosen in such a way that the derivative (11) of $V^{(i)}(t, \tilde{x})$ is minimized in each simplex $\Omega^{(i)}$. However, taking into account the piecewise defined nature of this function, there was ambiguity in the choice of $y_k^{(i)}$. To eliminate it, the controls were additionally adjusted, and this negatively affected the resulting solution.

In this paper, we demonstrate that the method allows the use of controls obtained on the basis of alternative approaches, reinforcement learning in particular. As a result, the constructed approximation of the value function (6) can be more accurate.

Reinforcement learning [16] is a domain of machine learning, where the agent's behavior is adjusted by repeated interaction with the environment, depending on the rewards received from it

for each action performed. In our task, the agent implements the control strategy $u = u(t, x)$ and we choose

$$\mathcal{L}(t,x) = \begin{cases} 0, & t < t_1 \\ -d^2(x, \mathcal{X}_1), & t = t_1, \end{cases} \tag{19}$$

as a reward function. Here $d(x, \mathcal{X}_1)$ is the distance between a point x and a set $\mathcal{X}_1$.

Proximal Policy Optimization (PPO) is one of the reinforcement learning algorithms in which the control strategy is represented using a neural network, and its weights are updated by gradient descent while optimizing some objective function. The objective is to maximize the cumulative reward at the end of the experiment; however, this function is described by a more complex expression [17] to ensure a stable learning process.

The advantage of the PPO algorithm is possibility of its application to continuous dynamics, including the system (1). Some other algorithms also have this property, for example, DDPG [18] and SAC [19]. They can also be used in the proposed approach. However, they showed lower accuracy in the examples discussed below.

Let the set $\mathcal{P}$ admit finite-dimensional parametrization. In this case, a vector $u \in \mathcal{P}$ is defined by parameters $\theta \in \mathbb{R}^r$, where $\theta_i \in [\theta_i^{\min}, \theta_i^{\max}]$, $i = \overline{1,r}$. The goal is to determine these parameters for each fixed position (t, x). However, since the PPO algorithm is designed for stochastic strategies, θ is usually assumed to be a random vector with a multidimensional normal distribution $\theta \sim \mathcal{N}(\mu, \Sigma)$ with a diagonal covariance matrix. When using the algorithm, at first a neural network is trained, which predicts the parameters of this distribution, and then realizations of the corresponding random vector are generated during the calculation of values $u(t, x)$. Nevertheless, having a trained neural network, it is easy to obtain deterministic control. Instead of generating a random vector, one can take the corresponding expected value: $\theta = \mu$.

Note that the values of θ_i are subject to interval constraints, while the support of a normal random vector is the entire space $\mathbb{R}^r$. In order to meet the requirements, the parameter values are "truncated" [26]. New values are obtained using the formula $\tilde{\theta}_i = \min\{\theta_i^{\max}, \max\{\theta_i, \theta_i^{\min}\}\}$, although other transformations are allowed. In addition, distributions with a bounded support [27] can be used for the specified random variables.

Such deterministic controls, which are based on a neural network model and satisfy the constraint (2), are further denoted as $\hat{u}(t, x)$. The resulting piecewise affine control used in this work is determined by formula (10):

$$u(t,x) = \sum_{k=1}^{n_x+1} \alpha_k^{(i)}(x) \hat{u}(t, g_k^{(i)}), \quad x \in \Omega^{(i)}. \tag{20}$$

The function $\hat{u}(t, x)$ will be continuous in (t, x) due to the structure of a neural network. It also follows that as the diameter of the partition of Ω into simplices tends to zero, the resulting control (20) will converge pointwise to $\hat{u}(t, x)$.

6. MAIN RESULT

The constructions above allow us to prove the following theorem.

Theorem 1. *Let the matrix functions $K^{(i)}(t) \in \mathbb{R}^{(n_x+1)\times(n_x+1)}$ be a solution of the Cauchy problem* (18)*. Let $V(t, \tilde{x})$ be a continuous piecewise quadratic function defined on $[t_0, t_1] \times \Omega \times \{1\}$ and determined by the equation $V^{(i)}(t, \tilde{x}) = \langle \tilde{x}, K^{(i)}(t) \tilde{H}^{(i)} \tilde{x} \rangle$ in each simplex $\Omega^{(i)}$. Then the set $\mathcal{W}_\varepsilon^{int}(t_0) = \left\{ x \in \Omega \;\middle|\; V(t_0, \tilde{x}) \leqslant \varepsilon \right\}$ (assuming that it is not empty) is an internal estimate of the solvability set of the original nonlinear system* (1)*, i.e.*

$$\mathcal{W}_\varepsilon^{int}(t_0) \subseteq \mathcal{W}_\varepsilon(t_0, t_1, \mathcal{X}_1).$$

The proof is based on trajectory analysis of the nonlinear system (1), closed by control (10). However, it does not depend on the method of finding the vectors $y_k^{(i)}(t) \in \mathcal{P}$ at the vertices of the simplices. The proof follows the scheme presented in [13].

7. EXAMPLES

7.1. Nonlinear System

Consider the motion of a pendulum on a trolley, taking the frictional force into account [28]. It is described by the system of equations

$$\begin{cases} \dot{x}_1 = x_2 \\ \dot{x}_2 = -w^2 \sin(x_1) - 2\gamma x_2 - w^2 \cos(x_1) \times u, \end{cases} \tag{21}$$

where ω and γ are parameters, x_1 and x_2 are the angle of pendulum deflection and the angular velocity, respectively. The control u denotes acceleration of the cart. We consider $\omega = 1$, $\gamma = 0.1$. It is required to steer the system from the initial position $(-0.3,\, 0.6)^T$ at time $t_0 = 0$ to a small neighborhood of the origin at time $t_1 = 1$. The control is bounded by $u \in [-1, 1]$.

For neural networks used in the PPO algorithm, we chose a two-layer perceptron [29] with activation function $\tanh(x)$ due to its simplicity. During training, 10 000 test trajectories of the system (21) were generated, starting from various random points $x^0 \in \Omega$ at time t_0. The control strategy $\hat{u}(t, x)$ was updated based on the penalties (19). Figure 1 shows the trajectory obtained using the PPO algorithm without any additional modifications. The distance between the end point of the trajectory and the origin is 0.027.

To calculate the piecewise quadratic function (9), at first we fixed the vertices $g_k \in \mathbb{R}^2$ located on a rectangular grid with sides of length $\Delta = 0.1$. These vertices were used to partition the set $\Omega = [-1, 1] \times [-1, 1]$ into $N = 800$ equal simplices. Figure 2 shows the results obtained using the control selection algorithm described in [13]. The dotted line indicates the boundary of the set which a trajectory of the system is a priori guaranteed to hit. The distance between $x(t_1)$ and the target set is 0.043.

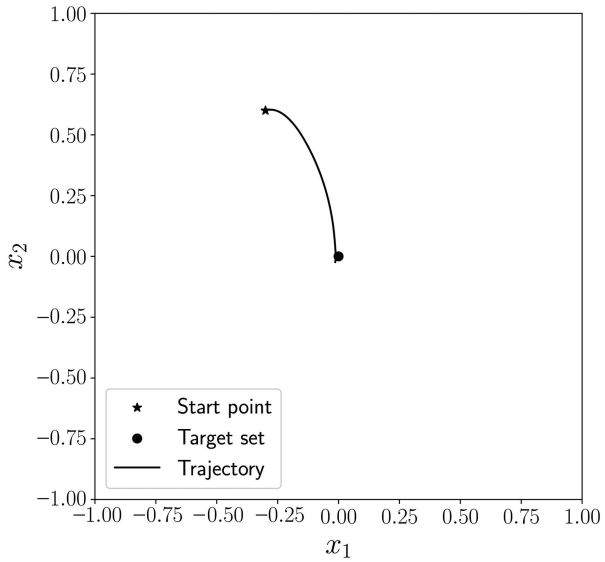

Fig. 1. The trajectory based on control $\hat{u}(t, x)$.

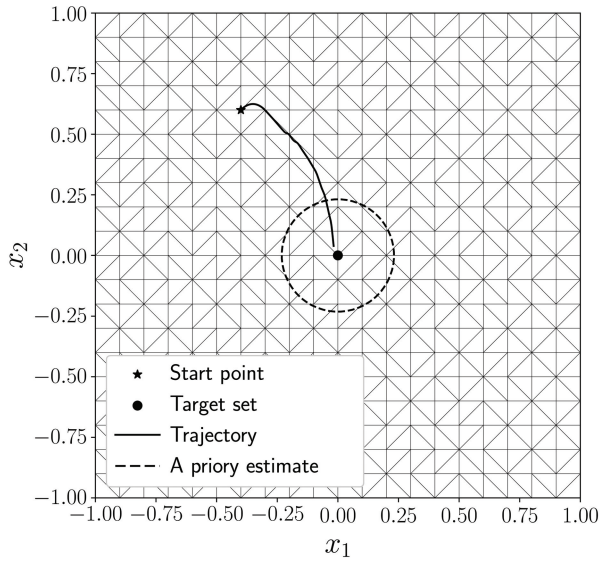

Fig. 2. The trajectory based on control strategy described in [13].

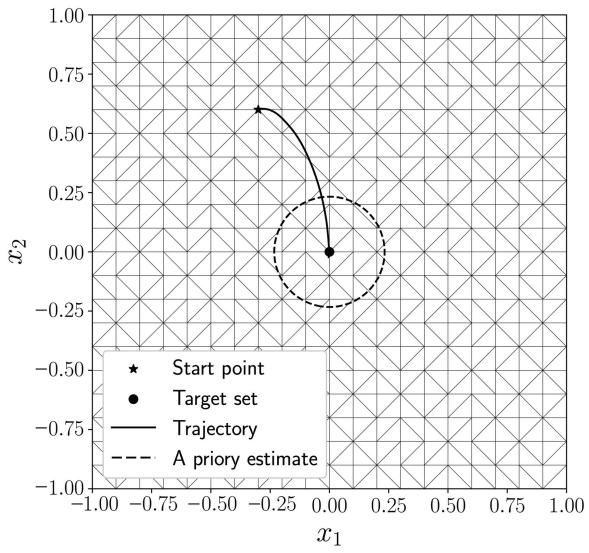

Fig. 3. The trajectory based on approximation (20) of neural network control $\hat{u}(t, x)$.

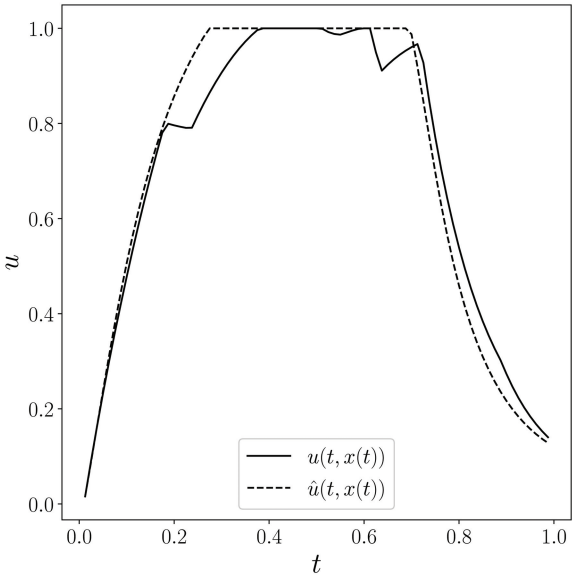

Fig. 4. Neural network control $\hat{u}(t, x(t))$ and the resulting control $u(t, x(t))$.

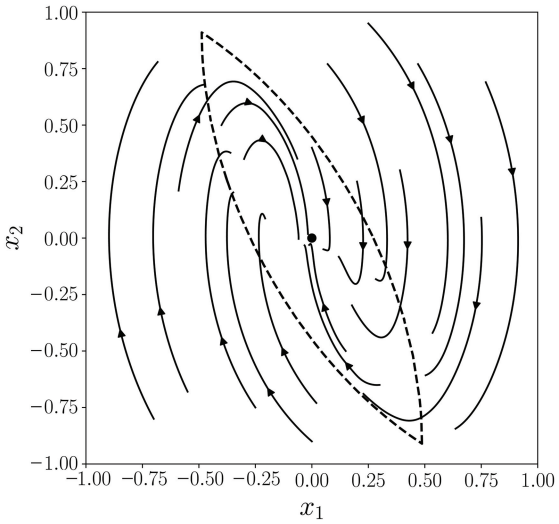

Fig. 5. The boundary of solvability set at $t = t_0$ and trajectories of the system (21) closed by the resulting control $u(t, x)$.

Figure 3 shows the trajectory obtained by the combination of methods described in the current work. The same partition into simplices is used. The distance from the origin in this case is 0.023. The change in error is explained by the difference between the original neural network control $\hat{u}(t, x)$ and its approximation (20). Figure 4 shows the controls corresponding to the trajectories shown in Figs. 1 and 3. The a priori error is less for the presented method than for the algorithm [13]. This example confirms that the a priori estimate obtained from the value function approximation (9) is guaranteed in each case.

In Fig. 5, continuous lines indicate the trajectories obtained by the proposed method when starting from various starting points. Arrows indicate the direction of movement along the trajectories. In addition, the dotted line stands for the boundary of the solvability set using the class of piecewise continuous program controls, calculated on the basis of the Pontryagin's maximum principle [30, pp. 336–344].

7.2. Linear System

To better understand accuracy of the proposed approach, consider a linear system

$$\dot{x}_1 = x_2, \quad \dot{x}_2 = u \tag{22}$$

on the segment $t \in [0, 1]$. In this case, the method of piecewise linearization described above is not needed, however, this system is well studied in literature [30]. Let the control satisfy $u \in [-2, 2]$. It is required to transfer the system to the origin at time $t = 1$. Then it can be proved that the point $x^0 = (0.5, 0)^T$ lies on the boundary of the solvability set at the moment $t = 0$, and it is achieved by piecewise constant control $u^*(t) = 2 \times \mathrm{sgn}(t - 0.5)$.

A neural network model of the same structure as in the previous example was chosen for numerical experiments. The model was trained on a personal computer for one hour, and then piecewise quadratic functions of the form (9) were constructed for different diameters of simplices $\Omega^{(i)}$. We consider the set $\Omega = [-1.5, 1.5] \times [-1.5, 1.5]$.

Figure 6 shows the resulting trajectory and the a priori estimate of hitting the origin from the point x^0 when step of the rectangular grid was $\Delta = 0.25$. This corresponds to the division into 288 simplices shown in the figure. Figure 7 shows the corresponding control $u(t, x(t))$ of the form (20). Figure 8 shows the solvability set calculated on the basis of the Pontryagin's maximum principle as well as the trajectories obtained by the proposed method when starting from various points.

Figure 9 shows dependencies of the a priori and a posteriori errors on the number of simplices in the partition $\Omega = \bigcup_{i=1}^{N} \Omega^{(i)}$ for the same starting point $x^0 = (0.5, 0)^T$. As the partition diameter decreases, the a posteriori error converges to 0.104, which corresponds to the accuracy of the original neural network control $\hat{u}(t, x)$. Note that this accuracy can be improved by considering other neural network models, which can require more parameters. In addition, it follows from Fig. 9 that the a priori error decreases at first, yet at some point it begins to increase again. This increase is explained by imperfection of auxiliary optimization problems (17): their solutions in neighboring vertices can differ significantly from each other, and it affects the stability of the method when using a small partition diameter. This problem can be eliminated by replacing the objective in

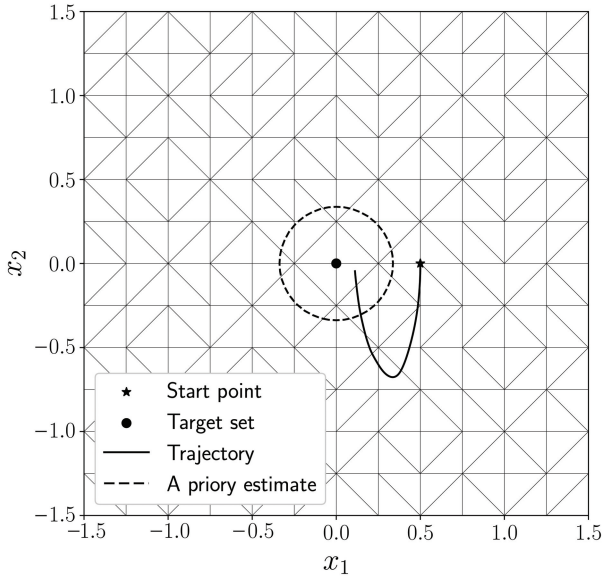

Fig. 6. Trajectory of the system (22) and a priori estimate of hitting the target point.

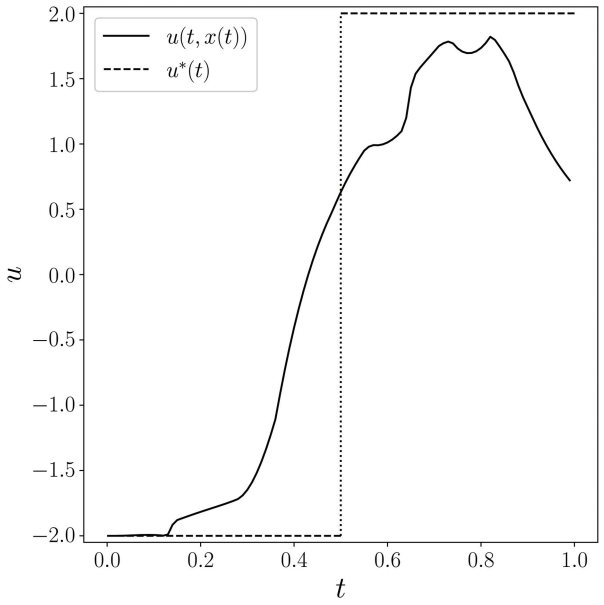

Fig. 7. The resulting control $u(t, x(t))$ for the system (22), and the optimal control $u^*(t)$.

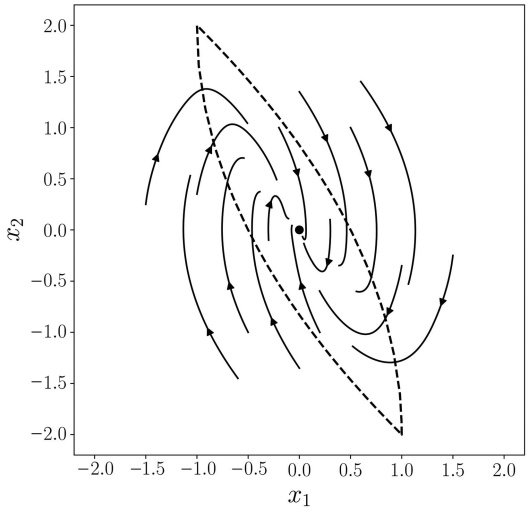

Fig. 8. Boundary of the solvability set at $t = t_0$ and trajectories of the system (22) when using the resulting control $u(t, x)$.

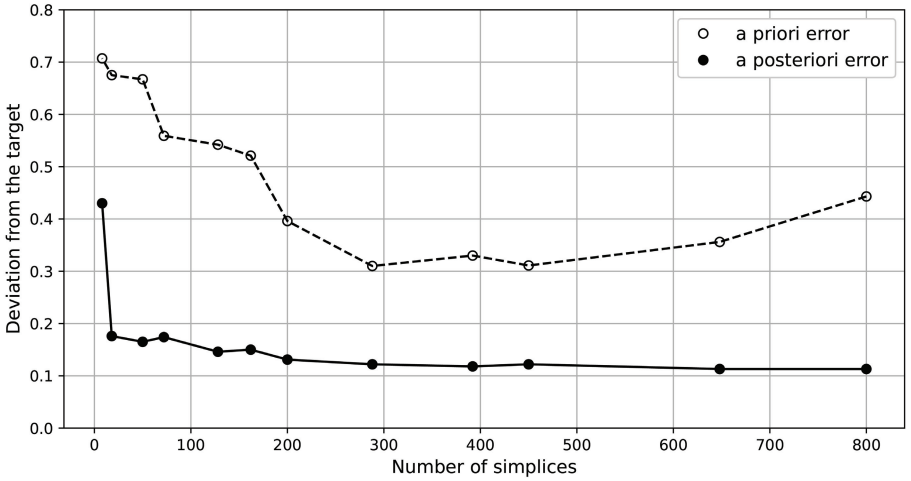

Fig. 9. Deviation from the target point $x^1 = (0, 0)^T$ depending on the number of partition simplices.

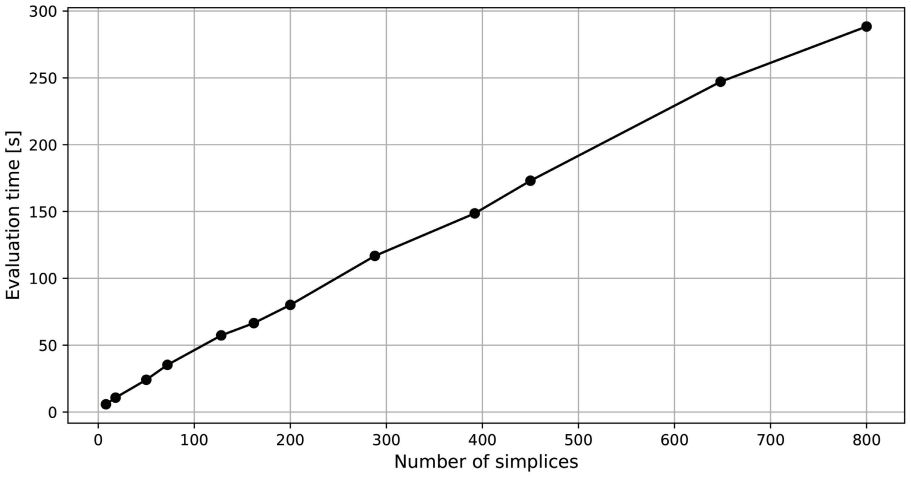

Fig. 10. Computation time of value function approximation for a fixed control strategy $\hat{u}(t, x)$.

problems (17) or by introducing additional "regularizing" terms into the system (18), which were proposed in [11].

Figure 10 shows computation times of the value function estimate depending on the number of simplices, using a fixed neural network strategy $\hat{u}(t,x)$. Time costs increase linearly as the number of simplices becomes greater. If this number is not too large, the computation time is small compared to the training time of a neural network.

8. CONCLUSION

The formulas presented in this paper make it possible to obtain a feedback control strategy that solves the problem approximately, as well as a piecewise affine approximation of this strategy on a set of simplices. The latter is used to construct a continuous piecewise quadratic function which defines an internal estimate of the solvability set in a target control problem. For the obtained piecewise affine control, a guaranteed a priori error estimate of hitting the target set is valid. The proposed approach can be used in solving control problems for nonlinear systems in case of a small state space dimension.

FUNDING

This work was carried out with financial support from the Ministry of Science and Higher Education of the Russian Federation within the framework of the program of the Moscow Center for Fundamental and Applied Mathematics under the agreement no. 075-15-2022-284.

REFERENCES

1. Neznakhin, A.A. and Ushakov, V.N., A discrete method for constructing an approximate viability kernel of a differential inclusion, *Zh. Vychisl. Mat. Mat. Fiz.*, 2001, vol. 41, no. 6, pp. 895–908.
2. Goubault, E. and Putot, S., Inner and Outer Reachability for the Verification of Control Systems, *Proceedings of the 22nd ACM International Conference on Hybrid Systems: Computation and Control*, 2019, pp. 11–22.
3. Shafa, T. and Ornik, M., *Reachability of Nonlinear Systems with Unknown Dynamics*, 2021.
4. Garrido, S., Moreno, L.E., Blanco, D., et al, Optimal control using the Fast Marching Method, *35th Annual Conference of IEEE Industrial Electronics*, 2009, pp. 1669–1674.
5. Subbotina, N.N. and Tokmantsev, T.B., Classical characteristics of the Bellman equation in constructions of grid optimal synthesis, *Proceedings of the Steklov institute of mathematics*, 2010, vol. 271, no. 1, pp. 246–264.
6. Xue, B., Fränzle, M., and Zhan, N., Inner-Approximating Reachable Sets for Polynomial Systems with Time-Varying Uncertainties, *IEEE Transactions on Automatic Control*, 2019, vol. 65, no. 4, pp. 1468–1483. https://doi.org/10.1109/TAC.2019.2923049
7. Lee, D. and Tomlin, C.J., Efficient Computation of State-Constrained Reachability Problems Using Hopf–Lax Formulae, *IEEE Transactions on Automatic Control*, 2023, pp. 1–15.
8. Cheng, T., Lewis, F.L., and Abu–Khalaf, M., Fixed-Final-Time-Constrained Optimal Control of Nonlinear Systems Using Neural Network HJB Approach, *IEEE Transactions on Neural Networks*, 2007, vol. 18, no. 6, pp. 1725–1737.
9. Onken, D., Nurbekyan, L., Li, X., et al., A Neural Network Approach for High-Dimensional Optimal Control Applied to Multiagent Path Finding, *IEEE Transactions on Control Systems Technology*, 2023, vol. 31, no. 1, pp. 235–251.
10. Sánchez–Sánchez, C., Izzo, D., and Hennes, D., Learning the optimal state-feedback using deep networks, *2016 IEEE Symposium Series on Computational Intelligence*, 2016, pp. 1–8.

11. Tochilin, P.A., Piecewise affine feedback control for approximate solution of the target control problem, *IFAC-PapersOnLine*, 2020, vol. 53, no. 2, pp. 6127–6132.

12. Tochilin, P.A., On the construction of a piecewise affine value function in an infinite-horizon optimal control problem, *Trudy Instituta Matematiki i Mekhaniki UrO RAN*, 2020, vol. 26, no. 1, pp. 223–238.

13. Chistyakov, I.A. and Tochilin, P.A., Application of Piecewise Quadratic Value Functions to the Approximate Solution of a Nonlinear Target Control Problem, *Differential Equations*, 2020, vol. 56, no. 11, pp. 1513–1523.

14. Kurzhanski, A.B., Comparison principle for equations of the Hamilton-Jacobi type in control theory, *Proceedings of the Steklov Institute of Mathematic*, 2006, vol. 253, pp. 185–195.

15. Kurzhanski, A.B. and Varaiya, P., *Dynamics and control of trajectory tubes. Theory and computation*, Birkhäuser, 2014.

16. Sutton, R.S. and Barto, A.G., *Reinforcement learning: An introduction*, MIT press, 2018.

17. Schulman, J., Wolski, F., Dhariwal, P., et al., Proximal policy optimization algorithms, 2017. https://doi.org/10.48550/arXiv.1707.06347

18. Lillicrap, T.P., Hunt, J.J., Pritzel, A., et al., Continuous control with deep reinforcement learning, 2019. https://doi.org/10.48550/arXiv.1509.02971

19. Haarnoja, T., Zhou, A., Abbeel, P., et al., Soft Actor-Critic: Off-Policy Maximum Entropy Deep Reinforcement Learning with a Stochastic Actor, 2018. https://doi.org/10.48550/arXiv.1801.01290

20. Pshenichnyi, B.N., *Vypuklyi analiz i ekstremal'nye zadachi* (Convex Analysis and Extremum Problems), Moscow: Nauka, 1980.

21. Skvortsov, A.V. and Mirza, N.S., *Algoritmy postroeniya i analiza trianguyatsii* (Algorithms for constructing and analyzing triangulation), Tomsk: Izd-vo Tom. un-ta, 2006.

22. Rajan, V.T., Optimality of the Delaunay triangulation in $\mathbb{R}^d$, *Discrete & Computational Geometry*, 1994, vol. 12, no. 2, pp. 189–202.

23. Brown, K.Q., Voronoi diagrams from convex hulls, *Information processing letters*, 1979, vol. 9, no. 5, pp. 223–228.

24. Liberzon, D., *Switching in Systems and Control*, Birkhäuser, 2003.

25. Bardi, M. and Capuzzo-Dolcetta, I., *Optimal control and viscosity solutions of Hamilton–Jacobi–Bellman equations. Ser. Systems & Control: Foundations & Applications*, Boston: Birkhäuser, 2008.

26. Raffin, A., Hill, A., Gleave, et al., Stable-Baselines3: Reliable Reinforcement Learning Implementations, *Journal of Machine Learning Research*, 2021, vol. 22, no. 268, pp. 1–8.

27. Petrazzini, I.G.B. and Antonelo, E.A., Proximal Policy Optimization with Continuous Bounded Action Space via the Beta Distribution, *2021 IEEE Symposium Series on Computational Intelligence (SSCI)*, 2022, pp. 1–8.

28. Reissig, G., Computing Abstractions of Nonlinear Systems, *IEEE Trans. Automatic Control*, 2011, vol. 56, no. 11, pp. 2583–2598.

29. Golubev, Yu.F., Neural networks in mechatronics, *Journal of Mathematical Sciences*, 2007, vol. 147, pp. 6607–6622.

30. Lee, E.B. and Markus, L., *Foundations of Optimal Control Theory*, Wiley, 1967.

This paper was recommended for publication by P.V. Pakshin, a member of the Editorial Board

ISSN 0005-1179 (print), ISSN 1608-3032 (online), Automation and Remote Control, 2025, Vol. 86, No. 1, pp. 74–85.

Stability Analysis of "Bridge–Pedestrians" System Based on Tsypkin Criterion

I. S. Zaitceva[*,**,a] **and A. L. Fradkov**[*,***,b]

[*] *Institute for Problems in Mechanical Engineering, Russian Academy of Sciences, St. Petersburg, Russia*
[**] *St. Petersburg State Electrotechnical University "LETI", St. Petersburg, Russia*
[***] *St. Petersburg State University, St. Petersburg, Russia*
e-mail: [a] *zyus@ipme.ru,* [b] *alf@ipme.ru*

Received June 27, 2024
Revised November 20, 2024
Accepted November 28, 2024

Abstract—A novel cybernetic model has been developed to analyze the dynamics of the "bridge–pedestrians" system in the transverse direction, incorporating the functional state of the pedestrians. An analytical expression has been derived for the critical number of pedestrians capable of inducing rocking in the bridge. Additionally, the stability region of the system has been assessed using the frequency criterion established by Ya.Z. Tsypkin, specifically applied to the parameters of the London Millennium Bridge. The results of this study indicate that the rocking of the bridge may be attributed to a minor neuromuscular delay among pedestrians, rather than to the synchronization of their steps, as suggested in several existing publications. Furthermore, the obtained results may have broader implications for other classes of oscillatory human–machine systems.

Keywords: stability, reliability of structures, swinging bridge, footbridges, London Millennium Bridge

DOI: 10.31857/S0005117925010063

1. INTRODUCTION

Over the past two centuries, numerous incidents involving pedestrian bridges have been documented, including the notable swaying of London's Millennium Bridge [1]. Constructed to commemorate the arrival of the third millennium, the bridge features a lightweight suspension structure characterized by cables positioned below deck level. The Millennium Bridge stands out as one of the few structures for which extensive and valuable observational data has been gathered. Notably, it has been observed that lateral sway increases with the number of pedestrians and diminishes when pedestrian traffic decreases or comes to a halt.

The incident involving the Millennium Bridge prompted a significant surge of publications by esteemed researchers in prestigious scientific journals [2–5]. Initial studies concluded that the large amplitude of oscillations was primarily induced by the synchronous stepping of pedestrians. This finding not only resonated with public perception but also aligned well with the theoretical framework of synchronization in coupled oscillators [6]. However, subsequent observational data emerged that could not be solely explained by synchronization. For instance, oscillations unrelated to the average step frequency were recorded, as well as the identification of a specific critical number of pedestrians capable of inducing rocking in the bridge [1, 7]. In light of this evidence, several researchers proposed that synchronization may be a consequence rather than a causative factor in the rocking of the bridge [4, 5, 8–10].

In this paper, a novel model for the dynamics of the "bridge–pedestrians" system in the transverse direction, incorporating the functional state of pedestrians through a delay link, is proposed. Based on this new model, an innovative approach to analyze the stability of the system is introduced.

Existing approaches to the analysis of the "bridge–pedestrians" system often describe the system model in terms of mechanics and the influence of dynamic forces in both time and frequency domains [11, 12]. The most commonly encountered dynamic model of a bridge in the literature is represented by the following equation [8, 12, 13]

$$M\ddot{x}(t) + C\dot{x}(t) + Kx(t) = F(t), \tag{1}$$

where M, C and K are the mass, damping and stiffness matrices, $\ddot{x}(t)$, $\dot{x}(t)$ and $x(t)$ are the acceleration, velocity and displacement vectors, $F(t)$ is the vector of external forces, which is defined as [14]

$$F(t) = G_p + \sum_{i=1}^{n} G_p \alpha_i \sin(2\pi i f t - \phi_i), \tag{2}$$

where G_p is the human weight, α_i is the Fourier coefficient of the ith harmonic, $f(t)$ is the frequency, ϕ_i is the phase shift of the ith harmonic, i is the ordinal number of the harmonic, and n is the total number of harmonics.

By analogy with (1), the dynamics of pedestrians can be modeled as an oscillator characterized by its own mass, stiffness, and damping coefficient. This methodology has been applied to analyze vertical oscillations in [15, 16], where the "bridge–pedestrians" system is expressed as

$$\begin{bmatrix} m_s & 0 \\ 0 & m_c \end{bmatrix} \begin{Bmatrix} \ddot{x}_s(t) \\ \ddot{x}_c(t) \end{Bmatrix} + \begin{bmatrix} c_s + c_c & -c_c \\ -c_c & c_c \end{bmatrix} \begin{Bmatrix} \dot{x}_s(t) \\ \dot{x}_c(t) \end{Bmatrix} + \begin{bmatrix} k_s + k_c & -k_c \\ -k_c & k_c \end{bmatrix} \begin{Bmatrix} x_s(t) \\ x_c(t) \end{Bmatrix} = \begin{Bmatrix} f_s(t) \\ f_c(t) \end{Bmatrix}. \tag{3}$$

In equation (3), m, c, and k denote the mass, damping coefficient, and stiffness, respectively; the index s corresponds to the bridge, while c pertains to the pedestrian.

The inverted pendulum model with a rigid support and limited motion in the frontal plane effectively captures key features of pedestrian behavior on a horizontally oscillating surface, including both kinematics and kinetics [9, 17]. One of the assumptions underlying this model is that ground surface oscillations do not influence the timing of pedestrian steps. However, as demonstrated in [18], this assumption does not always hold true in practice. In this paper, a law for controlling foot placement that accounts for the delay in foot contact with the ground is proposed.

Recent advancements in addressing the stability of pedestrian bridges are presented in works such as [8–10], where results are derived based on the assumption that step synchronization arises as a consequence of bridge swaying. This condition facilitates the formulation of a relationship between the amplitude and phase balance of pedestrians and the bridge, allowing for the determination of a critical number of pedestrians that satisfy this relationship. In [8–10], pedestrian dynamics are modeled using the Van der Pol oscillator

$$f(x, \dot{x}) = \lambda(\dot{x}^2 + x^2 a^2)\dot{x} + \omega^2 x, \tag{4}$$

where x is the coordinate of the pedestrian's center of mass, λ is the damping, a is the limit cycle amplitude, ω is the step frequency. In the subsequent work by the authors [8], the force $F(t)$ exerted on the bridge by pedestrians is articulated in terms of the average pedestrian damping coefficient $\overline{\sigma}(\overline{\omega_i}, \Omega)$. This coefficient is significantly influenced by the ratio of the bridge oscillation frequency Ω to the pedestrian step frequency $\overline{\omega_i}$. It was found that there is a large range of

pedestrian step frequencies and bridge oscillations for which $\overline{\sigma}(\overline{\omega_i}, \Omega) < 0$. This means that, at a certain critical number of pedestrians, the overall modal damping of the bridge may become negative. Consequently, the authors proposed a straightforward formula for calculating the critical number of pedestrians

$$N_{cr} = -c_0/\overline{\sigma}, \tag{5}$$

where c_0 is the passive damping coefficient of the bridge.

The paper is structured as follows: Section 2 presents the problem statement. Section 3 describes the model of the "bridge–pedestrians" system. Section 4 discusses the stability analysis of this system and provides analytical expressions for the critical number of pedestrians. Finally, Section 5 outlines the results and their potential applications.

2. PROBLEM STATEMENT

The existing literature employs an approach to modeling pedestrian behavior that emphasizes understanding the mechanisms of walking as governed by the central nervous system. However, the high sensitivity of humans to surface vibrations elicits a response that triggers subsequent muscular actions. This observation underscores the necessity of conceptualizing humans as integral components within a closed system, taking into account their physical and psychophysiological properties. This perspective is well-established in the field of human-machine systems and is predicated on the characterization of human functional states [19]; however, it has yet to be applied to the dynamics of gait.

Without delving into the causes of bridge swaying, we will assume that individuals traverse the bridge at an average step frequency, exerting force on the surface equivalent to their body weight while simultaneously striving to maintain balance through visual and vestibular information processed by the central nervous system. The corresponding block diagram for such a system is presented in Fig. 1. In this context, this paper proposes the development of a cybernetic model for the "bridge–pedestrians" system and aims to investigate its applicability for designing and analyzing bridge structural vibrations using methodologies from automatic control theory. To achieve this, it is essential to delineate the dynamics of movement for each component within the "bridge–pedestrians" system through dynamic links.

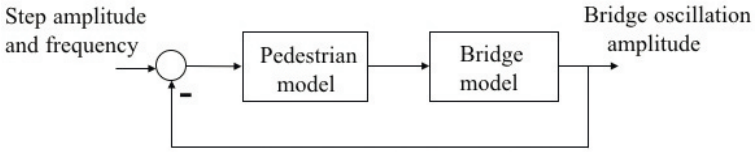

Fig. 1. General diagram of the "bridge–pedestrians" system.

3. MODEL OF THE "BRIDGE–PEDESTRIANS" SYSTEM

Human movement encompasses a variety of types that are often difficult to characterize due to their inherent randomness. Consequently, existing literature has examined the effects of groups of individuals engaged in walking [15], running [20], and jumping [21] on structural design considerations. By defining specific tasks and categorizing human movements, it becomes possible to introduce an approximate mathematical description of these actions that captures the fundamental properties of locomotion. Such descriptions are particularly relevant in the fields of bipedal robot design and human–machine systems.

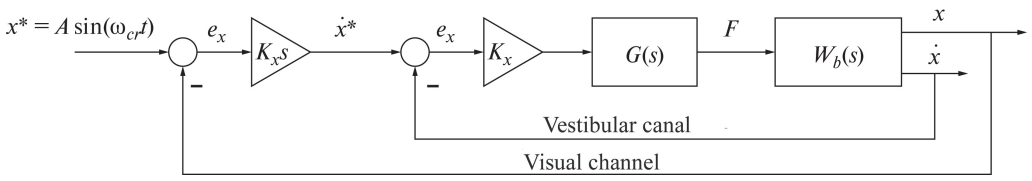

Fig. 2. Block diagram of the "bridge–pedestrians" system.

In this context, the findings from cybernetic models of pilot control actions — specifically concerning error tracking and pitch deviation rates — are well-documented. These models have contributed to our understanding of oscillatory phenomena induced by pilot actions [22, 23]. Research into the interaction between human pilots and aircraft has revealed a tendency for individuals to strive for optimal system control, which manifests as an adaptive property of neuromuscular dynamics in response to the changing dynamics of the system [19, 22–25].

The concept of optimality in human movement is frequently discussed in relation to the energy expenditure associated with executing specific actions. This characteristic is particularly applicable to periodic and repetitive movements, such as sustained walking. On a stable surface, the primary objective is to maintain balance, a task that individuals typically perform reflexively, without conscious thought. However, when navigating an unstable surface, individuals must exert effort or control to sustain balance. This process requires time for the central nervous system to process information and make decisions, which introduces a certain degree of delay.

A clear illustration of the interaction between a person and a structure can be observed in everyday situations, such as when traversing a relatively lightweight suspension bridge on a two-wheeled vehicle (e.g., a bicycle). In such scenarios, the bridge begins to sway noticeably. Notably, the more actively an individual attempts to maintain balance, the more pronounced the oscillations of the bridge become. In all instances, consciously reducing one's efforts to maintain balance — essentially decreasing the proportional gain coefficient "in the head" — can mitigate these oscillations.

The cybernetic model of human behavior in the frequency domain is structured as a series of interconnected blocks, each representing the processes of perception, strategy development, and control action processing [25, 26]. Three primary stimuli facilitate the perception of information: visual, vestibular, and proprioceptive. Within the framework of a structural approach, it is posited that the processes of information processing and strategy formulation occurring within the central nervous system are analogous for each type of perceptual stimulus. Each action performed necessitates a specific duration of time, which can be effectively characterized by a delay link; this delay tends to increase as the complexity of the control process escalates.

The aforementioned adaptive property of humans is represented through correction blocks corresponding to each perceived stimulus, with the cumulative response subsequently directed to the motor system. This structure ultimately delineates the transfer function governing human control actions [25, 27–29].

The most extensively studied model is the correction model developed by individuals based on visual perception of a command stimulus. Numerous studies have demonstrated that individuals possess the ability to amplify, differentiate, and smooth the perceived signal [27–29].

Figure 2 illustrates the model of a pedestrian who utilizes both visual and vestibular channels for information perception while walking. According to this model, a pedestrian attempts to compensate for discrepancies in the angle and angular velocity of roll to maintain balance during locomotion. Thus, the pedestrian operates within a closed-loop system, with their behavior being influenced by the dynamics of the bridge.

The transfer function of the pedestrian model relating the error in angle deviation to the roll angle can be expressed as [24, 30, 31]

$$W_p(s) = NK_x s K_{\dot{x}} G(s), \tag{6}$$

$$G(s) = \frac{T^2 e^{-\tau s}}{s^2 + 2\xi T s + T^2}, \tag{7}$$

where N represent the number of pedestrians, while K_x and $K_{\dot{x}}$ denote the gain factors, $G(s)$ is the transfer function governing the neuromuscular dynamics of pedestrians, ξ and T refer to the damping factor and frequency, respectively, whereas τ is the neuromuscular lag time. It is important to note that, as demonstrated in [31], the value of $K_{\dot{x}}$ is negative.

Considering the bridge model as described in equations (1) and (6), the transfer function of the open-loop system comprising the "bridge–pedestrians" interaction — from the displacement in the transverse direction of the bridge x to the deviation error e_x — can be expressed as follows

$$W(s) = W_p(s)W_b(s) = \frac{NK_pT^2 s e^{-\tau s}}{(s^2 + 2\xi T s + T^2)(Ms^2 + Cs + K)}, \tag{8}$$

where $K_p = K_x K_{\dot{x}}$.

4. STABILITY ANALYSIS OF THE "BRIDGE–PEDESTRIANS" SYSTEM

The remaining parameters of the system are assumed to be constant. The following parameters of the London Millennium Bridge are known: mass $M = 81\,000$, stiffness $K = 3\,390\,733$ kg/s^2, damping coefficient $C = 7681$ kg/s, and natural frequency $\Omega = \sqrt{K/M} = 6.5$ rad/s [8, 33]. Additionally, the parameters related to the neuromuscular dynamics of a pedestrian are $T = 30$, $\xi = 0.7$ [31].

The comfortable time required for information processing in the central nervous system and the transmission of signals along neuromuscular fibers for pilots in manual control mode is approximately 0.2 seconds [25, 27]. Due to the movement of the bridge surface, the pedestrian's orientation angle changes, presenting a non-standard situation that triggers the adaptation process to new conditions. This adaptation is reflected in the settings of the parameters defined in equation (6), including the delay time. Depending on external circumstances, an individual may either decrease or increase the neuromuscular delay time. For instance, a reduction in the delay to 0.08 seconds is associated with an increase in neuromuscular tension [22].

To evaluate the magnitude of the delay time and its corresponding frequency, which affect the stability of the system, it is convenient to employ the frequency criterion established by Ya.Z. Tsypkin [34, 35]. The critical frequency ω_{0i} is determined from the following equation

$$|W(\omega_{0i}, N)| - 1 = 0, \tag{9}$$

where $|W|$ denote the amplitude-frequency response (AFR) of an open-loop system without the delay link, as presented in (8). Subsequently, the resulting value of ω_{0i} is substituted into the expression for the phase relationship, which generally assumes the following form

$$\tau_{0i}(n) = \frac{\theta(\omega_{0i})}{\omega_{0i}} + \frac{2\pi n}{\omega_{0i}}, \quad n \in \mathbb{N}, \tag{10}$$

where $\theta(\omega_{0i}) = \arctan(W(\omega_{0i}))$. This critical delay time τ_{0i} delineates the transition of the system's roots through the imaginary axis, thereby establishing the stability boundary of the system. The system under investigation will be considered stable when (9) yields has no solutions with respect to ω_{0i}; in other words, when the hodograph of the system remains within the unit circle.

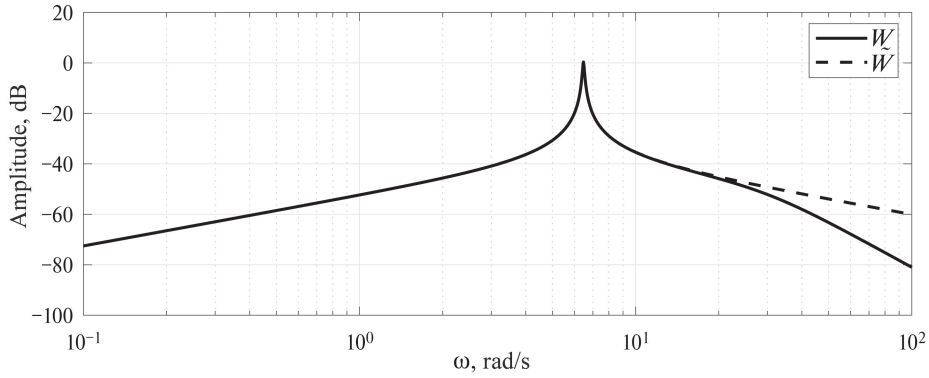

Fig. 3. Amplitude-frequency response of the "bridge–pedestrians" system with and without the neuromuscular dynamics link.

Let us apply the criteria outlined in (9) and (10) to (8). It is noteworthy that the AFR (8) coincides with the AFR that does not account for the neuromuscular dynamics link across a broad frequency range of 1–10 rad/s (see Fig. 3). This observation allows us to infer that for the purpose of assessing the stability of the system, the neuromuscular dynamics link can be neglected within this frequency range. Consequently, equation (8) can be reformulated as follows

$$\tilde{W}(s) = \frac{NK_p s e^{-\tau s}}{(Ms^2 + Cs + K)}. \tag{11}$$

Let us move from s to $j\omega$ in (8) and isolate the real and imaginary components without taking into account the delay link

$$\tilde{W}(j\omega) = K_p N \left[\frac{j\omega(K - M\omega^2)}{(K - M\omega^2)^2 + C^2\omega^2} + \frac{C\omega^2}{(K - M\omega^2)^2 + C^2\omega^2} \right]. \tag{12}$$

Then (9) can be written as

$$\frac{K_p^2 N^2 \left[(C\omega^2)^2 - \omega^2 (K - M\omega^2)^2 \right]}{\left[(K - M\omega^2)^2 + C^2\omega^2 \right]^2} - 1 = 0, \tag{13}$$

by expanding the brackets, we derive an eighth-order equation represented as

$$A_8\omega^8 + A_6\omega^6 + A_4\omega^4 + A_2\omega^2 + A_0 = 0, \tag{14}$$

where $A_8 = -M^4$, $A_6 = 4KM^3 - K_p^2 M^2 N^2 - 2C^2M^2$, $A_4 = 2KK_p^2 MN^2 - 6K^2M^2 + C^2K_p^2N^2 + 4C^2KM$, $A_2 = 4K^3M - K^2K_p^2N^2 - 2C^2K^2$, $A_0 = -K^4$.

We perform a variable substitution in equation (14) by letting $\omega^2 = t$. This substitution is essential for the subsequent analysis of the obtained solution. The solution to equation (14) with respect to ω, expressed symbolically using MATLAB, yields the following expression

$$t^2 = \left[\frac{2}{4M^2} \sqrt{C^4 + \frac{\sigma_7}{2} + 4KM^3\sigma_3 + 3C^2 \mathrm{K_p}^2 N^2 - 2C^2M^2\sigma_3 - \sigma_2 - \mathrm{K_p}^2 M^2 N^2 \sigma_3 - \sigma_1} - 2C^2 \right.$$
$$\left. + 2M^2 \sqrt{\frac{{\sigma_4}^2}{4M^8} + \frac{\sigma_6 - 8MK^3 + \sigma_5}{\sigma_4} + \frac{-C^4 + \sigma_2 + C^2 \mathrm{K_p}^2 N^2 - 6K^2M^2 + \sigma_1}{M^4}} - \mathrm{K_p}^2 N^2 + 4KM \right]^{\frac{1}{2}}, \tag{15}$$

where $\sigma_1 = 2K{\mathrm{K_p}}^2MN^2$, $\sigma_2 = 4C^2KM$, $\sigma_3 = \sqrt{\frac{\sigma_7}{4M^4} - \frac{2K^2}{M^2} - \frac{8K^3M}{\sigma_4} + \frac{\sigma_6}{\sigma_4} + \frac{2C^2{\mathrm{K_p}}^2N^2}{M^4} + \frac{\sigma_5}{\sigma_4}}$,
$\sigma_4 = 2C^2M^2 + {\mathrm{K_p}}^2M^2N^2 - 4KM^3$, $\sigma_5 = 2K^2{\mathrm{K_p}}^2N^2$, $\sigma_6 = 4C^2K^2$, $\sigma_7 = {\mathrm{K_p}}^4N^4$.

The expression in equation (15) appears under the square root and is dependent on the variable parameter representing the number of pedestrians N. Consequently, numerically, equation (15) can assume any values, including complex ones. However, the physical context of the problem necessitates that only real quantities are considered. Therefore, it is imperative to establish a condition for the existence of a real non-negative solution. One such condition is the non-negativity of the radical expression in equation (15). Based on this, all conditions for a real solution are derived symbolically using MATLAB

$$\begin{aligned} N \in \mathbb{R} \wedge 2\,M^2\sqrt{\frac{{\sigma_5}^2}{4\,M^8} + \frac{\sigma_7 - 8\,M\,K^3 + \sigma_6}{\sigma_5} + \frac{-C^4 + \sigma_3 + C^2\,\mathrm{Kp}^2\,N^2 - 6\,K^2\,M^2 + \sigma_1}{M^4}} \\ + 2\sqrt{C^4 + \frac{\sigma_8}{2} + 4\,K\,M^3\,\sigma_4 - 2\,C^2\,M^2\,\sigma_4 + 3\,C^2\,\mathrm{Kp}^2\,N^2 - \sigma_3 - \mathrm{Kp}^2\,M^2\,N^2\,\sigma_4 - \sigma_1} - \sigma_2 \\ = 2\,C^2 - 4\,K\,M \wedge 2\,C^2 + \sigma_2 \neq 4\,K\,M \wedge 0 < N, \end{aligned} \tag{16}$$

where $\sigma_1 = 2\,K\,\mathrm{Kp}^2\,M\,N^2$, $\sigma_2 = \mathrm{Kp}^2\,N^2$, $\sigma_3 = 4\,C^2\,K\,M$,
$\sigma_4 = \sqrt{\frac{\sigma_8}{4\,M^4} - \frac{2\,K^2}{M^2} - \frac{8\,K^3\,M}{\sigma_5} + \frac{\sigma_7}{\sigma_5} + \frac{2\,C^2\,\mathrm{Kp}^2\,N^2}{M^4} + \frac{\sigma_6}{\sigma_5}}$, $\sigma_5 = 2\,C^2\,M^2 + \mathrm{Kp}^2\,M^2\,N^2 - 4\,K\,M^3$,
$\sigma_6 = 2\,K^2\,\mathrm{Kp}^2\,N^2$, $\sigma_7 = 4\,C^2\,K^2$, $\sigma_8 = \mathrm{Kp}^4\,N^4$.

After conducting both numerical and analytical analyses of the aforementioned constraints in MATLAB, we determine that the smallest N for which a real solution exists is governed by the condition

$$K_p^4N^4 + (4MKK_p^2 - 2C^2K_p^2)N^2 + C^4 - 4MKC^2 \geqslant 0. \tag{17}$$

By setting the left side of equation (17) to zero and substituting $N^2 = t_2$, we obtain an expression for the discriminant

$$D_2 = (4MKK_p^2 - 2C^2K_p^2)^2 - 4K_p^4(C^4 - 4MKC^2) = 16K_p^4M^2K^2, \tag{18}$$

$$\sqrt{D_2} = \pm 4K_p^2MK, \tag{19}$$

then the roots of (17) can be found from the expression

$$t_2^1 = \frac{-4MKK_p^2 + 2C^2K_p^2 + 4K_p^2MK}{2K_p^4}, \tag{20}$$

$$t_2^2 = \frac{-4MKK_p^2 + 2C^2K_p^2 - 4K_p^2MK}{2K_p^4}. \tag{21}$$

Substituting the numerical parameters into equations (20) and (17), we find that $t_2^1 > 0$ and $t_2^2 < 0$. We will subsequently perform the inverse substitution of t_2 back to N^2 and extract the root of t_2. Therefore, we will discard $t_2^2 < 0$, leading to

$$N^2 = \frac{-4MKK_p^2 + 2C^2K_p^2 + 4K_p^2MK}{2K_p^4}, \tag{22}$$

from where, leaving only the positive root, we get:

$$N = \frac{C}{K_p}. \tag{23}$$

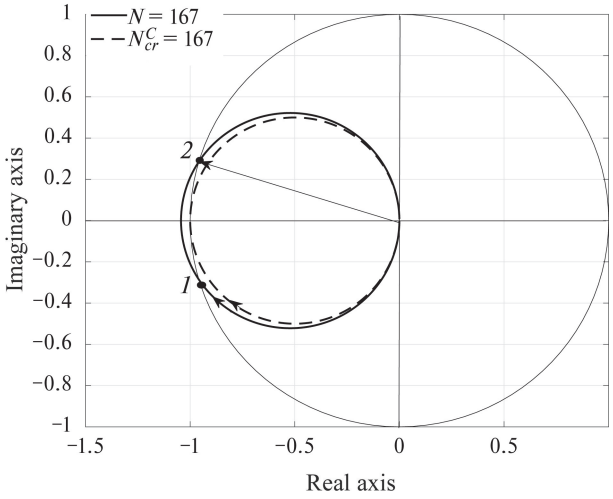

Fig. 4. Amplitude-phase frequency response of an open-loop system with varying numbers of pedestrians.

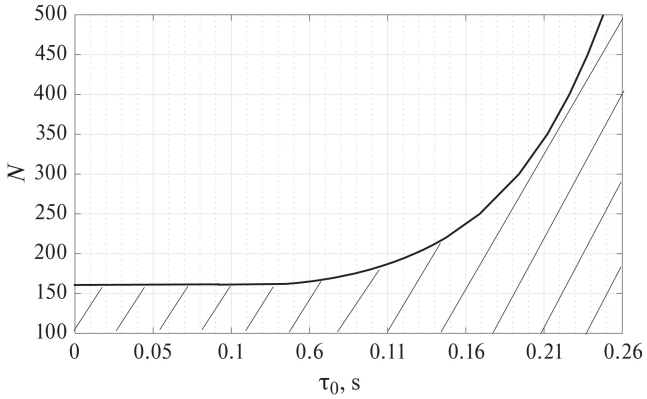

Fig. 5. The dependence of the number of pedestrians on the critical neuromuscular delay is indicated. The region of stability is marked with hatching.

By substituting the system parameters into equation (23), we obtain $N = 160.0208$, which corresponds to the critical number of pedestrians derived from Ya.Z. Tsypkin's criterion, denoted as $N_{cr}^{C} = 160$. Thus, this value represents the maximum possible number of pedestrians at which the system remains stable, independent of delay. The graphical representation of solution (9) is illustrated in Fig. 4, where the numerical result coincides with that obtained from equation (23).

Further increases in N lead to the intersection of the hodograph with the unit circle at two points. For instance, at $N = 167$, we find two solutions: $\omega_{01} = 6.45$ rad/s and $\omega_{02} = 6.48$ rad/s, with the corresponding points indicated in Fig. 4. Since $\omega_{02} > \omega_{01}$, it follows that $\tau_{02} < \tau_{01}$, where τ_{02} represents the critical delay time. For the given hodograph, this can be determined from the expression

$$\tau_{02} = \frac{\pi - \theta(\omega_{02})}{\omega_{02}}. \tag{24}$$

Substituting the numerical values into equation (24), we obtain $\tau_{02} = 0.086$ s. Thus, for $N = 167$, the critical delay for stability is $\tau_{02} = 0.086$ s, which corresponds to excessive neuromuscular tension in individuals [22]. An increase in the number of pedestrians further leads to an escalation in the critical delay required for maintaining stability.

Figure 5 illustrates the relationship between the number of pedestrians and the neuromuscular delay $N(\tau_0)$, as derived from the solutions of equations (9) and (24). The figure clearly indicates

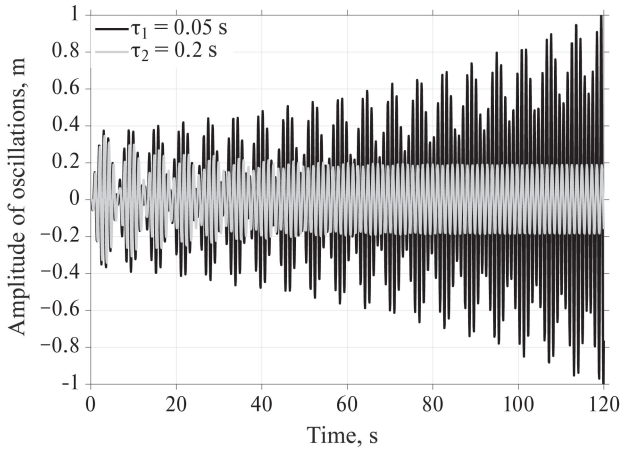

Fig. 6. Dependence of the amplitude of bridge oscillations on time for 250 pedestrians walking at a frequency of 5.4 rad/s.

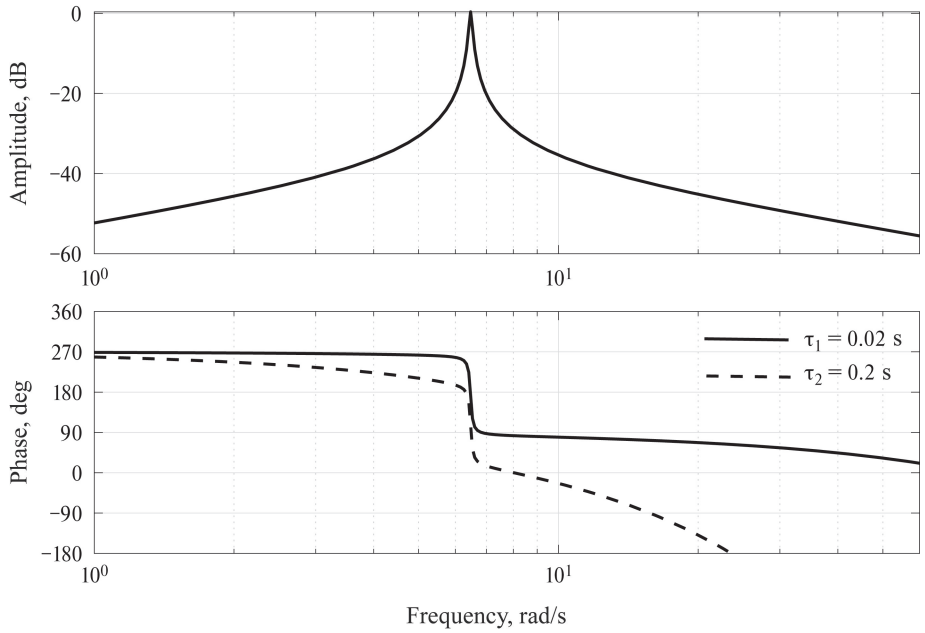

Fig. 7. Frequency response of the "bridge–pedestrians" system with different values of neuromuscular delay.

that the stability region is constrained by the number of pedestrians at minimal delays, with a sharp increase observed in the region of delay values that are typical for humans.

The dependence of the bridge oscillation amplitude on time, influenced by 250 pedestrians walking at an average frequency of 5.4 rad/s and exhibiting varying delays, is depicted in Fig. 6. At a normal delay of $\tau_2 = 0.2$ s, the bridge exhibits stable oscillations with an amplitude of approximately 20 cm. In contrast, the neuromuscular tension associated with a smaller delay of $\tau_1 = 0.05$ s results in a gradual increase in oscillation amplitude.

Figure 7 presents the amplitude-phase frequency response (APFR) of the "bridge–pedestrians" system for different values of neuromuscular delay (0.02 s and 0.2 s), which introduces a corresponding phase shift between the input and output of the system.

Thus, the stability of the system is influenced not only by the number of pedestrians but also by the delays they introduce due to the characteristics of their neuromuscular systems. This factor had not been previously considered in the analysis of the "bridge–pedestrians" system.

5. CONCLUSION

This paper proposes a novel approach to studying the stability of human-machine systems with oscillatory dynamics, exemplified by the "bridge–pedestrians" system. A linear model of the closed-loop "bridge–pedestrians" system is examined, incorporating both pedestrian muscle dynamics and processes occurring within the central nervous system. This approach enables us to represent the closed-loop system as a transfer function that includes a delay element, thereby facilitating stability assessment using methods from automatic control theory.

The applicability of this approach is demonstrated through an analysis of the swinging of the London Millennium Bridge during its opening day, when pedestrians traversed it. Utilizing Ya.Z. Tsypkin's frequency criterion across various delay values, we derived conditions pertaining to the number of pedestrians that ensure the stability of the closed-loop system is not compromised. Numerical results indicate that significant bridge oscillations can be attributed to reduced neuromuscular delays among pedestrians. Specifically, due to their heightened sensitivity to minor surface vibrations, pedestrians require time to adapt to changing conditions, which manifests as excessive neuromuscular tension. A rapid pedestrian response introduces a minimal phase shift between the input and output of the "bridge–pedestrians" system, resulting in bridge swaying and potential loss of stability. Conversely, a slower response introduces a phase shift of approximately 90 degrees, which contributes to stabilization.

The proposed approach provides a more nuanced framework for analyzing and designing structures utilized by people that exhibit oscillatory dynamics. Future research could focus on refining the parameters of the neuromuscular dynamics model while considering nonlinearities in the bridge model and the impact of external disturbances.

FUNDING

This work was supported by the Ministry of Science and Higher Education of the Russian Federation, project no. 124041500008-1.

REFERENCES

1. Dallard, P., Fitzpatrick, A., Flint, A., Le Bourva, S., Low, A., Ridsdill Smith, R.M., and Willford, M., The London Millennium footbridge, *Structural Engineers*, 2001, vol. 79, no. 22, pp. 17–33.
2. Strogatz, S., Abrams, D., Mcrobie, F., Eckhardt, B., and Ott, E., Crowd synchrony on the Millennium Bridge, *Nature*, 2005, vol. 438, pp. 43–44. https://doi.org/10.1038/43843a
3. Eckhardt, B., Ott, E., Strogatz, S.H., Abrams, D.M., and McRobie, A., Modeling walker synchronization on the Millennium Bridge, *Phys. Rev. E*, 2007, vol. 75, pp. 021110. https://doi.org/10.1103/PhysRevE.75.021110
4. Josephson, B., Out of step on the bridge, *Letter to the Editor. The Guardian. UK*, 2000.
5. Barker, C., Some observations on the nature of the mechanism that drives the self-excited lateral response of footbridges, *International Conference on the Design and Dynamic Behaviour of Footbridges*, Paris, 2002.
6. Kuramoto, Y., Self-entrainment of a population of coupled non-linear oscillators, in *International Symposium on Mathematical Problems in Theoretical Physics*, Araki, H., Rd., Berlin, Heidelberg: Springer, 1975, pp. 420–422.
7. Macdonald, J., Pedestrian-induced vibrations of the Clifton Suspension Bridge, UK, *Proceedings of The Ice-Bridge Engineering*, 2008, vol. 161, no. 2, pp. 69–77. https://doi.org/10.1680/bren.2008.161.2.69
8. Belykh, I., Bocian, M., Champneys, A., Daley, K., Jeter, R., Macdonald, J.H.G., and McRobie, A., Emergence of the London Millenium Bridge instability without synchronization, *Nature Communications*, 2021, vol. 12, no. 1, p. 7223. https://doi.org/10.1038/s41467-021-27568-y

9. Belykh, I., Jeter, R., and Belykh, V., Foot force models of crowd dynamics on a wobbly bridge, *Science Advances*, 2017, vol. 3, no. 11, p. e1701512. https://doi.org/10.1126/sciadv.1701512

10. Belykh, I.V., Daley, K.M., and Belykh, V.N., Pedestrian-induced bridge instability: the role of frequency ratios, *Radiophys. Quant. Electron.*, 2022, vol. 64, no. 10, pp. 700–708. https://doi.org/10.1007/s11141-022-10172-5

11. Živanović, S., Pavic, A., and Reynolds, P., Vibration serviceability of footbridges under human-induced excitation: a literature review, *J. Sound Vibrat.*, 2005, vol. 279, no. 1–2, pp. 1–74. https://doi.org/10.1016/j.jsv.2004.01.019

12. Chopra, A.K., *Dynamics of structures: Theory and applications to earthquake engineering*, Englewood Cliffs: Prentice Hall, 1995.

13. Clough, R. and Penzien, J., *Dynamics of Structures*, New York: McGraw-Hill, 1993.

14. Bachmann, H., Pretlove, A., and Rainer, H., *Dynamic forces from rhythmical human body motions, in: Vibration Problems in Structures: Practical Guidelines*, Birkhauser, Basel, 1995, Appendix G.

15. Shahabpoor, E., Pavic, A., Racic, V., and Zivanovic, S., Effect of group walking traffic on dynamic properties of pedestrian structures, *J. Sound Vibrat.*, 2017, vol. 387, pp. 207–225. https://doi.org/10.1016/j.jsv.2016.10.017

16. Van Nimmen, K., Pavic, A., and Van den Broeck, P., A simplified method to account for vertical human-structure interaction, *Structures*, 2021, vol. 32, pp. 2004–2019. https://doi.org/10.1016/j.istruc.2021.03.090

17. Macdonald, J., Lateral excitation of bridges by balancing pedestrians, *Proc. R. Soc. Lond.*, 2009, vol. 465, pp. 1055–1073. https://doi.org/10.1098/rspa.2008.0367

18. Czaplewski, B., Bocian, M., and Macdonald, J.H.G., Calibration of inverted pendulum pedestrian model for laterally oscillating bridges based on stepping behaviour, *J. Sound Vibrat.*, 2024, vol. 572, no. 22, pp. 118141. https://doi.org/10.1016/j.jsv.2023.118141

19. Bukov, V.N., Optimization of human-machine systems based on prediction of the functional state of the operator, *AiT*, 1995, vol. 12, pp. 124–137.

20. Racic, V. and Morin, J.B., Data-driven modelling of vertical dynamic excitation of bridges induced by people running, *Mechanical Systems and Signal Processing*, 2014, vol. 43, no. 1, pp. 153–170. https://doi.org/10.1016/j.ymssp.2013.10.006

21. Yao, S., Wright, J., Pavic, A., and Reynolds, P., Forces generated when bouncing or jumping on a flexible Structure, *International Conference on Noise and Vibration*, Leuven, Belgium, 2002, pp. 563–572.

22. Byushgens, G.S. and Studnev, R.V., *Aerodinamika samoleta. Dinamika prodol'nogo i bokovogo dvizheniya* (Aerodynamics of the aircraft. Dynamics of longitudinal and lateral movement,) Moscow: Mashinostroenie, 1979.

23. McRuer, D., Pilot-Induced Oscillations and Human Dynamic Behavior: Tech. Rep. 4683: NASA, 1995.

24. Kurochkin, I.V. and Maltsev, A.A., On static optimization of interaction of components of human-machine systems, *AiT*, 1981, vol. 8, pp. 35–45.

25. Efremov, A.V., Ogloblin, A.V., Predtechensky, A.N., and Rodchenko, V.V., *Letchik kak dinamicheskaya sistema* (The pilot as a dynamic system), Moscow: Mashinostroenie, 1992.

26. Hess, R., A Model for the Human Use of Motion Cues in Vehicular Control, *Guidance, Control, Dynam.*, 1990, vol. 13, no. 3, pp. 476–482.

27. McRuer, D., Graham, D., Krendel, E., and Reisener, W., Human Pilot Dynamics in Compensatory Systems: Theory, Models and Experiments with Controlled-Element and Forcing Function Variations. Amsterdam, The Netherlands: Elsevier Ltd., 1965. AFFDL-TR-65-15.

28. Hess, R.A., A Model-Based Theory for Analyzing Human Control Behavior, *Advances in Man-Machine Systems Research.*, 1985, vol. 2, pp. 129–175.

29. Liang, H., Xie, W., Wei, P., Dehao, A., and Zhiqiang, Z., Identification of Dynamic Parameters of Pedestrian Walking Model Based on a Coupled Pedestrian-Structure System, *Appl. Sci.*, 2021, vol. 11, no. 14, pp. 1–23. https://doi.org/10.3390/app11146407

30. Magdaleno, R. and McRuer, D., Experimental Validation and Analytical Elaboration for Models of the Pilot's Neuromuscular Subsystem in Tracking Tasks: Tech. Rep. CR-1757: NASA, 1971.

31. Hess, R., Moore, J.K., and Hubbard, M., Modeling the Manually Controlled Bicycle, *IEEE Transactions on Systems, Man, and Cybernetics. Part A: Systems and Humans*, 2012, vol. 42, no. 3, pp. 545–557. https://doi.org/10.1109/TSMCA.2011.2164244

32. Andriacchi, T., Ogle, J., and Galante, J., Walking speed as a basis for normal and abnormal gait measurements, *J. Biomech.*, 1977, vol. 10, no. 4, pp. 261–268.

33. Han, H., Zhou, D., Ji, T., and Zhang, J., Modelling of lateral forces generated by pedestrians walking across footbridges, *Appl. Math. Modell.*, 2021, vol. 89, pp. 1775–1791. https://doi.org/10.1016/j.apm.2020.08.081

34. Tsypkin, Ya.Z., Stability of systems with delayed feedback, *AiT*, 1946, vol. 7, no. 2–3, pp. 107–129.

35. Nikolsky, A.A., Generalized stability criteria for special linear automatic control systems with delay, *Electricity*, 2020, vol. 1, pp. 38-46. https://doi.org/10.24160/0013-5380-2020-11-38–46

This paper was recommended for publication by N.V. Kuznetsov, a member of the Editorial Board

ISSN 0005-1179 (print), ISSN 1608-3032 (online), Automation and Remote Control, 2025, Vol. 86, No. 1, pp. 86–98.

Algebraic Methods of the Synthesis of Models Based on the Graphical Representation of Finite State Machines

V. V. Menshikh[*,a] **and V. A. Nikitenko**[*,b]

[*] *Voronezh Institute of the Ministry of Internal Affairs of Russia, Voronezh, Russia*
e-mail: [a] *menshikh@list.ru,* [b] *vitalijnikitenko82043@gmail.com*

Received April 10, 2024
Revised July 24, 2024
Accepted September 2, 2024

Abstract—The issues of modeling objects and systems based on the graphical representation of finite state machines using algebraic methods are considered. The problem of finite state machines synthesis based on the construction of the algebra of their graphoids is solved. With this aim existing operations on finite state machines are transferred to their graphoids. Subject to additional requirements, that may emerge during the analysis of the subject area new operations are introduced. This defines the algebra of finite state machines graphoids, which enables the synthesis of graphoids for finite state machines models using the algorithm proposed by the authors. Statements confirming the correctness of the algorithm are proven. A numerical example of the finite state machines model graphoid synthesis for the joint actions of functional groups in an emergency area.

Keywords: finite state machines graphoids, operations on graphoids, algebra of graphoids, the parallel synchronous change of automata states, parallel synchronous state transitions of automata of finite state machines states, invalid states, invalid vertex, graphoid synthesis

DOI: 10.31857/S0005117925010075

1. INTRODUCTION

An effective tool for modeling the dynamics of object and system functioning in various subject areas is finite automata [1]. However, as the complexity of the modeled objects and systems increases, the size of the input, output, and state alphabets of the automaton grows significantly. This substantially complicates the modeling process, makes the models excessively cumbersome, and hinders the interpretation of the modeling results. In this case, an effective approach is the use of a systemic methodology, according to which the object or system is initially decomposed into components, automata models for individual components are developed, and a general model is synthesized [2, 3]. The implementation of each of the aforementioned stages largely depends on the specific characteristics of the subject area of the modeled objects or systems. The most challenging stage is the synthesis of the general model, as it has the greatest impact on its adequacy. For instance, in [4, 5], automata theory methods were used to model the behavior of digital production twins based on automata algebra, which included not only well-known operations but also operations introduced by the authors to account for the peculiarities of the modeled object. Other examples of introducing domain-specific operations on automata and utilizing automata algebra can be found in [6–8]. Another challenge arising during the synthesis of automata models is the presence of significant constraints on the selection of possible components for the general model. If the component models must correspond to predefined objects or systems, specific requirements may be imposed on the synthesis process of the general model. These requirements include the

necessity to eliminate invalid combinations of states in the components of the general model. An example of this is the task of modeling the joint actions of several functional groups involved in responding to an emergency situation [9, 10]. Constraints may arise, for instance, from the need to prevent conflicts between functional groups or to account for synergistic effects during their coordinated actions [11]. Automata that model the functioning of these groups serve as components of the general model for the emergency response process. It should be noted that the set of states of the components of the general model is often fully known. In this case, the automaton is represented as a labeled graph (a graphoid), where the vertices correspond to states, the edges represent transitions between states, and the edge weights describe the automaton's responses to various input symbols. This circumstance enables the synthesis of the graphoid of the general model by combining the graphoids of the automata models of its components. The solution to this problem can be achieved using algebraic methods. In [12, 13], the concept of an algebra of finite deterministic automata was introduced based on a set of composition operations, which are also applicable to automata graphoids. In particular, necessary and sufficient conditions for the decomposition of an automaton into a network of component automata were established using the introduced operations and by solving automaton equations through a specially defined language of paired algebras. The approaches used are naturally applicable to automata graphoids, whose representation is simply augmented with descriptions of the corresponding automata. However, in some subject areas, the solution obtained using the approach described in these works may fail to produce meaningful results because it does not account for potential constraints on the joint functioning of the components. In this regard, the task of developing a universal approach to synthesizing the graphoid of the general model, which takes into account the constraints on the joint functioning of the modeled objects or systems, is particularly relevant. In this work, this problem is addressed through the use of algebraic methods, and the correctness of the proposed approach is also substantiated.

2. THE ALGEBRA OF FINITE STATE MACHINES GRAPHOIDS

By the algebra $\mathcal{A} = \langle \mathcal{N}, \mathcal{S} \rangle$, according to [14], we mean the set $\mathcal{N}$ along with the operations defined on it.

$$\mathcal{S} = \{f_{11}, f_{12}, \ldots, f_{1n_1}, f_{21}, f_{22}, \ldots, f_{2n_2}, \ldots, f_{m1}, f_{m2}, \ldots, f_{mn_m}\},$$

where $\mathcal{N}$ is the carrier, and $\mathcal{S}$ is the signature of the algebra (f_{kl} is the lth k-ary operation).

A graphoid G of a finite deterministic non-initial abstract Moore automaton A is a quadruple [15] (Q, F, X, Y), where Q is the set of numbered vertices corresponding to the states of automaton A; F is the operator describing weighted edges, i.e., transitions between states and their corresponding output symbols depending on the input symbols; X is the input alphabet of automaton A; Y is the output alphabet of automaton A.

The notation $A\langle G$ will be used when automaton A corresponds to graphoid G.

We will now provide descriptions of operator F that are convenient for further use.

Expression

$$F^{x/y}q^i = q^{i_s}(x/y).$$

It means that if the automaton is in a state corresponding to the vertex of the graphoid q^i and the input symbol $x \in X$, is received, the automaton will transition to the state corresponding to the vertex of the graphoid q^{i_s} and an output symbol $y \in Y$ will be generated.

Denote

$$Fq^i = \bigcup_{\substack{x \in X \\ y \in Y}} \left\{F^{x/y}q^i\right\}.$$

In these notations, the result of the operation of the operator F can be described as

$$\left\{Fq^i = \{q^{i_1}(x^{j_1}/y^{k_1}), \ldots, q^{i_l}(x^{j_l}/y^{k_l}), \ldots, q^{i_{n_i}}(x^{j_{n_i}}/y^{k_{n_i}})\}, i = \overline{1, |Q|}\right\}.$$

It is assumed that in general, $\{x^{j_1}, \ldots, x^{j_{n_i}}\} \subseteq X$, i.e., the automaton can be partial.

The operator F can be represented as a symbolic matrix, where the elements are pairs x/y. The algebra of such matrices described in [3] simplifies the process of developing numerical methods for operating with graphoids. However, this requires justification for the correctness of the operations used.

The introduction of the concept of the algebra of automata graphoids, where the carrier $\mathcal{N}$ is some set of graphoids $\mathcal{G}_0$, allows formalizing the procedure for synthesizing the graphoid of the general model of objects or systems, whose automata models are described by graphoids contained in the set $\mathcal{G}_0$, using various operations.

Let us now turn to the description and justification of the correctness of these operations.

3. ALGEBRA OF FINITE STATE MACHINE'S GRAPHOIDS OPERATIONS

Define the operation $\times$ on finite non-empty pairwise disjoint sets $M_1 = \left\{m_1^1, \ldots, m_{|M_1|}^1\right\}, \ldots, M_n = \left\{m_1^n, \ldots, m_{|M_n|}^n\right\}$:

$$M_1 \times \ldots \times M_n = \left\{\left\{m_{i_1}^1, \ldots, m_{i_n}^n\right\} | i_1 = \overline{1, |M_1|}, \ldots, i_n = \overline{1, |M_n|}\right\}.$$

In this case $\times$ is not the Cartesian product because a result doesn't depend on order of operation. It enables to provide the commutativity of operations on of finite state machine's graphoids.

Suppose $G_1, G_2 \in \mathcal{G}_0$ — graphoids

$$G_1 = (Q_{G_1}, F_{G_1}, X_{G_1}, Y_{G_1}); \tag{1}$$
$$G_2 = (Q_{G_2}, F_{G_2}, X_{G_2}, Y_{G_2}). \tag{2}$$

If graphoids (1) and (2) satisfy the conditions

$$Y_{G_1} \cap X_{G_2} = \varnothing; \tag{3}$$
$$Y_{G_2} \cap X_{G_1} = \varnothing, \tag{4}$$
$$\Pi = G_1 \times G_2 = (Q_\Pi, F_\Pi, X_\Pi, Y_\Pi),$$

then $q_\Pi \in Q_\Pi$ will be define like $q_\Pi = \{q_{G_1}, q_{G_2}\}$ and $Q_\Pi, F_\Pi, X_\Pi, Y_\Pi$ will be set by equation:

$$Q_\Pi = Q_{G_1} \times Q_{G_2};$$
$$F_\Pi q_\Pi = F_{G_1} q_{G_1} \times F_{G_2} q_{G_2};$$
$$X_\Pi = X_{G_1} \times X_{G_2};$$
$$Y_\Pi = Y_{G_1} \times Y_{G_2}.$$

The graphoid Π corresponds to the parallel operation of automata described by graphoids G_1 and G_2, with synchronized state transitions.

If graphoids (1) and (2) satisfy the condition

$$X_{G_1} \cap X_{G_2} = \varnothing, \tag{5}$$

then the $+$ of graphoids (1) and (2) is defined as the graphoid

$$\Sigma = G_1 + G_2 = (Q_\Sigma, F_\Sigma, X_\Sigma, Y_\Sigma),$$

where $q_\Sigma \in Q_\Sigma$ is defined as $q_\Sigma = \{q_{G_1}, q_{G_2}\}$, and $Q_\Sigma, F_\Sigma, X_\Sigma, Y_\Sigma$ are determined by the following formulas

$$Q_\Sigma = Q_{G_1} \times Q_{G_2};$$
$$F_\Sigma q_\Sigma = (F_{G_1} q_{G_1} \times \{q_{G_2}\}) \cup (\{q_{G_1}\} \times F_{G_2} q_{G_2});$$
$$X_\Sigma = X_{G_1} \cup X_{G_2};$$
$$Y_\Sigma = Y_{G_1} \cup Y_{G_2}.$$

The graphoid Σ corresponds to the parallel operation of automata described by graphoids G_1 and G_2, with asynchronous state transitions.

Condition (5) eliminates the possibility of ambiguity during state transitions after performing the + operation, i.e., it prevents the emergence of a nondeterministic automaton.

It should be noted that from the definition of the $\times$ and + operations for graphoids (1) and (2), it follows that

$$Q_{G_1 \times G_2} = Q_{G_1 + G_2}. \tag{6}$$

Thus, the algebra $\mathcal{A}_1 = \langle \mathcal{G}_1, \mathcal{S}_1 \rangle$, where $\mathcal{S}_1 = \{\times, +\}$ is described and possesses the following properties:

$$(G_1 \times G_2) \times G_3 = G_1 \times (G_2 \times G_3);$$
$$G_1 \times G_2 = G_2 \times G_1;$$
$$(G_1 + G_2) + G_3 = G_1 + (G_2 + G_3);$$
$$G_1 + G_2 = G_2 + G_1.$$

Consequently, the algebra $\mathcal{A}_1$ is a commutative semigroup with respect to each operation in the signature $\mathcal{S}_1$.

4. THE COMPOSITION OF GRAPHOIDS

When simulating real systems, it is necessary to take into account the characteristics of the subject area, which lead to additional requirements for the synthesis of automatic models, which in turn imposes some restrictions on the operations on their graphs. The most common requirements are:

1) changing the state of one object or system can trigger a change in the state of another object or system;

2) an object or system obtained by performing operations may contain invalid states.

In this connection, there is a need to extend the $\mathcal{S}_1$ signal of algebra $\mathcal{A}_1$ by introducing operations that allow taking into account the described features.

The first feature is implemented by introducing the concept "state-trigger," which assumes that the transition of one automaton into this state initiates the transition of another automaton to a certain specified state depending on its current state, i.e. at least one of the conditions (3) or (4) is not met. Consider the process of operation of the automata, which are described by graphs (1) and (2), in this case.

If the vertex $q^i_{G_1}$ corresponds to the state-trigger of $A_1\langle G_1$, automaton, which initiates state change in $A_2\langle G_2$ automaton, then for convenience of further description we will designate this vertex as ${}^{T_{G_2}}q^i_{G_1}$.

Let the $A_1\langle G_1$ have a trigger state corresponding to the vertex of ${}^{T_{G_2}}q^i_{G_1}$, and in this finite state machine corresponds to the output character $y^k_{G_1}$. This symbol simultaneously serves as an input symbol for the automaton $A_2\langle G_2$ and initiates a state transition in it as follows: if $A_2\langle G_2$ was in a certain state corresponding to the vertex $q^s_{G_2}$, and the set of its input symbols that trigger a state

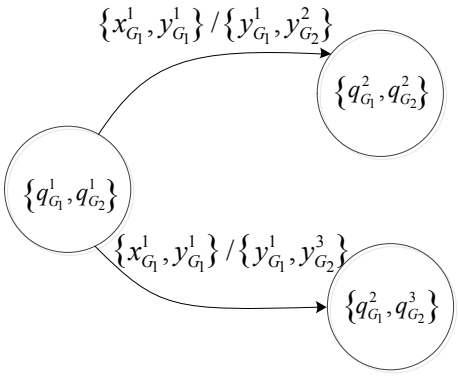

Fig. 1. Graphoid of the sub-automaton of automaton $A_{1,2}\langle K$.

transition includes $y^k_{G_1}$, then $A_2\langle G_2$ transitions from the state corresponding to the vertex $q^s_{G_2}$ a new state based on the input symbol $y^k_{G_1}$.

It is also possible that the automaton $A_2\langle G_2$ initiates state transitions in the automaton $A_1\langle G_1$, i.e., $A_2\langle G_2$ contains a trigger state corresponding to the vertex ${}^{T_{G_1}}q^i_{G_2}$.

Thus, there arises the need to describe a graphoid that represents the joint operation of two automatons, at least one of which contains a trigger state that influences the operation of the other.

If for graphoids (1) and (2) at least one of the conditions (3) or (4) is not satisfied, the composition $\circ$ of the graphoids is called a graphoid.

$$K = G_1 \circ G_2 = (Q_K, F_K, X_K, Y_K),$$

if Q_K, F_K, X_K, Y_K satisfy the following conditions:

$$Q_K = Q_{G_1} \times Q_{G_2};$$
$$F_K q_K = \bigcup_{\substack{t \in Y_{G_2} \\ l \in Y_{G_1}}} F^{t/l}_{G_1} q_{G_1} \times F^{l/t}_{G_2} q_{G_2};$$
$$X_K = X_{G_1} \times X_{G_2};$$
$$Y_K = Y_{G_1} \times Y_{G_2},$$

where $F^{t/l}_{G_1} q_{G_1}$is the transition mapping of the automaton from the state corresponding to the vertex q_{G_1} of graphoid G_1 when its input symbol $t \in X_{G_1} \cap Y_{G_2}$ appears, resulting in the output symbol $l \in Y_{G_1}$,

Similarly, $F^{l/t}_{G_2} q_{G_2}$ is the transition mapping of the automaton from the state corresponding to the vertex q_{G_2} of graphoid G_2, when its input symbol $l \in X_{G_2} \cap Y_{G_1}$ appears, resulting in the output symbol $t \in Y_{G_2}$.

It is worth noting that from the definition of the operations $\circ$, $\times$ and $+$ for graphoids (1) and (2), it follows that:

$$Q_{G_1 \circ G_2} = Q_{G_1 \times G_2} = Q_{G_1 + G_2}. \tag{7}$$

Proposition 1. *Let the graphoids* (1) *and* (2) *correspond to deterministic automata A_1 and A_2, and do not satisfy at least one of the conditions* (3) *or* (4)*. Then, $K = G_1 \circ G_2$ is a graphoid of a deterministic automaton.*

Proof. Assume that the automaton $A_{1,2}\langle K$ is nondeterministic. Without loss of generality, we can assume that it contains a subautomaton whose graphoid is shown in Fig. 1, where $y^1_{G_1} = x^1_{G_2}$ appears.

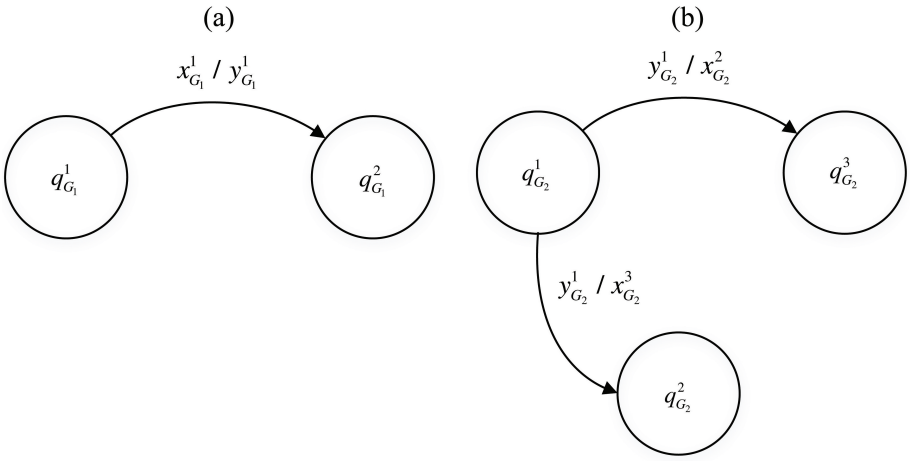

Fig. 2. (a) Graphoid of the sub-automaton A_1, (b) graphoid of the sub-automaton A_2.

Then, in automata A_1 and A_2, there will be subautomata whose graphoids are shown in Fig. 2.

Therefore, in this case, automaton A_2 would be nondeterministic, which contradicts the condition of the theorem.

Note that due to the associativity and commutativity of the operations $\times, \cup$, the composition operation $\circ$ also possesses these properties:

$$(G_1 \circ G_2) \circ G_3 = G_1 \circ (G_2 \circ G_3);$$
$$G_1 \circ G_2 = G_2 \circ G_1.$$

It is evident that if conditions (3) and (4) are satisfied, then $G_1 \circ G_2 = G_1 \times G_2$.

Let us define a new algebra $\mathcal{A}_2 = \langle \mathcal{G}_2, \mathcal{S}_2 \rangle$ with the signature $\mathcal{S}_2 = \{\circ, \times, +\}$, which, like the algebra $\mathcal{A}_1$, forms a commutative semigroup under each operation.

5. THE OPERATION OF GRAPHOID FILTERING

After performing the binary operations of the signature $\mathcal{S}_2$ a new graphoid of the algebra $\mathcal{A}_2$ is obtained. The automaton corresponding to this graphoid may not satisfy the constraints for the joint functioning of the components of the overall model because the resulting automaton may contain invalid combinations of their states, considering the specific characteristics of the domain. That is, conflict situations arise in the resulting automaton (it is assumed that the set of conflict situations is defined by the decision-maker). As a result, there is a need to introduce a filtering operation ∇, which allows excluding vertices of the graphoid that correspond to invalid states of the automaton. These vertices will also be referred to as invalid.

It should be noted that in [12, 13], only the issues of finding and removing unreachable states of automata were studied, which helps reduce the dimensionality of the problem, but may not meet the requirements of the domain.

Let $\Omega_1, \ldots, \Omega_n$ be the generators of the algebra $\mathcal{A}_2$, i.e., the graphoids from which, using the operations signature $\mathcal{S}_2$ of the all other graphoids of the carrier $\mathcal{G}_2$ can be obtained.

Let us define the set $\Psi = \{\Psi_1, \ldots, \Psi_k, \ldots, \Psi_r\}$ of invalid vertices of some graphoid. Each vertex Ψ_k corresponds to the set $\left\{q^{l_{k_1}}_{\Omega_{k_1}}, \ldots, q^{l_{|\Psi_k|}}_{\Omega_{k_{|\Psi_k|}}}\right\}$ of vertices, which are the generators of the algebra $\mathcal{A}_2$.

Let the graphoid $H = (Q_H, F_H, X_H, Y_H)$ be obtained by transforming the graphoid $G_1, \ldots, G_m \in \mathcal{G}_2$ using the operations of the signature $\mathcal{S}_2$. Then, the set of all vertices of the graphoid H is as follows:

$$Q_H = \Big\{Q_{G_1}, \ldots, Q_{G_m}, \{Q_{G_i j} | Q_{G_i j} = Q_{G_i} \times Q_{G_j}, \forall i, j \in \{1, m\}, i \neq j\}, \ldots,$$
$$\{Q_{G_{i_1,\ldots,i_n}} | Q_{G_{i_1,\ldots,i_n}} = Q_{G_{i_1}} \times \ldots \times Q_{G_{i_n}}, \forall i_1, \ldots, i_n \in \{1, m\}, i_1 \neq \ldots \neq i_n\}\Big\}.$$

Let us define the function

$$\pi(q_H, \Psi_k) = \begin{cases} 1, & \text{if } \Psi_k \subseteq q_H \\ 0, & \text{otherwise.} \end{cases}$$

Then the vertex $q_H \in Q_H$ is invalid if:

$$\sum_{k=1}^{r} \pi(q_H, \Psi_k) \neq 0.$$

Let us denote as

$$\Xi_H = \left\{ q_H \in Q_H | \sum_{k=1}^{r} \pi(q_H, \Psi_k) \neq 0 \right\}$$

a set of invalid vertexes.

For exclude invalid states, we introduce a unary filtering operation ∇.

The graphoid $\nabla_{\Xi_H} H$ is called the filtration of the graphoid H by the set Ξ_H if it is a subgraph of the graphoid H with the set of vertices $Q_{\nabla_{\Xi_H} H} = Q_H \setminus \Xi_H$.

Thus, the algebra $\mathcal{A}_3 = \langle \mathcal{G}_3, \mathcal{S}_3 \rangle$ with the signature $\mathcal{S}_3 = \{\nabla, \circ, \times, +\}$ is obtained.

6. ALGORITHM FOR GRAPHOID SYNTHESIS OF A FINITE STATE MACHINE MODEL

To develop this algorithm, we first define the algebra of graphoids, whose signature contains only the operations necessary to solve the problem of synthesizing graphoids for automaton models, taking into account the features described above.

Consider automata functioning simultaneously, which are described by graphoids (1) and (2). Their state transitions can occur either simultaneously or at different times. Therefore, the operation of the automata can be:

- Either synchronized, which in the synthesis process is described by:
  - — the operation $\times$, if they do not contain triggers that influence each other's functioning;
  - — the operation $\circ$, if they contain triggers that influence each other's functioning;
- or asynchronous, which is described by the operation $+$.

Both possibilities for the functioning of the automata must be taken into account during the synthesis process. Based on this, it is necessary to combine the operations $\circ, \times$ and $+$. For this, we introduce the union operation $\cup$ of graphoids.

Let the condition (5) hold for graphoids (1) and (2), and $Q_{G_1} = Q_{G_2}$, then the union $\cup$ of the graphoids is called the graphoid

$$C = G_1 \cup G_2 = (Q_C, F_C, X_C, Y_C),$$

where Q_C, F_C, X_C, Y_C are defined by following formulas:

$$Q_C = Q_{G_1} = Q_{G_2};$$
$$F_C q_C = F_{G_1} q_{G_1} \cup F_{G_2} q_{G_2};$$
$$X_C = X_{G_1} \cup X_{G_2};$$
$$Y_C = Y_{G_1} \cup Y_{G_2}.$$

This operation has the following properties:

$$(G_1 \cup G_2) \cup G_3 = G_1 \cup (G_2 \cup G_3);$$
$$G_1 \cup G_2 = G_2 \cup G_1.$$

Considering the properties (6) and (7) of the operations $\circ, \times$ and $+$ introduced above, the synthesis process of graphoids for automaton models can be carried out using the following combinations of these operations:

$$G_1 \otimes G_2 = (G_1 \times G_2) \cup (G_1 + G_2);$$
$$G_1 \odot G_2 = (G_1 \circ G_2) \cup (G_1 + G_2).$$

The graphoids obtained after performing the operations $\otimes$ and $\odot$ may correspond to automata that contain unacceptable states. To exclude them, the filtration operation ∇ must be used.

The above leads to the conclusion that the algebra $\mathcal{A} = \langle \mathcal{G}, \mathcal{S} \rangle$, where $\mathcal{S} = \{\nabla, \otimes, \odot\}$, can be used for synthesizing graphoids of automaton models.

Now, let's consider the algebraic properties of the operations in the signature $\mathcal{S}$.

From the commutativity and associativity of the operations $\circ, \times, +, \cup$, it follows that the operations $\otimes$ and $\odot$ are also commutative and associative. Therefore, the order in which the synthesis of the overall model is carried out using these operations does not matter.

Let $\bullet$ denote one of the operations in the set $\{\otimes, \odot\}$. Suppose the graphoids $G_{i_1}, G_{i_2}, G_{i_3}, \ldots, G_{i_s}$ are obtained by transforming the graphoids $G_1, \ldots, G_m \in \mathcal{G}$ using operations from the signature $\mathcal{S}$. Then the following statement holds.

Proposition 2.

$$\nabla(G_{i_1} \bullet G_{i_2} \bullet G_{i_3} \bullet \ldots \bullet G_{i_s}) = \nabla\Big(\nabla\Big(\ldots\Big(\nabla((\nabla G_{i_1}) \bullet G_{i_2}) \bullet G_{i_3}\Big) \bullet \ldots\Big) \bullet G_{i_s}\Big).$$

Proof. We will use the method of mathematical induction.

Let $\Xi_{G_{i_t}}$ be the set of unacceptable vertices of the graphoid G_{i_t}, and let Ξ contain all possible unacceptable vertices of combinations of the graphoids $G_{i_1}, G_{i_2}, G_{i_3}, \ldots, G_{i_s}$.

(1) Base case $s = 2$. We need to prove that $\nabla(G_{i_1} \bullet G_{i_2}) = \nabla\big((\nabla G_{i_1}) \bullet G_{i_2}\big)$.
The set of vertices $\nabla(G_{i_1} \bullet G_{i_2})$ is $Q_{G_{i_1} \bullet G_{i_2}} = \widehat{Q}_{G_{i_1} \bullet G_{i_2}} \setminus \Xi$, and the set of vertices of $\nabla((\nabla G_{i_1}) \bullet G_{i_2})$ is $Q_{G_{i_1} \bullet G_{i_2}} = ((\widehat{Q}_{G_{i_1}} \setminus \Xi_{G_{i_1}}) \times \widehat{Q}_{G_{i_2}}) \setminus \Xi$.
Now, let us transform the last expression:

$$Q_{G_{i_1} \bullet G_{i_2}} = \Big((\widehat{Q}_{G_{i_1}} \setminus \Xi_{G_{i_1}}) \times \widehat{Q}_{G_{i_2}}\Big) \setminus \Xi = \Big((\widehat{Q}_{G_{i_1}} \times \widehat{Q}_{G_{i_2}}) \setminus (\Xi_{G_{i_1}} \times \widehat{Q}_{G_{i_2}})\Big) \setminus \Xi. \qquad (8)$$

In the set $\Xi_{G_{i_1}} \times \widehat{Q}_{G_{i_2}}$ all vertices are unacceptable, so, $\Xi_{G_{i_1}} \times \widehat{Q}_{G_{i_2}} \subseteq \Xi$, and we can rewrite the expression (6) as: $(\widehat{Q}_{G_{i_1}} \times \widehat{Q}_{G_{i_2}}) \setminus \Xi$, which corresponds to $\nabla(G_{i_1} \bullet G_{i_2})$.

(2) Assume that the statement is true for $s = k$ We now need to prove that it holds for $s = k+1$. We have:

$$\nabla(G_{i_1} \bullet G_{i_2} \bullet G_{i_3} \bullet \ldots \bullet G_{i_s} \bullet G_{i_{s+1}})$$
$$= \nabla\Big(\nabla\Big(\nabla\Big(\ldots\Big(\nabla(\nabla(G_{i_1}) \bullet G_{i_2}) \bullet G_{i_3}\Big) \bullet \ldots\Big) \bullet G_{i_s}\Big) \bullet G_{i_{s+1}}\Big),$$

since the graphoids $G_{i_1}, G_{i_2}, G_{i_3}, \ldots, G_{i_s}$ are obtained by transformations using the operations of the signature $\mathcal{S}$, the expression $G_{i_1} \bullet G_{i_2} \bullet G_{i_3} \bullet \ldots \bullet G_{i_s}$ can be replaced by the equivalent graphoid $H = G_{i_1} \bullet G_{i_2} \bullet G_{i_3} \bullet \ldots \bullet G_{i_s}$. Thus, we obtain the expression $\nabla(G_{i_1} \bullet G_{i_2} \bullet G_{i_3} \bullet \ldots \bullet G_{i_s} \bullet G_{i_{s+1}})$ is $\nabla(H \bullet G_{i_{s+1}})$. Therefore, it is necessary to show the validity of the equality $\nabla(H \bullet G_{i_{s+1}}) = \nabla\big((\nabla H) \bullet G_{i_{s+1}}\big)$, which was proven in part 1).

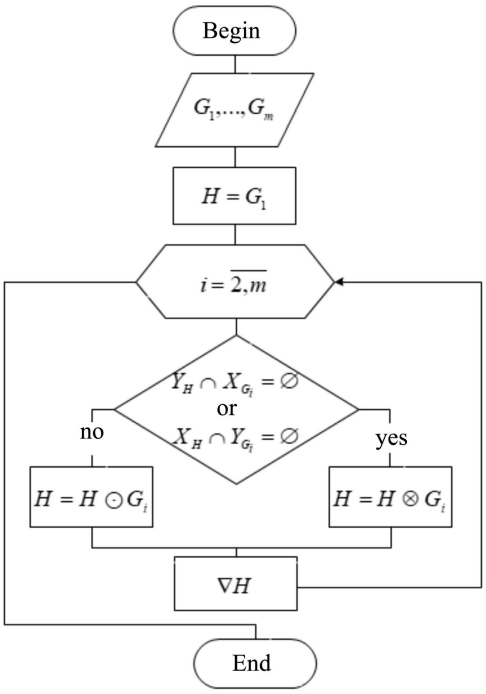

Fig. 3. Algorithm for synthesizing graphoids of automaton models.

Thus, the algorithm for synthesizing graphoids from $\mathcal{G}$ is as shown in Fig. 3. Its correctness follows from the algebraic properties of the operations of the signature $\mathcal{S}$ and the theorem proven above.

7. NUMERICAL EXAMPLE

As an example, consider the process of access control to an emergency zone, the organization of search and rescue operations, and the evacuation of people and material assets from this zone [10], which involves the use of the following standard functional groups:

(1) Organization of access to the emergency zone, whose actions are modeled by automaton $A_1\langle(G_1 = (Q_{G_1}, F_{G_1}, X_{G_1}, Y_{G_1}))$;
(2) Organization of the search for people and material assets to be evacuated, whose actions are modeled by automaton $A_2\langle(G_2 = (Q_{G_2}, F_{G_2}, X_{G_2}, Y_{G_2}))$;
(3) Organization of evacuation to a safe area, whose actions are modeled by automaton $A_3\langle(G_3 = (Q_{G_3}, F_{G_3}, X_{G_3}, Y_{G_3}))$.

During the development of the emergency situation, the listed functional groups can be in states corresponding to the vertices indicated in table.

Description of the vertices of the graphoids corresponding to the states of the automata $A_1\langle G_1, A_2\langle G_2, A_3\langle G_3$, modeling the actions of functional groups

$q^1_{G_1}$	Full perimeter control of the emergency zone
$q^2_{G_1}$	Implementation of access control
$q^1_{G_2}$	Waiting in the initial area
$q^2_{G_2}$	Movement to the search area
$q^3_{G_2}$	Searching for people and material valuables to be evacuated
$q^4_{G_2}$	Escorting people and material valuables to the assembly evacuation point
$q^1_{G_3}$	Waiting for the formation of the evacuation convoy
$q^2_{G_3}$	Accounting for the injured and forming the evacuation convoy
$q^3_{G_3}$	Movement to the safe zone

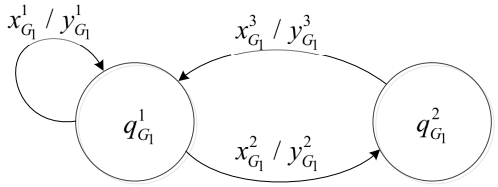

Fig. 4. Graphoid G_1.

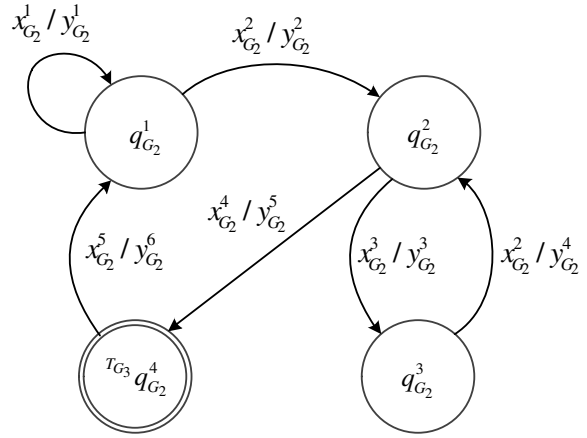

Fig. 5. Graphoid G_2.

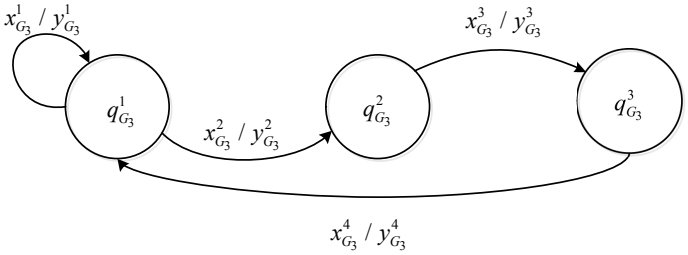

Fig. 6. Graphoid G_3.

The graphoids G_1, G_2, G_3 of finite state machines A_1, A_2, A_3 are shown in Figs. 4–6.

It is necessary to synthesize, using the developed algebra $\mathcal{A}$ a graphoid H, that defines the joint activities of the functional groups. The analysis of the task revealed:

1) potential conflict situations and the determination of the set of unacceptable vertices

$$\Xi = \left\{\left\{q^1_{G_1}, q^2_{G_2}\right\}, \left\{q^2_{G_1}, q^1_{G_2}\right\}, \left\{q^2_{G_1}, q^3_{G_2}\right\}, \left\{q^2_{G_1}, q^4_{G_2}\right\}, \left\{q^1_{G_1}, q^4_{G_2}, q^1_{G_3}\right\}, \left\{q^1_{G_1}, q^4_{G_2}, q^3_{G_3}\right\}\right\};$$

2) the need for automaton A_3 to be triggered by automaton A_2: if the output symbol of automaton A_2 is $y^5_{G_2}$, then the input symbol of automaton A_3 is $x^2_{G_3}$.

For example, the state corresponding to the vertex is a conflict state because the functional group described by automaton A_1, is advancing into the search area at the moment when the functional group described by automaton A_2, is performing territorial control.

We will describe the process of synthesizing the graphoid H in accordance with the algorithm shown in Fig. 1.

In the first iteration, the synthesis of graphoids H and G_2 is carried out:

It is assumed that $H = G_1$ and $Y_H = Y_{G_1}$;

Since there are no state triggers, as $Y_H \cap X_{G_2} = \varnothing$, the operation $H = H \otimes G_2$ is performed;

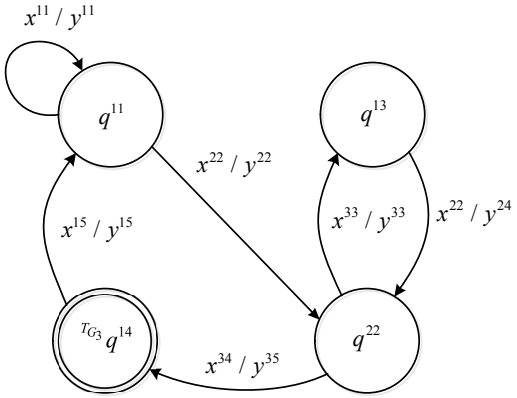

Fig. 7. Graphoid $H = \nabla(G_1 \otimes G_2)$.

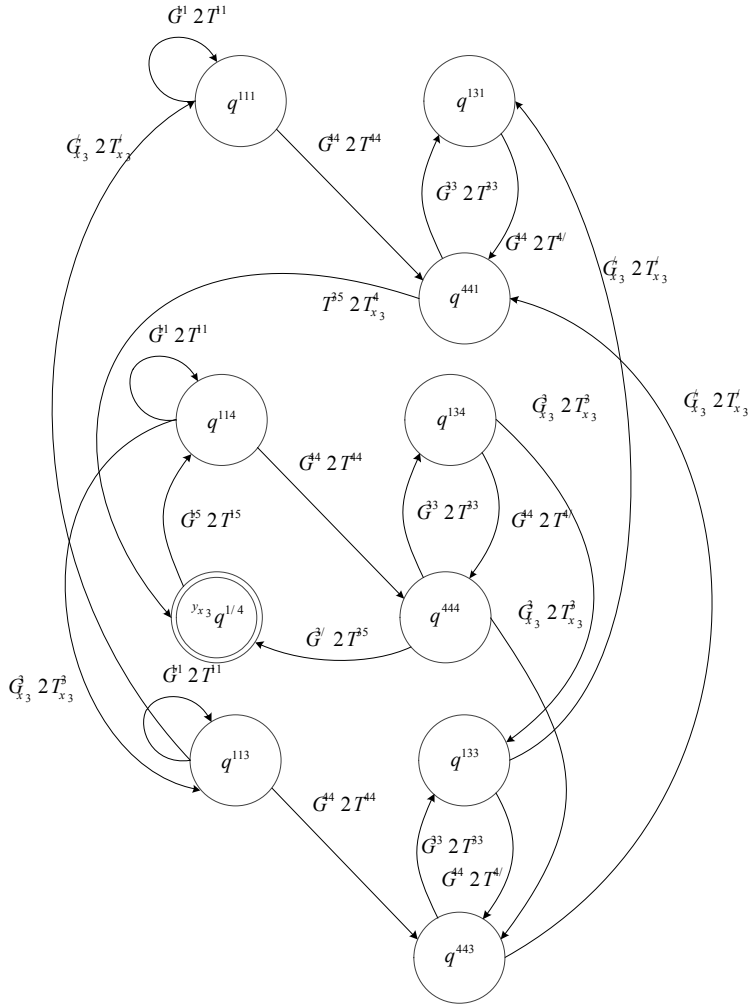

Fig. 8. Graphoid $= \nabla(\nabla(G_1 \otimes G_2) \odot G_3)$.

Invalid states, determined by the vertices $\{q^1_{G_1}, q^2_{G_2}\}$, $\{q^2_{G_1}, q^1_{G_2}\}$, $\{q^2_{G_1}, q^3_{G_2}\}$, $\{q^2_{G_1}, q^4_{G_2}\}$ are excluded from graphoid H, i.e., the operation $H = \nabla H$ is performed. The resulting graphoid is shown in Fig. 7, where the vertices $q^{ij} = \{q^i_{G_1}, q^j_{G_2}\}$, input symbols $x^{ij} = \{x^i_{G_1}, x^j_{G_2}\}$ and output symbols $y^{ij} = \{y^i_{G_1}, y^j_{G_2}\}$ are defined.

In the next iteration, the synthesis of graphoids H and G_3 is performed:

Since $Y_H \cap X_{G_3} \neq \varnothing$ the operation $H = H \odot G_3$ is performed;

Invalid vertices $\{q^1_{G_1}, q^4_{G_2}, q^1_{G_3}\}, \{q^1_{G_1}, q^4_{G_2}, q^3_{G_3}\}$ are excluded from graphoid H, i.e., the operation $H = \nabla H$, is performed. The resulting graphoid is shown in Fig. 8, with vertices $q^{ijk} = \{q^i_{G_1}, q^j_{G_2}, q^k_{G_3}\}$.

Thus, the graphoid H corresponds to an automaton that describes the parallel synchronous and asynchronous functioning of automata A_1, A_2, as well as the initialization of state transitions of automaton A_3.

In the resulting graphoid H, all interrelated actions of the three functional groups are considered. Their activities are directed at controlling access to the emergency zone, organizing the search for victims, and evacuating people and material valuables from the zone.

8. CONCLUSION

The article presents an algebra of graphoids of automata, which allows synthesizing a graphoid for the general model of automaton functioning. In constructing this algebra, operations on automata were partially transferred to the graphoids of these automata, and operations were introduced to account for additional domain-specific requirements. An algorithm for synthesizing the graphoids of automata based on this algebra has been developed, which allows constructing a generalized model of object functioning independently of the sequence in which they are connected, due to the commutativity of the operations. A numerical example of synthesizing the graphoid of an automaton is provided, describing the interrelated actions of three functional groups used in the event of an emergency. These functional groups carry out control of access to the emergency zone, organize the search for victims, and evacuate people and material valuables from the zone. As a result, a mathematical apparatus has been developed, enabling the modeling of joint actions of the functional groups involved in emergency response. This mathematical apparatus can later be used in models for assessing the effectiveness of functional group actions and optimizing the selection of their composition and tactics, by populating it with the contents of the input and output symbols of the automata.

REFERENCES

1. Kalman, R.E., Falb, P.L., and Arbib, M.A., *Topics in Mathematical System Theory*, New York: McGraw-Hill, 1969. Translated under the title *Ocherki po matematicheskoi teorii sistem*, Moscow: Mir, 1971.

2. Sysoev, V.V., Menshikh, V.V., Solodukha, R.A., and Zabiyako, S.V., Study of Interactions in a Network of Finite Deterministic Automata, *Radio Engineering*, 2000, no. 9, pp. 65–67.

3. Menshikh, V.V. and Nikitenko, V.A., Numerical Method for Aggregating Automaton Models Using Algebraic Operations on Automata, *Control Problems*, 2000, no. 9, pp. 65–67.

4. Gapanoich, D.A. and Sukhomlin, V.A., Algebra of Finite Automata as a Mathematical Model of Digital Twin for Smart Manufacturing, *Modern Information Technologies and IT Education*, 2022, vol. 18, no. 2, pp. 353–366.

5. Gapanoich, D.A. and Sukhomlin, V.A., Modeling of Mine Operations Using Algebra of Finite Automata DTA, *Modern Information Technologies and IT Education*, 2022, vol. 18, no. 3, pp. 634–643.

6. Volkova, K.M., Bulletin of the South Ural State University. Series: Computer Technologies, *Automatic Control, Radio Electronics*, 2022, vol. 21, no. 1, pp. 49–58.

7. Shirokova, E.V. and Yevtushenko, N.V., Synthesis of Safe Web Service Components Based on the Solution of Automaton Equations, *Modern Science: Actual Problems of Theory and Practice. Series: Natural and Technical Sciences*, 2023, no. 8, pp. 143–150.

8. Solovyev, V.V., Synthesis of Fast Finite Automata on Programmable Logic Integrated Circuits by Splitting Internal States, *Izv. RAS. Theory and Systems of Control*, 2022, no. 3, pp. 69–80.

9. Menshikh, V.V. and Korchagin, A.V., Structural Models of Interactions of Units of Law Enforcement Agencies in Case of Technogenic Emergencies, *Proceedings of the Academy of Management of the Ministry of Internal Affairs of Russia*, 2015, no. 2(34), pp. 54–58.

10. Menshikh, V.V., Samorokovskyi, A.F., Sereda, E.N., Gorlov, and V.V., *Modeling Collective Actions of Internal Affairs Officers*, Voronezh: Voronezh Institute of the Ministry of Internal Affairs of the Russian Federation, 2017.

11. Menshikh, V.V., Gorlov, V.V., and Nikitenko, V.A., Consideration of Synergistic Effects in the Composition of Automaton Models of Actions of Units of Law Enforcement Agencies Involved in Emergency Response, *Bulletin of Voronezh Institute of the Ministry of Internal Affairs of Russia*, 2023, no. 2, pp. 60-68.

12. Harmanis, J. and Stearns, R., *Algebraic Structure Theory of Sequential Machines*, New York: Prentice-Hall Inc., 1966.

13. Villa, T., Yevtushenko, N., Brayton, R.K., Mishchenko, A., Petrenko, A., and Sangiovanni Vincentelli, A.L., *The Unknown Component Problem: Theory and Applications*, Springer, 2012.

14. Gorbatov, V.A., *Fundamental'nye osnovy diskretnoi matematiki. Informatsionnaya matematika* (Fundamentals of Discrete Mathematics. Information Mathematics), Moscow: Nauka, 2000.

15. Melikhov, A.N., *Orientirovannye grafy i konechnye avtomaty* (Directed Graphs and Finite Automata), Moscow: Nauka, 1971.

This paper was recommended for publication by M.F. Karavai, a member of the Editorial Board